

Gasification of Biomass: Production of Methanol

Ally Smith, Abby Williams, Samuel Kwon and Teeb Alnaji

Department of Chemical and Biological Engineering, University of Colorado Boulder

CHEN 4520: Final Design Project

Professor Alan Weimer and Professor Wendy Young

Dec 8, 2022

Table of contents

Table of contents	1
Executive Summary	3
1. Project Description, Scope and Background	4
2. Environmental, Health & Safety Considerations	6
2.1. State and Federal Permits and Regulations	6
2.2. Waste Stream Considerations	7
2.3. Primary Safety, Environmental, and Health Concerns	8
2.4. Material Safety and Data Sheet	8
2.5. Plant Safety Equipment	15
2.6. Safe Plant Operating Procedures	15
2.7. Employee Safety Precautions and Personal Protection Equipment Requirements	15
2.8. Worst Case Scenario	15
2.9. HAZOP (Solar Thermal Reactor and Distillation Column)	16
3. Approach and Premises	19
3.1. Overview of Project	19
3.2. Project Management	20
3.3. Process Description and Flow Diagram	22
3.4. Battery Limits and Design & Economic Premises	24
3.5. Material Balances	26
3.6. Energy Balances	31
4. Process Description & Simulation	33
4.1. Aspen Plus Simulation	33
4.2. Aspen HYSYS Simulation	38
5. Process Details & Equipment Specifications	41
5.1. Reactors	41
5.1.1. Solar-Thermal Gasification	41
5.1.2. Catalytic Gas Cleaning Bed	47
5.1.3. Methanol Fixed Bed Reactor	50
5.2. Separators	60
5.3. Heat Exchangers	68
5.3.1. Spray Quench Tank	68
5.3.2. Shell-and-Tube	72

5.4. Pumps & Compressors	77
5.4.1. Pumps	77
5.4.2. Compressors	81
5.5 Heliostat Design	84
6. Utilities Summary & Heat Integration	87
7. Estimation of Capital Investment, Cash Flow, & Profitability Analysis	93
References	98
Table of Nomenclature	103
Appendices	108
Appendix A (Sample Calculations)	108
3.6 Energy Balances	108
5.2 Separators	110
5.3 Heat Exchangers	110
5.4 Pumps and Compressors	111
5.5 Heliostat Design	112
Appendix B: Excel	114
Appendix C: Code	132

Executive Summary

The main objective of this report is utilization of a solar thermal reactor to gasify feed biomass and convert it into syngas. The chemical plant is divided into an upstream that operates eight hours a day, 365 days a year, and a downstream that operates 24 hours a day, 365 days a year and a total of 8000 hours per year. The upstream segment of the plant contains major equipment such as: solar reactor, spray quench, cyclone, ZnO cleaning bed reactor, shell-and-tube heat exchangers and methanol bed reactor. As for the downstream, major components are a storage tank and a distillation column. Both sections of the plant are located in Daggett, California. The consumer's request is to produce 56 million methanol gallons per year, with a purity of 99.97%. Ingredients that are fed into the reactor are water, cellulose, lignin, ash, nitrogen, chlorine and methane. The overall biomass flow rate fed into the reactor is a value of 72 kmol/hr, water is 4.7E+6 kmol/hr and methane is 8.6E+06. Constituents afterwards enter a water-gas-shift reactor, which in reality is not implemented because WGS reaction would occur within the solar reactor itself. However, the stream coming out of the WGS reactor is at a temperature of 800 °C. In order to cool down the stream, a spray quench is employed with cooling water as a utility and to decrease the temperature to a value of 210 °C. However since the amount of natural gas fed is considerably large, the stream was cooled down to a value of 488 °C. Subsequently, components enter the cyclone where ash is withdrawn and other materials enter a shell-and-tube heat exchanger which cools it down to 210 °C. Moving on the ZnO cleaning bed, 1200 kmol/hr is fed into the reactor as the other incoming components enter. A compressor is located after that step of the simulation for materials to undergo pressure changes and heat exchanger is located consecutively. The methanol bed reactor is a highly pressurized system with a value of 80 bar and 270 °C, the raw methanol product stream exits the methanol bed reactor with a flow rate of 4.5E+6 kmol/hr containing mainly water, methanol, hydrogen and residual gasses. It contains a methanol mole fraction of 0.65 and 0.32 of water. The raw methanol stream enters the storage tank downstream with a flow rate of 8.6E+06 kmol/hr, where the distillate flow rate exits with a value of 1.79E+6 kmol/hr which is the desired specification of 56 million gallons per year. Moreover, considering that the solar reactor is powered by a heliostat field, a concentration of 8000 suns have been chosen, resulting in five towers each with a height of 184.4 m. Another major consideration is design of all three reactors where the volumes of solar, ZnO and methanol are 30 L, 0.5 L and 8000 L, respectively. As for the number of tubes, there are 16 for the methanol bed and 4663 for the solar. Proceeding with economic feasibility, at a base case of 12.5% IRR, the selling price of methanol was a value of \$2.3 per gallon, a NPV of \$10,000 and a capital investment of \$35,256 per year. The payback period of the base case is around 5.3 years, as for the ROI it amounted to 18.9%. As per sensitivity analysis, as IRR increases, the number of operators and ingredients costs result in a maximization of methanol selling price to a value of \$2.6. It can be concluded from such figures that it takes more than five years to start making a profit, which might affect the system in a negative manner due to lack of capital. As for matters in regards to the system overall, it is scientifically feasible with the space of development as it is still a growing field in research. A recommendation that can be implemented in the system to reduce waste and cost is to recycle the bottoms stream of the distillation column, considering that it is 99% water which can be utilized as utilities in the system, or re-fed into the solar reactor itself for the water requirement. As for cost-effectiveness, an optimization process in regards to sizing up equipment would be of major assistance to

minimize costs and maximize efficiency of equipment such as pumps, compressors and heat exchangers.

1. Project Description, Scope and Background

As climate conditions worsen due to the excessive usage of carbon-enriched fuels, industries finally started to acknowledge the dangers of such a practice and started to shift into more environmentally friendly and renewable resources. This project essentially is the embodiment of implementing such practices. To begin with, gasification of biomass has been there for a while now and applied in different mediums in order to produce syngas and minimize the carbon dioxide emissions to almost zero. There are industry-based examples where such a reaction is occurring in an interconnected fluidized bed at relatively high operating conditions of temperature and pressure, as well as utilization of catalysts such as CaCO_3 (Zhang, 200). Another example that is found in industry is using a thermo-catalytic and bioconversion of biomass to produce H_2 rich syngas in which the steps are gasification, reforming and fermentation. Pyrolysis is employed in order to undergo biomass gasification without the need of oxygen and therefore avoiding combustion, as for fermentation is also anaerobic in which some enzymes and bacteria are used to convert biomass to a type of syngas like methanol, glycerol and ethanol (Ayodele et al., 2019). Even though there are loads of promising technologies out there that strive to minimize carbon emissions as much as possible, some factors such as electricity and waste products are not entirely within the picture in regards to the emissions produced by them. Here is where this project comes into play, by which a solar-thermal reactor that is powered by a heliostat field of solar panels is utilized to gasify biomass feed. What makes this approach promising is the absence of the need to combust a certain amount of feedstock in order to capture the energy released. Prior to delving into design parameters of such a design, the inert species are water, cellulose, lignin, ash, nitrogen, chlorine and methane. The plant is divided into two sections: upstream methanol production and downstream methanol purification. Water is pumped into the reactor at a pressure of 35 bar and 25 °C, biomass is delivered to the plant and fed into the reactor, as well as methane. In order to maximize the hydrogen-carbon ratio, natural gas is one of the feed inlets to produce hydrogen enriched syngas. Other materials are fed into the solar thermal reactor at standard conditions. Moreover, the operating conditions for the solar reactor are very high with values of 1450 °C and 35 bar, which relinquishes the need of a catalyst because it essentially is autocatalytic due to high temperature. Outlets of the reactor enter a mixer and a spray quench heat exchanger to cool down the components from around 800 °C to a value of 210 °C. Afterwards, they enter a cyclone in order to dispense all lingering, unreacted solids such as ash, as liquid and vapor phase enter another shell-and-tube heat exchanger to cool down materials if the specification temperature was not reached in the previous spray quench. After that, components enter a ZnO cleaning bed to get rid of H_2S and HCl that resulted from previous reactions in the process. Entering another mixer, materials undergo pressure and temperature changes due to a compressor prior to entering the methanol bed reactor. Operating conditions of a methanol bed reactor is a temperature of 270 °C and a pressure of 80 bar, where the outlet

stream enters a separator to isolate methanol into the downstream process and the other unreacted outlets are recycled back into the system. Entering the downstream segment, methanol is stored in a storage tank in the downtime of the plant, and is distilled in a distillation column in the operating hours of the plant. The amount of methanol that needs to be produced is 56 million gallons per year with a purification level of 99.97%.

For further background information, other than gasification of biomass, methanol production has also been practiced with different approaches, be it renewable or nonrenewable. For example, some famous ways to produce methanol is through a steam-reforming process of natural gas, partial oxidation of methanol and methanol-water electrolysis. A study was conducted by Xiaoti Cui et al. in which a comparative process was conducted between three different reactors that fostered methanol production. The reactors were adiabatic, water-cooled and gas-cooled to navigate which approach enhances the hydrogenation of carbon dioxide, alongside different types of flows: radial and axial. It appeared that both gas-cooled and adiabatic reactors exhibit low heat transfer as a result of the hindrance of the water gas shift reaction that keeps cooling the system due to its endothermic nature. That being said, the choice of a water-cooled reactor would have a more distributed heat transfer ratio upon a certain surface area of a tube, and hence the choice of a multi-tubular fixed bed. More information in terms of type of flow, heat transfer and pressure drop of the system are discussed in depth in the upcoming sections in the report.

The scope of this project vast and keeps expanding the more research is conducted in all the variations and the parameters that are implemented in the process. Especially that solar energy is still undergoing rigorous research in terms of energy storage, energy capture and production with minimum heat losses. Some aspects that have not been touched upon are process control routes and equipment. Therefore, a brief description of some process control matters are to be discussed. Safety is an important factor in any chemical plant design, thanks to advancement of technology there are some aspects that are dangerous to be operated by a human and therefore automated apparatus are administered as a part of process synthesis. Considering that the solar reactor operates at very high temperatures, thermocouples are required to be placed in various yet specific regions such as top, bottom and middle of the reactor to ensure a safe range of temperature. widely used kinds of thermocouples in such a setting are type K and type C (Omega, n.d.) Another piece of equipment that is important is a flow rate regulator, also known as flow controllers for certain species in the system, such as hydrogen and/or nitrogen (Weimer et al, 2013). Moreover, pressure transducers are also to be placed, especially in high pressure regions such as streams coming out the solar reactor, pumps and compressors. Control valves are to be placed in almost every inlet and outlet of each existing piece of equipment, in order to direct flow rates into the correct route with the right amount of basis. To mitigate errors that could be as a result of these automated apparatus, a centralized computer is placed in almost

every chemical plant with a human operator to ensure that levels of temperature, pressure and flow rates are in the accepted range.

Even though this report mostly navigates the industrial feasibility of such a process synthesis, one of the main important questions to ask is: is it economically feasible? Generally, a very large chemical plant will require a huge amount of capital for construction, equipment, ingredients and most importantly production. One of the most apparent obstacles that solar industries face is large expenses which makes it less attractive for usage, especially in start ups or already established companies with a fixed income. Therefore, an implementation of a heliostat field alone is quite expensive, let alone the execution of the process itself overall. Economics are studied and analyzed in the following sections of this report to answer the ultimate question in terms of cost-effectiveness.

2. Environmental, Health & Safety Considerations

2.1. State and Federal Permits and Regulations

The upstream process plant is located in Dagget, California. When deciding a spot to place the downstream process plant, it is important to consider raw materials supply, location with respect to market, transportation, utilities, land, and environmental impact. The downstream process starts with a tank of the raw methanol produced upstream. Since the upstream process is already located in Dagget, California, it would be beneficial to place the downstream process near the upstream process plant because of transportation costs. Placing the two processes in the same city would drastically reduce the cost of transportation between the two plants. Furthermore, Dagget, California, is an ideal location to place the methanol production plant because it is a rural area with a limited human population. Access to raw materials and the market is easy in California. Before designing the process plant, there are state and federal permits and regulations to keep in mind.

Chemical process plan permits can be divided into agency permits and state permits. Agency permits are issued through a federal or local agency that enforces certain regulations. The Occupational Safety and Health Administration (OSHA) sets guidelines regarding employee safety. The OSHA work permit is a document signed by the employee and employer that places safeguards. Through this permit, process plants place guidelines that mitigate chemical and ignition hazards to workers. The Environmental Protection Agencies (EPA) issue permits to the chemical manufacturing sector where laws and regulations are in place regarding air quality control, toxic substances, and water. Specifically, the Department of Toxic Substance Control administers permits that review hazardous waste facility design and operations. Any process plan that stores, treats, or disposes of hazardous waste must obtain a permit. The Resource Conservation and Recovery Act (RCRA) issues hazardous waste and solid waste management permits. Besides agency permits, state permits are also issued to process plants to initiate the

plant-building process. The process plant must gain a building permit through the local building department. The permit will enforce local codes and fire prevention programs and design checkpoints. Before the building process, plants must have a detailed civil and structural drawing, fire protection system drawing, site drawing, and electrical drawing. In addition to the building permit, the plant must also have permits issued by the city or county regarding zoning conditions, emergency planning and response, and wastewater management. The water treatment facility will review the amount of wastewater produced to install the correct equipment and treatment methods.

Below is a table of permits required for operation in Daggett, California.

Table 1: Required Operation Permits

Permit Name	Issuing Institute
Hazardous Waste Permit	EPA: Department of Toxic Substance and Control
Hot Work Permit	OSHA
Wastewater Discharge Permit	California Water Boards
Building Permit	San Bernardino County
Site Plan Permit	San Bernardino County: Planning Division
Construction Waste Management Plan	San Bernardino County: Solid Waste Management
Greenhouse Gas Reporting Program	Environmental Protection Agency
Title V Permit	Environmental Protection Agency
Risk Management Plan	Environmental Protection Agency

2.2. Waste Stream Considerations

Waste streams include the purge streams, solid waste stream, and ZnCl₂ stream. The ZnCl₂ waste stream contains majority ZnCl₂ and some concentrations of ZnO and ZnS. The purge stream contains hydrogen. The waste streams should be treated appropriately by disposing of waste as hazardous waste. Hazardous waste can be processed chemically, thermally, biologically, or physically. Chemical waste should be kept in a controlled container with the appropriate inert absorbent material. Furthermore, the hazardous waste should be addressed by sending it to a licensed disposal facility.

2.3. Primary Safety, Environmental, and Health Concerns

Primary safety, environmental, and health concerns are associated with chemical hazards, combustion, and ventilation. As the MSDS table records, chemicals such as H₂S, Cl₂, CO, HCl, and ZnCl₂ have an NFPA health rating greater than or equal to three, indicating that the chemical substance is dangerous and can cause severe health damage. Exposure to these chemicals can cause respiratory and digestive tract irritation and irreversible damage. In addition, excessive ingestion of methanol can cause damage to internal organs and the central nervous system. When dealing with these substances, it is important to follow OSHA personal protective equipment guidelines. Besides chemical hazards, gasses utilized in this process are pressurized in a container. Dealing with pressurized gasses comes with the risk of explosion if punctured, heated, or dented. This can cause physical and environmental damage. In addition to combustible material, gasses and airborne solids pose health and safety concerns. Therefore, working in a cool, dry, and well-ventilated area is key to avoiding the ignition of chemicals and respiratory irritation.

2.4. Material Safety and Data Sheet

Table 2: Material Safety and Data Sheet

Chemical	Flash Point	Flammability	Health	Reactivity	Special Considerations
Cellulose	N/A	NFPA Rating: Flammability: 1	May cause eye and skin irritation. May cause respiratory and digestive tract irritation.	Material should be kept in a dry area to avoid spontaneous combustion. Avoid bromine pentafluoride, hydrogen peroxide, sodium hypochlorite, sodium nitrate, fluorine, and strong oxidizing agents.	NFPA Rating: Flammability: 1 Health: 1 Instability: 1 Store in tightly closed containers and avoid oxidizing materials.
Ligin	N/A	May form combustible dry dust if not	May cause eye and skin irritation.	Material is relatively stable under ambient	NFPA Rating: Flammability: 1 Health: 1

		<p>maintained adequately. Hazardous combustion production includes sulfur oxides and carbon oxides.</p>	<p>May cause respiratory and digestive tract irritation. Chronic exposure may lead to long term damage.</p>	<p>conditions. Incompatible with oxidizers, reducers, and organic material.</p>	<p>Reactivity: 0 Store in ambient conditions away from dust, static electricity, moist areas.</p>
Ash	N/A	Solid and gas not combustible	<p>May cause eye and skin irritation.</p> <p>May cause respiratory and digestive tract irritation.</p>	<p>Material is inert and no known incompatible materials.</p>	<p>NFPA Rating: Health: 2 Flammability: 1 Reactivity: 0 Should be stored in closed containers cause it can become airborne. If stored outside, place damp cloth on top.</p>
N₂	N/A	If the container is heated, it will burst since it is under pressure.	<p>May cause burns or frostbites if contact with eyes or skin.</p> <p>May cause suffocation if inhaled in large quantities.</p>	<p>Material is relatively stable and no known incompatible materials.</p>	<p>NFPA Rating: Health: 0 Flammability: 0 Reactivity: 0 Store away from direct sunlight in dry, cool, and well ventilated areas. Close the valve after each use and put on appropriate PPE.</p>

H₂	N/A	Extremely flammable gas. Avoid any oxidizing agents. Container is under pressure so it may explode if heated.	May cause burns or frostbites if contact with eyes or skin. May cause suffocation if inhaled in large quantities.	Oxidizer is incompatible. The product is relatively stable.	NFPA Rating: Health: 0 Flammability: 4 Reactivity: 0 Store away from direct sunlight in dry, cool, and well ventilated areas. Close the valve after each use and put on appropriate PPE.
S	207 °C	Flammable solid. Sulfur dust easily ignites in air. Static discharge may ignite dust.	Contact with molten sulfur may cause burns and blindness. Sulfur vapor may cause eye irritation. Contact with dust may cause abrasions and discomfort.	Sulfur is incompatible with chlorates, nitrates, oxidisers, carbides, halogens, phosphorus, and heavy metals.	NFPA Rating: Health: 2 Flammability: 1 Reactivity: 0 Store away from high temperatures, open flames, welding, and ignition sources.
H₂O	N/A	Non Flammable	No significant hazard when used under normal conditions.	Avoid extremely high or low temperatures. Metallic sodium is an incompatible material.	NFPA Rating: Health: 0 Flammability: 0 Reactivity: 0 Keep the container closed when not in use.

H₂S	N/A	Extremely flammable gas. Gas is under pressure which may lead to explosion if heated.	May lead to respiratory irritation.	Incompatible with oxidizers. Product should be stable under normal conditions.	NFPA Rating: Health: 4 Flammability: 4 Reactivity: 0 Avoid all sources of ignition. Avoid cutting, welding, or grinding the container.
Cl₂	N/A	Contact with combustible material may cause fire. Heating the pressurized container may cause an explosion. Flammable material is dangerous to water sources and sewer.	Can cause serious eye damage. Fatal if inhaled. Can cause serious burns or frostbite.	Incompatible with combustible materials, reducing agents, grease, oil.	NFPA Rating: Health: 4 Flammability: 0 Reactivity: 0 Store away from direct sunlight. Should be stored in a dry and well ventilated area. Utilize appropriate PPE.
CO	N/A	Extremely flammable gas. Avoid open flames, sparks, static discharge, and oxidizing materials. May explode if heated since gas is under pressure.	Toxic if inhaled. May cause fertility damage or damage to unborn children. Can cause damage to organs if	Incompatible with oxidizing agents.	NFPA Rating: Health: 3 Flammability: 4 Reactivity: 0 Store away from direct sunlight. Should be stored in a dry and well

			prolonged exposure. May cause asphyxiation.		ventilated area. Utilize appropriate PPE. Empty containers may contain residue products so store away from heat, sparks, open flame, or any form of ignition.
CO₂	N/A	Could explode if heated.	May cause suffocation if prolonged exposure. May increase respiration and heat rate.	No specific data available on incompatible materials.	NFPA Rating: Health: 3 Flammability: 0 Reactivity: 0 Store away from direct sunlight. Should be stored in a dry and well ventilated area. Utilize appropriate PPE.
CH₄	-104 °C	Extremely flammable gas., May form explosives if mixed with air. May explode if the container is headed while under pressure.	May cause burns or frostbites.	Avoid all sources of ignition. Avoid any oxidizing agents.	NFPA Rating: Health: 2 Flammability: 4 Reactivity: 0 Store away from direct sunlight. Should be stored in a dry and well ventilated area. Utilize

					appropriate PPE and respirator.
HCl	N/A	Product is non combustible.	<p>May cause severe eye injury such as irritation and severe burns.</p> <p>Contact with skin will cause severe burns and ulcerations.</p> <p>Contact with the digestive tract will cause permanent tissue damage.</p> <p>Contact with the respiratory tract will cause severe damage to mucous membranes.</p>	<p>Incompatible with metals, oxidizing agents, reducing agents, bases, acetic anhydride, alcohols, amines, sulfuric acid, vinyl acetate, spoxides, carbides, cyanides.</p> <p>For a full list please reference citations.</p>	<p>NFPA Rating: Health: 3 Flammability: 0 Reactivity: 1</p> <p>Store in a cool, dry, and well ventilated area. Avoid storing in metal containers and away from alkalies.</p>
ZnO	N/A	Product is noncombustible .	<p>May cause eye, skin, and respiratory irritation.</p> <p>Inhalation of fumes may be toxic.</p>	<p>Incompatible with magnesium and chlorinated rubber.</p>	<p>NFPA Rating: Health: 1 Flammability: 0 Reactivity: 0</p> <p>Store in a tightly closed container. Store in a cool, dry, and well ventilated area.</p>

ZnS	N/A	Product is noncombustible	May cause irritation, shortness of breath, headache, nausea, dizziness.	Incompatible with strong oxidizing agents, strong acids, iodine pentachloride.	NFPA Rating: Health: 0 Flammability: 0 Reactivity: 0 Store in a cool and well ventilated area. Store away from strong acids. Protect from freezing and physical damage.
ZnCl₂	N/A	Product is noncombustible	May cause eye and skin burns. Can cause gastrointestinal burns if ingested. Harmful to the respiratory tract if inhaled for a long time.	Incompatible with metals and strong oxidizing agents.	NFPA Rating: Health: 3 Flammability: 0 Reactivity: 1 Store in dry, cool, and well ventilated areas Avoid corrosives and do not store in metal containers.
CH₃OH	12 °C	Combustible vapor and liquid. Water may spread the fire since the product is lighter. Vapors will cause ignition and flash back.	May cause blindness if swallowed. Can cause eye, skin, and respiratory tract irritation. May cause central	Incompatible with oxidizing agents, reducing acids, acids, alkali metals, potassium, sodium, acid chlorides, powdered aluminum, powdered	NFPA Rating: Health: 1 Flammability: 3 Reactivity: 0 Store in cool, dry, and well ventilated areas. Keep away from ignition sources and incompatible

			nervous system damage.	magnesium.	products. Keep the container closed tight.
--	--	--	------------------------	------------	--

2.5. Plant Safety Equipment

Besides personal protective equipment, the plant will also have safety equipment for chemical spills and fire hazards. Safety equipment such as absorbent materials, neutralizing agents, oxidizing agents, reducing agents, and pumps and hoses will be supplied for chemical spills. Fire protection systems such as fire extinguishers, sprinkler systems, fire alarms, and toxic gas monitors will be installed for fire safety management. First aid kits and emergency medical kits are key in any industrial plant. Chemical burn stations will be installed, which requires a water supply network.

2.6. Safe Plant Operating Procedures

OSHA requires that all employees comply with the safety and health standards and provide a place of employment free from recognized hazards. In order to provide a hazard-free environment, it is key to implement operating procedures. Operating procedures include pre operational checks, safe operation of equipment, carrying out multiple inspections, performing frequent repair and maintenance when required, and establishing traffic rules and emergency procedures.

2.7. Employee Safety Precautions and Personal Protection Equipment Requirements

Providing the correct personal protective equipment is key to avoiding future hazards. Since the chemical plant deals with hazardous chemicals, operators must utilize eye and face protection. Chemical safety goggles and face shields are required protective equipment. In addition, chemical-resistant suits, protective gloves, and footwear are a must when dealing with chemicals. Since the chemical plant deals with various gas and particulate matter, respirators are also important protective equipment. When the operator is near the process plant, all protective equipment is expected to be worn.

2.8. Worst Case Scenario

A few worst-case scenarios can occur when managing the plant. The first worst-case scenario would be a leak in a valve or piping, causing vapor to accumulate outside the process plant. Some of the gasses utilized in this process plant are highly combustible and can cause chronic health damage if exposed for a long time. Accumulation of gasses outside the process flow can cause a combustion reaction which will start a fire in the process plan. If a leak is present, the procedure would be to shut down the plant or the reactor unit that is causing the accumulation of vapor. Generally, it is not ideal to shut down the whole plant; therefore, it would

be more desirable if the problematic unit or section of pipe were isolated from the rest of the process. In order to mitigate this issue, the design should include additional pipes that divert the flow away from the leaking section. During normal operations, the process will not flow through the backup pipes; however, if a leak is detected, the backup pipes will open to divert the flow. Leaks can be detected by measuring the flow rate through the pipe, meaning that mass flow controllers can be installed to monitor changes.

The second worst-case scenario is the buildup of pressure. It is important to note that the process deals with solids, vapors, and liquids. Residual solids can accumulate in piping or reactor tanks if the equipment is poorly managed or the proper components need to be chosen. Accumulation of residue in reactor tanks or pipings can cause an increase in pressure which will impact the efficiency of the processes and the overall safety of the process units. If this scenario occurs, the operators should activate pressure relief valves to decrease pressure buildup. When designing the plant, it is important to install pressure relief valves that automatically activate when a threshold pressure value is reached.

The third worst-case scenario is a sudden increase in reaction temperature. The most dangerous situations occur when heat transfer is not properly accounted for during heat exchanger design. Furthermore, a change in chemical kinetics can cause the reaction to have exponential temperature growth. When the process exceeds normal temperature values, the operator should shut down the process plant if emergency systems are not in place. Emergency systems such as extra pumps or sprinklers can be installed for future mitigation. Reactor tanks can have a sprinkling system that activates if the temperature of the reactor exceeds the operation conditions. Since heat exchangers utilize a cold medium, extra water pumps can be installed. If the heat exchanger fails to transfer heat at its normal rate, additional cooling pumps will assist with normalizing the heat transfer process.

2.9. HAZOP (Solar Thermal Reactor and Distillation Column)

Table 3. Solar Thermal Reactor HAZOP

Deviation	Possible Causes	Consequences	Safeguards	Recommendations
No Flow	1. Feed pipe is plugged. 2. Pump is broken 3. Broken pipeline	1. No inlet biomass flow to the solar reactor, thus, reaction is limited. 2. NNC	1. PT presents high pressure 2. FT presents no flow into reactor 3. NNC	1. Consider changing piping material. Upgrading component. 2. Consider changing pumps or performing pump maintenance. 3. NNR
More Flow	1. FC broken	1. Flow not	1. FT with high	1. Consider changing

	2. Broken valve	properly regulated impacting reaction. 2. Could present a leak creating a hazardous work environment.	flow alarm. 2. Additional overflow piping.	the flow rate controller. 2. Update valve component.
High Pressure	1. Blocked pipeline 2. PC Broken	1. Explosion of reactor tank. 2. NNC	1. PC 2. Pressure relief valves	1. Change pipe material. Upgrade component. 2. Change PC components.
Low Pressure	1. Crack or hole in tank	1. Leaks present a hazardous environment.	1. PT with a low pressure alarm	1. Consider reactor tank maintenance or replacing the tank.
High Temperature	1. Recycle stream can have high temperature	1. Can impact pipes that cannot take on high temperatures. Reactor product stream temperature is high.	1. TC presents a high temperature alarm.	1. Optimize product flow conditions after the methanol reactor.
Low Temperature	1. Heliostat failure.	1. Limited reaction kinetics	1. TC presents a low temperature alarm	1. Consider Heliostat maintenance or replacement.

Table 4. Distillation Column HAZOP

Deviation	Possible Causes	Consequences	Safeguards	Recommendations
No Flow	1. Blocked pipeline 2. Broken pipeline 3. Broken pump 4. FC broken	1. No inlet flow rate into the distillation column. 2. NCC	1. PT presents a low pressure alarm. 2. FT presents low flow rate 3. NNC	1. Consider replacement of pipes. 2. Consider replacement of pumps. 3. NNR
More Flow	1. FC broken 2. Valve broken 3. Broken pipeline	1. Flow not properly regulated impacting reaction. 2. Could present a leak creating a hazardous work environment. 3. NNC	1. FT with high flow alarm. 2. Additional overflow piping.	1. Consider changing the flow rate controller. 2. Update valve component.
High Pressure	1. PC broken 2. Blocked pipeline	1. Explosion of reactor tank. 2. NNC	1. PC 2. Pressure relief valves	1. Change pipe material. Upgrade component. 2. Change PC components.
Low Pressure	1. PC broken 2. Hole in column wall	1. Leaks present a hazardous environment.	1. PT with a low pressure alarm	1. Consider distillation column replacement or maintenance
High Temperature	1. High inlet temperature 2. TC broken 3. Condenser doesn't work	1. Can impact pipes that cannot take on high temperatures.	1. TC presents a high temperature alarm. 2. Poor separation	1. Consider condenser replacement or maintenance. 2. NNR

		2. Impact efficiency of separation 3. NNR		
Low Temperature	1. TC broken 2. Reboiler doesn't work	1. Limited distillation efficiency	1. TC presents a low temperature alarm. 2. Impact separation and product purity	1. Consider reboiler replacement or maintenance. 2. NNR

3. Approach and Premises

3.1. Overview of Project

To effectively design and model this process, the first step was determining everything that needed to be done and assigning who would do each part. This was done by using a Gantt chart, which was created using Excel, and it included a timeline of when tasks should be completed. The mass and energy balances were the first items on the list of tasks. The mass balances were first done by hand using an Excel spreadsheet, and they were compared with the results of a model of the entire process done in Aspen Plus and Aspen HYSYS. The upstream process, which included the solar reactor, the spray quench tank, the zinc oxide cleaning bed, and the raw methanol production, was modeled in Aspen Plus, while the downstream methanol purification process was modeled in Aspen HYSYS. The two kinds of software were used because Aspen Plus models reactors better, and Aspen HYSYS models distillation columns better. The energy balances were first performed by hand using Excel, in which heat capacities and heats of formation of each component were calculated, as well as heats of reaction and heats of combustion for respective reactions. Excel was also used to do a hand calculation of the energy requirement of the solar reactor. Each reactor was also modeled in MATLAB, which included differential equations to model temperature, pressure, and component flow rates. Plots for each differential were created by MATLAB. The heliostat field was modeled using Excel spreadsheets created by Allan Lewendowski, which were made to help in the design of heliostats used for 2000, 4000, and 8000 times solar concentration. The Analysis of utilities and heat integration was done using Aspen Energy Analyzer. Another Excel spreadsheet was used for economic analysis, which used macros and the Solver tool.

3.2. Project Management

Prior to assigning tasks for each member of the team, a discussion in regards to strengths and weaknesses in terms of conceptual understanding, technical matters and programming have been conducted in order to assign accordingly to maximize the strength of this report. A Gantt chart was assembled by which every task was delegated to the fitted group member. The timeline of this report started from 11/1/2022 to 12/8/2022. It was decided to leave small tasks such as introduction writings to the last interval of time allowable, and start heavy tasks on the earlier spectrum of time. Prior to delving into the Gantt chart, considering that the team consists of four people; Ally Smith, Williams, Sam Kwon and Teeb Alnaji, most tasks have been distributed in a pair-style, essentially for an extra eye to ensure that the tasks are to be completed on the right track. Table x below is a task distribution description that gives an outline of which member and when the tasks are required to be complete.

Table 5: Task Distribution

Task Name	Start Date	End Date	Start on Day	End on Day	Duration	Team Member(s)
Cover Page & Table of Contents	11/1	12/8	1	38	37	All
Executive Summary	11/1	12/8	1	38	37	Teeb
1. Project Description, Scope & Background	11/1	12/8	1	38	37	Ally
2. Environmental, Health & Safety Considerations	11/1	12/8	1	38	37	Sam
3.1. Overview of Project	11/1	12/8	1	38	37	Abby
3.2. Project Management	11/1	12/8	1	38	37	Teeb
3.3. Process Description and Flow Diagram	11/1	12/6	1	36	35	Sam
3.4. Battery Limits and Design & Economic Premises	11/29	12/6	29	36	7	Ally
3.5. Material Balance (overall hand MB to provide starting point for simulation)	11/1	11/8	1	8	7	Teeb and Sam
3.6. Energy Balances (incl. using heat capacity, etc. to determine heats of rxn)	11/1	11/8	1	8	7	Ally and Abby
4.1. Aspen Plus Simulation	11/1	11/15	1	15	14	Sam
4.2. Aspen HYSYS Simulation	11/1	11/15	1	15	14	Teeb
5.1. Reactors (math models should be developed and solved with Matlab or other solver)	11/1	11/20	1	20	19	Ally and Abby
5.1.1. Solar-Thermal Gasification	11/1	11/20	1	20	19	Ally and Abby

5.1.2. Catalytic Gas Cleaning Bed	11/1	11/20	1	20	19	Ally and Abby
5.1.3. Methanol Fixed Bed Reactor	11/1	11/20	1	20	19	Teeb and Sam
5.2 Separators	11/15	11/29	15	29	14	Teeb and Sam
5.3 Heat Exchangers	11/15	11/29	15	29	14	Teeb and Sam
5.4 Pumps & Compressors	11/15	11/29	15	29	14	Teeb and Sam
5.5 Heliostat Design (design based on lowest cost considering 2000, 4000, and 8000 suns)	11/15	11/29	15	29	14	Ally and Abby
6. Utilities Summary & Heat Integration including Energy Analyzer Analysis	11/15	11/29	15	29	14	Teeb and Sam
7. Estimation of Capital Investment & Cash Flow, and Profitability Analysis	11/20	12/6	20	36	16	All
References	11/1	12/8	1	38	37	All
Table of Nomenclature	11/1	12/8	1	38	37	All
Appendices	11/1	12/8	1	38	37	All
Formatting & Presentation	11/29	12/8	29	38	9	All
Mechanics of Writing, Grammar, Typos	11/1	12/8	1	38	37	All

The Gantt chart provides a visualization of the timeline of all the five weeks and the duration of time that is assigned for each task considering that each task requires a different amount of work. The solar reactor and the cleaning bed was assigned to Ally and Abby, as for the methanol bed reactor it was assigned to Sam and Teeb. The aspen plus simulation was started by Sam and continued by Teeb, as for the aspen HYSYS it was conducted by Teeb. Heliostat design was executed by Abby, whereas battery limits and economics were managed primarily by Ally. Separators, shell and tube heat exchangers and pumps were designed by Teeb, as compressors and spray quench tank were designed by Sam. As mentioned earlier, considering that the group is operating in pair-style, each pair is to proofread each other's work and to make sure everything is in its correct location. Due to the horizontal nature of a Gantt chart, it can be difficult to format it within the report and therefore it can be referred to in Appendix B.

3.3. Process Description and Flow Diagram

Figure 1 below is the overall process flow diagram. The upstream process deals with the feed stream, solar reactor, cyclone, zinc oxide reactor, and methanol production. The downstream process deals with the raw methanol produced upstream, which is processed using a distillation column. When modeling the overall process, the upstream process was modeled using Aspen Plus. The downstream process was modeled using Aspen HYSYS.

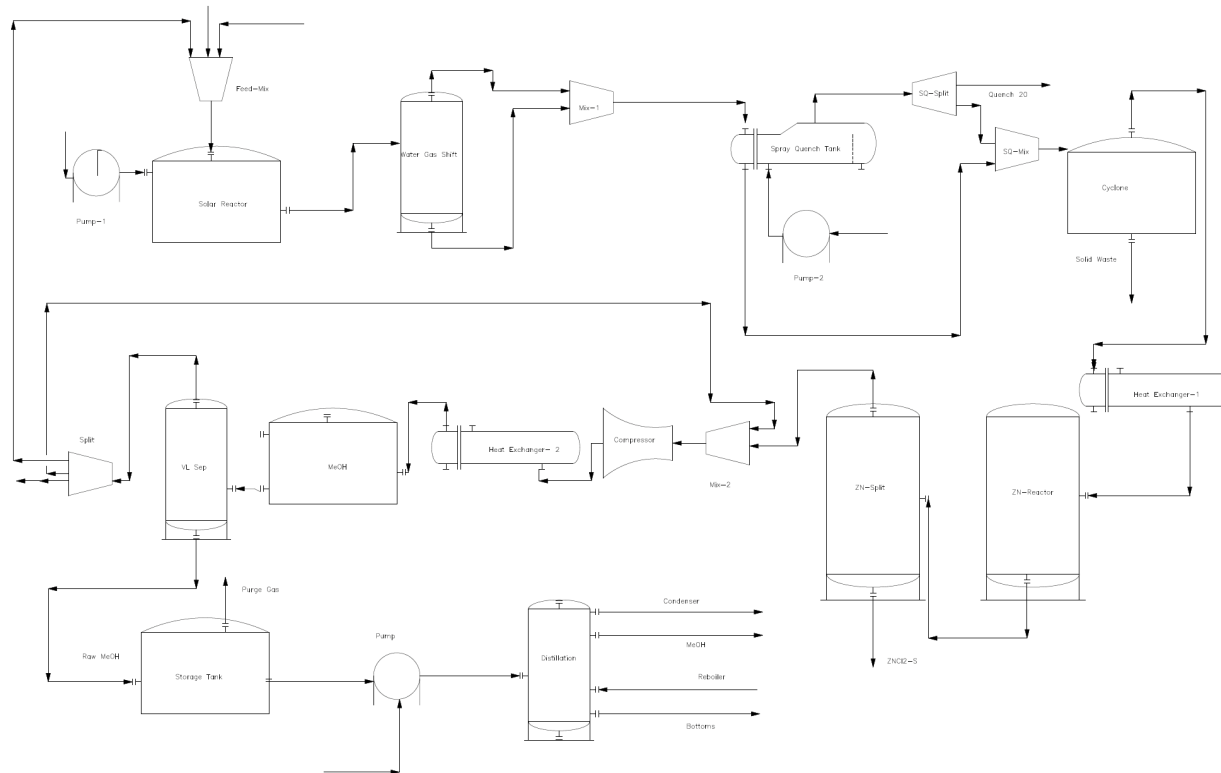


Figure 1. Overall Process Flow Diagram

The production process will be introduced in two sections: upstream and downstream. Figure 1 represents the upstream process flow diagram. The upstream can be divided into five different sections. The first section deals with the incoming raw biomass feed. Methanol, biomass, and recycled products are fed into the solar reactor at 25 °C and 1 bar. The biomass consists of 68.25% cellulose, 21.75% lignin, 8.78% ash, 0.61% N₂, 0.01% sulfur, and 0.6% Cl₂. Unlike a regular tank reactor, the solar reactor is operated by solar radiation from the heliostat field. The operation conditions of the reactor are 1450 °C and 35 bar. It is important to note that water is pumped into the reactor in addition to the feed mix. The resulting product stream from the solar reactor is fed into another reactor to perform rapid cooling through a water gas shift reaction. The operation conditions of the water gas shift reactor are 800 °C and 35 bar. Since a large temperature shift is present, the reactor separates the solids from the gas.

The second section is the cooling process of the stream through spray quench. The solid and vapor streams are mixed using a mixer and fed into a spray quench tank. The spray quench tank utilizes a hot/cold minimum approach with the hot stream coming in and cold water as the cooling medium. A pump at 35 bar is utilized to supply the cooling liquid. The overall product stream is mixed and results in a composition of 64 mol% H₂, 34 mol% CO, and contaminants. The third section is the cyclone, where the solid waste is removed. The cyclone takes in the product gas and separates the desired vapor from the solid. After the cyclone, the vapor stream is fed into a heat exchanger. The fourth section is the catalytic zinc oxide bed. The vapor is fed through a solid zinc oxide bed to remove H₂S and HCl. The solid zinc oxide bed operates at 210 °C and 35 bar. Since a mixed stream is present, it is important to note a particle distribution of 0.1. Following the zinc oxide bed separation, the stream enters a second reactor to separate the vapor and solid ZnCl₂ produced.

The fifth section is raw methanol production. The vapor stream is mixed with a recycled stream using a mixer. This is then fed into a compressor operating isentropically at 80 bar. After the compressor, the stream is fed into a methanol reactor tank operating at 270 °C and 80 bar. It is important to note the operating conditions of the methanol bed. Since the temperature of the product stream from the compressor will be higher than operation conditions, another heat exchanger was placed between the compressor and methanol reactor to match the reactor operating conditions. The stream leaving the methanol reactor is fed into a knock-out drum where the stream is decompressed to 35 bar and cooled to 50 °C. The stream leaving the knock-out drum is separated into three streams. The first is the recycling stream connected to the mixer after the zinc oxide bed. The zinc oxide recycling stream should contain around 90% of the product. The second is the purge stream containing around 0.5% of the product. The third is the feed recycling stream, which is connected to the initial feed. The feed recycling stream should contain around 9.5% of the product. The raw methanol produced from the upstream process is connected to the downstream process for further purification and concentration of methanol.

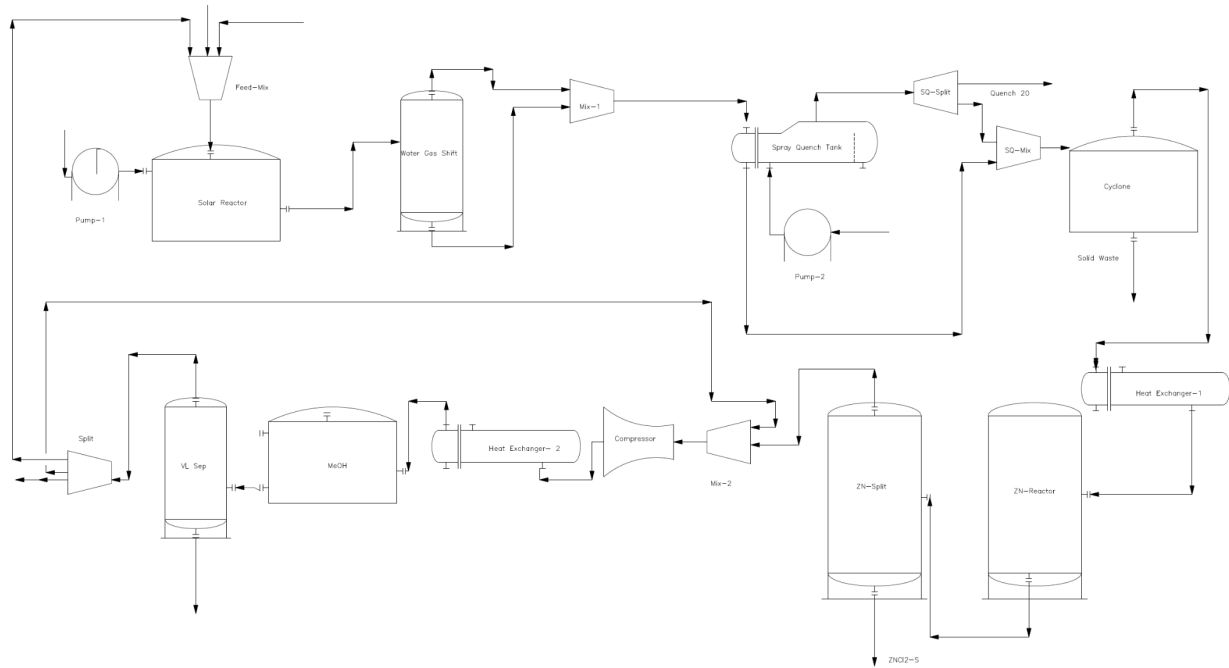


Figure 2. Upstream Process Flow Diagram

Moreover, Figure 3 below is the process flow diagram of the downstream process. The raw methanol is fed to a storage tank where purge gas is released, preparing the stream for purification using distillation. A pump is utilized to deliver the stream to the distillation column. The pure methanol leaving the column is around 99.97% methanol.

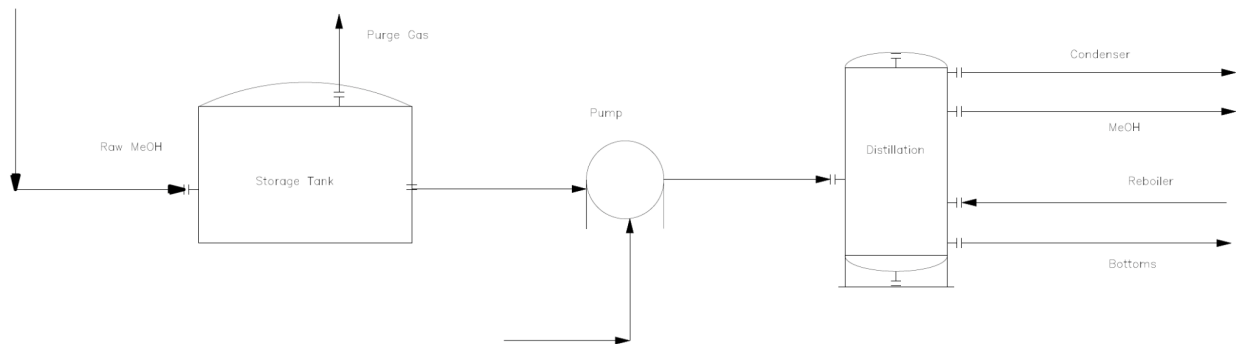


Figure 3. Downstream Process Flow Diagram

3.4. Battery Limits and Design & Economic Premises

Battery limits are defined boundaries throughout a plant that act as responsibility dividers. There are primarily two boundary limits: the inside battery limits, denoted as ISBL, and the outside battery limits, denoted as OSBL. Inside boundary limits contain essential components

for operation in addition to control and other instrumentation. Examples of elements found along an ISBL include; pumps, reactors, piping, columns, heat exchangers, compressors, etc. In the case of our system, the solar reactor, methanol reactor, zinc reactor, pumps, heat exchangers, compressors, spray quench tank, cyclone, separators, and distillation column would all be included in the ISBL. The OSBL incorporates non-essential elements for plant operation that contribute to utilities and infrastructure. Examples of items that would fall within the OSBL boundary include storage, offices, parking, breakrooms, sales and shipping areas, electricity, refrigeration, etc. While battery limits may separate a plant, everything is still connected and all elements factor into plant operation and cost.

- Plant Capacity: 56,000,000 Gal per Year, 19,178 Gal per hour
- Raw materials - biomass, water, methane, zinc - are all pure
- The composition of biomass is:

Table 6: Biomass Composition.

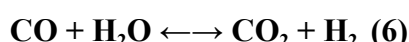
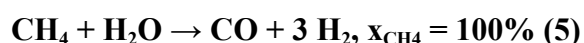
Component	Weight Percent %
Cellulose	68.25
Lignin	21.75
Ash	8.87
Nitrogen	0.61
Sulfur	0.01
Chloride	0.60

- Raw materials are easily accessible
- Raw materials with less accessibility have higher prices
 - Higher prices account for transportation or rarity
- Water is fed at 25°C and 1 bar
- Biomass is fed at 25°C and 35 bar
- Methane is fed at 25°C and 35 bar
- Zinc is being fed at 210°C and 35 bar
 - All classes have a 0.1 weight fraction particle size distribution
- Methanol product has a 99.97% mole fraction purity
- Upstream and downstream processes take place in Daggett, California
- Upstream process operates 8 hours per day for 365 days a year
- Downstream process operates 24 hours per day for 333 days per year
- New “grass root” plant hold both upstream and downstream processes
- The solar reactor utilizes silicon carbide tubes at a temperature of 1450°C and 35 bar

- All reactions in the solar reactor reach 100% conversion
 - Water-gas shift reaction is reversible and conversion is not considered
- The water-gas shift reaction occurs whilst leaving the reactor at 800°C and 35 bar
- All reactions in the zinc reactor reach 100% conversion
- The methanol reactors operates at a temperature of 270°C and 80 bar
- All reactions in the methanol reactor reach 45% conversion
- The separator processing decompresses methanol contents to 50°C and 35 bar
- Hot/cold minimum approach temperature in the spray quench tank is 0.5°C
- The spray quench tank operates at a pressure of 35 bar and 210°C exit temperature (stream 10)
- Stream 10 has a temperature of 210°C and is comprised H₂ (64 mol%) and CO (34 mol%)
- Stream 17 is split between a purge stream (0.5%), feed recycle stream (9.5%), and stream methanol recycle (90%)
- Carbon credit is accounted for in the financials, decreasing selling price by saving money on carbon reduction
- The plant runs a total of 25 years, with 2 years of construction

3.5. Material Balances

Material balances are conducted around pieces of equipment in the system as a whole, in order to determine the molar and mass flow rates that are fed into the system. The very first material balance is conducted around the solar reactor alongside the water-gas shift reactor, both material balances are intertwined considering that the water-gas shift essentially occurs within the solar reactor but for simulation purposes they have been separated. In order to get a head start, a mass flow rate of biomass is to be assumed with the following components and mass fractions: 68.25% cellulose, 21.75% lignin, 8.78% ash, 0.61% nitrogen, 0.01% sulfur and 0.60% chlorine. The chemical reactions that are occurring within the solar reactor is as follows:



As the syngas leaves the solar reactor it enters the water-gas shift reactor at a very high temperature where reaction 6 occurs. Such a reaction is extremely endothermic due to thermodynamically favoring operation at low temperatures. In reaction 5, addition of methane is to speed up the gasification process of biomass and potentially lower the amount of carbon dioxide emitted and for matter to take place a ratio of H₂/CO must equal 2. The flow rate of biomass must be estimated using such a ratio. The solar reactor is needless of a catalyst for two main reasons: it is once again running at 1450 C which makes it autocatalytic in some sense and addition of methane as feedstock that enhances the yield of raw methanol produced, hence the ratio discussed above of hydrogen and carbon monoxide. The estimated base flow rate of biomass was 10E+06 g/hr. Table X below exhibits biomass components scaled using given mass fractions.

Table 7. Mass Flow Rates of Biomass Components.

Species	wt%	Mass Flow Rate (g/hr)
C ₆ H ₁₀ O ₅	68.25%	6.8E+6
C ₁₀ H ₁₂ O ₃	21.75%	2.18E+6
Ash	8.78%	8.78E+5
N ₂	0.61%	6.10E+4
S	0.01%	1.00E+3
Cl ₂	0.60%	6E+4

A sample calculation using cellulose is as follows:

$$(68.25\% \frac{g}{g})(10E+06 \frac{g}{hr}) = 6.8E+6 \frac{g}{hr} \quad (1)$$

Subsequently, the biomass average molecular weight was also calculated in a similar manner where the mass fractions were multiplied by the molecular weight to obtain an average biomass molecular weight that is in accordance with the following system. Table 8 below exhibits values of molecular weights and estimated biomass molecular weight that is entering the system.

Table 8. Estimated Average of Biomass Molecular Weight in g/mol.

Species	wt%	True MW (g/mol)	Estimated MW (g/mol)
C ₆ H ₁₀ O ₅	68.25%	162	110
C ₁₀ H ₁₂ O ₃	21.75%	509	111
Ash	8.78%	76	7
N ₂	0.61%	28	0.34
S	0.01%	32	0.003
Cl ₂	0.60%	71	0.425
Average biomass MW (g/mol)		228.4	

A sample calculation using cellulose is as follows:

$$(68.25\% \frac{g}{g})(162 \frac{g}{mol}) = 110 \frac{g}{mol} \quad (2)$$

The actual inlet flow rates of biomass in units of kmol/hr are calculated afterwards while taking into account the stoichiometry to scale out each component with its own ratio. The following Table 9 will illustrate Reaction 1 calculations of true molar flow rates that are to be inputted in Aspen Plus.

Table 9. Inlet and outlet species of the first reaction of cellulose and water.

Inlet Species	Molar Flow Rate (kmol/hr)	Outlet Species	Molar Flow Rate (kmol/hr)
C ₆ H ₁₀ O ₅	41939	6 CO	251634
H ₂ O	41939	6 H ₂	251634

A sample calculation using cellulose is as follows:

$$(6.8E + 6 \frac{g}{hr}) / (162 \frac{g}{mol}) = 41939 \frac{kmol}{hr} \quad (3)$$

41939 $\frac{kmol}{hr}$ (6) = 251634 $\frac{kmol}{hr}$ of carbon monoxide and hydrogen

The same process is applied for all the rest of the six reactions in order to find the approximate values needed to be fed. Considering that water-gas shift is occurring, a value of equilibrium constant was calculated using the Equation 4 which is as follows. The main purpose of such a matter is to estimate the extent of reaction for water in this overall system considering that there is water as a reactant in all reactions occurring in both the solar reactor and the water-gas shift reactor. K_{eq} , is the variable representing the equilibrium constant also known as the extent of reaction for water. The WGS reactor is operating at 800 °C which is 1073 K.

$$K = \exp\left(\frac{4577.8}{T} - 4.33\right) \quad (\text{Moe, 1962}) \quad (4)$$

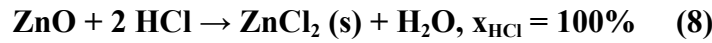
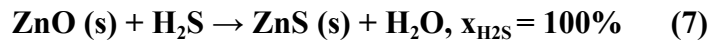
$$K = \exp\left(\frac{4577.8}{1073 \text{ K}} - 4.33\right) = 0.93$$

Moving on to determining the flowrate of methane using $\text{H}_2/\text{CO} = 2$, an iterative process was utilized in excel where the amount of 8.36E+5 kmol/hr of methane was fed into the solar reactor which resulted in a water flow rate of 2.6E+5 kmol/hr. However, in order to take into account the water-gas shift reaction, additional values of water must be added on top of the stoichiometric value where the ratio of water and biomass were calculated to amount to a value of 1.7. The ratio is multiplied by the amount of water obtained previously and summed up to be 5.33E+05 kmol/hr, which is the flow rate that is fed to the first pump in the system and the solar reactor afterwards. Refer to Appendix B for in depth calculations of water and methane flow rates. Table 10 below is showing the flow rates of all inlet components around the solar thermal bed reactor in both molar and mass basis.

Table 10. Molar and Mass Flow Rates of Inlet Species Into the Solar Reactor.

Inlet Species	Molar Flow Rate (kmol/hr)	Mass Flow Rate (kg/hr)
Biomass	72.1	10104
Methane	8619087.7	93448344.6
Water	266380	4798910.28

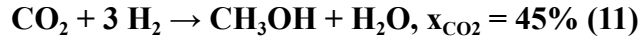
The second material balance was conducted around the ZnO bed, assuming 100% conversion of reactants as well. The following reaction are occurring in the reactor:



An amount of ZnO was assumed considering that hydrogen sulfide in the solar reactor has been consumed entirely since it undergoes full conversion. An amount of 100 kg/hr of ZnO

was fed into the ZnO fixed bed. The same methodology was applied in order to get the molar flow rate of ZnO, H₂S and HCl, in which they all amounted around a value of 12.29 kmol/hr with respect to stoichiometry. Inlets of the ZnO bed are incoming from the heat exchange section where constituents are cooled. Following the ZnO bed, a flash separator was utilized for waste ZnCl₂ where the outlets of the ZnO bed were the inlets.

As for the methanol bed reactor, incoming inlets have exited the Zn-Split enter a mixer and a compressor to undergo pressure changes prior to methanol bed reactor feed. The reactions that are taking place in such a reactor are as follows:



As per reactions nine, ten and eleven, the conversion of this system is 45% instead of 100%. In terms of material balances alongside inlets and outlets, the approach taken is quite similar to previous calculations however taking into account the conversion difference. To demonstrate, a sample calculation for reaction nine is presented after this paragraph. “ \dot{m} ” represents the molar flow rate of a species. The following calculations have been conducted for reaction ten and eleven as well.

$$\dot{m}_{\text{CO}_2, \text{in}} = \dot{m}_{\text{H}_2, \text{in}} = 7.36E+05 \text{ kmol/hr}$$

$$\dot{m}_{\text{CO}_2, \text{out}} = \dot{m}_{\text{H}_2, \text{out}} 7.36E+05 \text{ kmol/hr} (1-0.45) = 4.05e+5 \text{ kmol/hr}$$

$$\dot{m}_{\text{CO}, \text{in}} = \dot{m}_{\text{H}_2\text{O}, \text{in}} = 7.36E+05 \text{ kmol/hr} (0.45) = 331.2 \text{ kmol/hr}$$

Exiting the methanol bed reactor, ingredients go through a separation process in a flash separator where raw methanol is transferred to a storage tank in the downstream segment to undergo purification. A portion of the components are recycled back to the mixer, undergoing the same process in terms of pressure change, methanol bed reactor and raw methanol production. Whereas the other portion that generally contains residuals, unreacted elements, and inserts is recycled back to the solar thermal reactor. If recycle streams are to be taken into consideration for material balances, the difference it would pertain is an increase of conversion of the methanol bed reactor reactions to a close value of 100%. Therefore, it was left up to the simulation to gauge the divergence of flow rates. Table 11 below summarizes the outlet flow rates of streams 17 and 19 from Aspen Plus in contrast to previous estimations. All values are in units of kmol/hr.

Table 11: Streams 17 and 19 molar flow rates.

Species	Stream 17	Stream 19
CO	177	0.0006
H ₂	268978.14	0.98
CH ₃ OH	3024.77	3.58E-05
H ₂ O	411.6	0.0015

3.6. Energy Balances

In order to determine the energy balances on the system, the first step was to calculate the heat capacities of each component at the operating temperature of each reactor. The first reactor in this process was the solar reactor, and the heat capacities for each component reacted in it were calculated using heat capacity constants from Perry's Chemical Engineer's Handbook. These calculations are shown in Appendix A, and the heat capacities are shown below.

Table 12. Heat Capacities of Components Fed to the Solar Reactor.

Component	Heat Capacity at 1450°C in $\frac{kJ}{mol K}$
CH ₄	0.88904
C ₆ H ₁₀ O ₅	0.6675
C ₁₀ H ₁₂ O ₃	0.4300
Cl ₂	0.3793
CO ₂	0.63346
HCl	0.34063
H ₂ O	0.5276
O ₂	0.36533
H ₂	0.32248
H ₂ S	0.51432

CO	0.35208
----	---------

The heat capacities of each component were then integrated with respect to temperature between the feed and reactor temperatures to get the heat of reaction for each component in the reactor. The heats of reaction for the products and reactants for each reaction taking place in this reactor were then determined to be the sum of the product heats of reaction and the reactant heats of reaction, respectively. Similarly, the heats of combustion were calculated by using values from Perry's Chemical Engineer's Handbook and from Elementary Principles of Chemical Processes.

Since the vapor temperature of water at the operating pressure of this reactor, 35 bar, is 243°C, which is less than the reactor temperature, water is vaporized in this reactor. This was taken into account by calculating the heat capacity of liquid water below the boiling point, which was integrated with respect to temperature from the feed temperature to the vapor temperature. Then, the heat capacity of steam was calculated and integrated with respect to temperature from the vapor temperature to the reactor temperature. These values were used to calculate the heats of reaction of the products in a couple reactions that take place in the solar reactor. The values described above are shown below.

The Actual Heat of Reaction was the sum of the heats of reaction and the heat of combustion minus the heat of vaporization of water.

Table 13. Heat of Reaction Calculation for Cellulose Reaction in Solar Reactor.

Heat of Reaction of Reactants	-865.494 kJ/mol
Heat of Reaction of Products	641.746 kJ/mol
Heat of Combustion	601.339 kJ/mol
Heat of Vaporization of Water	40.8 kJ/mol
Actual Heat of Reaction	336.791 kJ/mol

Table 14. Heat of Reaction Calculation for Lignin Reaction in Solar Reactor.

Heat of Reaction of Reactants	-1212.885 kJ/mol
Heat of Reaction of Products	1228.508 kJ/mol
Heat of Combustion	2729.449 kJ/mol
Heat of Vaporization of Water	40.8 kJ/mol

Actual Heat of Reaction	2459.472 kJ/mol
-------------------------	-----------------

Table 15. Heat of Reaction Calculation for Methane Reaction in Solar Reactor.

Heat of Reaction of Reactants	-247.081 kJ/mol
Heat of Reaction of Products	212.912 kJ/mol
Heat of Combustion	250.150 kJ/mol
Heat of Vaporization of Water	40.800 kJ/mol
Actual Heat of Reaction	175.905 kJ/mol

Table 16. Heat of Reaction Calculation for Water-Gas Shift Reaction in Solar Reactor.

Heat of Reaction of Reactants	-139.707 kJ/mol
Heat of Reaction of Products	144.049 kJ/mol
Heat of Combustion	-174.446 kJ/mol
Heat of Vaporization of Water	40.800 kJ/mol
Actual Heat of Reaction	-210.905 kJ/mol

4. Process Description & Simulation

4.1. Aspen Plus Simulation

The upstream Aspen Plus simulation can be divided into the solar thermal reactor, the spray quench process, the zinc oxide reactor, and raw methanol production. During the solar thermal reaction process, the biomass stream is fed into the solar reactor. The feed stream consists of biomass, methane, and water. Water is provided through a pump configuration of 2 pumps in series and four in parallel. Then, the resulting product stream is fed into a reaction tank where a water gas shift reaction occurs.

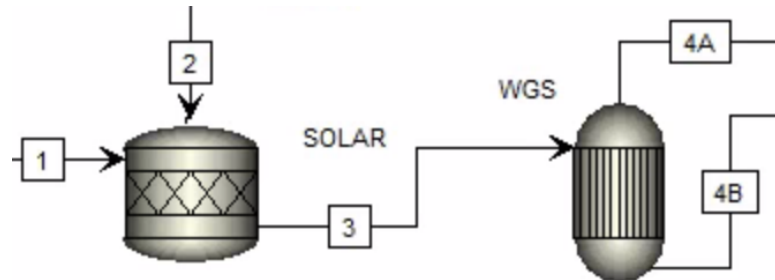


Figure 4: Solar and Water Gas Shift Reactor

It is important to note that the water gas shift reaction happens inside the solar reactor. In the simulation, it is hard to include the water gas shift reaction inside the solar reactor because the reaction hinders the biomass reaction kinetics. As a result, the water gas shift and solar reactions were modeled independently. The gas and vapor phases are mixed using a mixer and fed into the spray quench process. The spray quench process includes a spray quench tank, mixer, and pump. The spray quench tank utilizes cold water to perform heat transfer which is supplied using a pump. The pump configuration is five pumps in parallel.

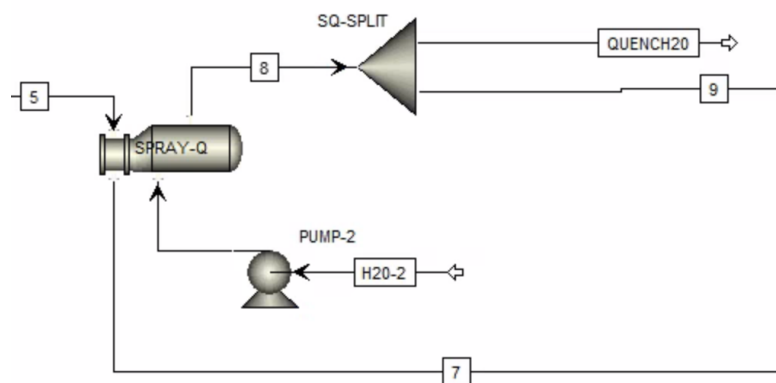


Figure 5: Spray Quench

After the spray quench, the solid and vapor stream is mixed and fed into a cyclone, where the solid waste is disposed of. In order to match the temperature specification of the zinc oxide reactor, the product stream is fed into a shell and tube heat exchanger. The zinc oxide reactor includes two reactors; the first removes H_2S and HCl , and the second removes solid ZnCl_2 .

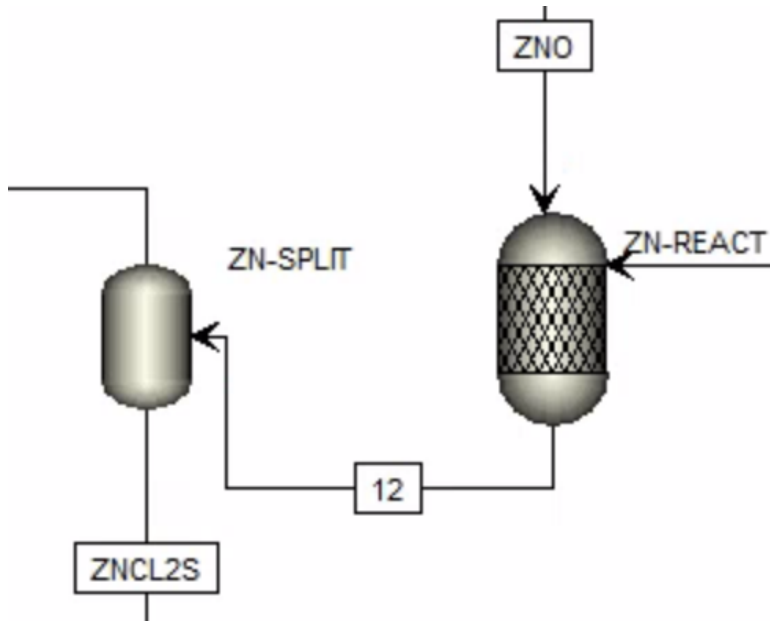


Figure 6: Zinc Oxide Reactors

It is important to note that the Zn-Split reactor occurs inside the zinc oxide reactor. The goal of this process is to remove solids such as $ZnCl_2$. In this simulation, the Zn-Split process is modeled independently from the Zn-React tank since it is hard to specify outlet conditions of the reactor. The products from the zinc oxide reactors are mixed and fed into a compressor. The compressor configuration is one in series and five compressors in parallel. Since the compressor changes the temperature of the stream, a heat exchanger is placed to meet the temperature specifications of the methanol reactor. The raw methanol production step includes a methanol tank and separator where the raw methanol stream is produced.

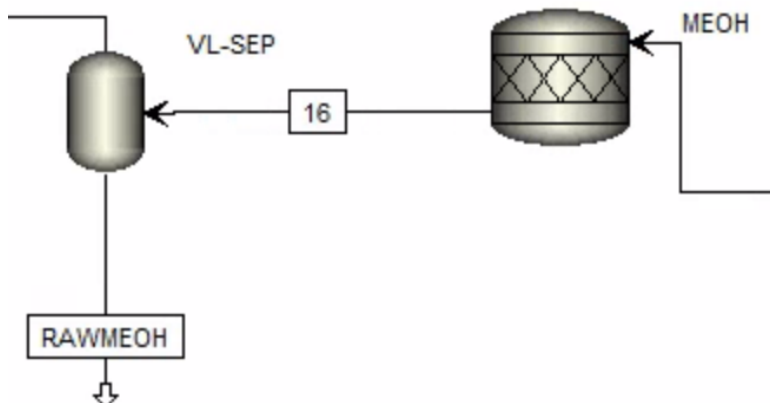


Figure 7: Raw Methanol Reactors

Important input streams in this process are biomass, solid waste, recycle to feed (stream 19), recycle to the mixer (stream 18), ZnCl₂, and raw methanol streams. A purge and quench stream is present, which is important to examine. The figure below is the overall Aspen Plus layout of the upstream process.

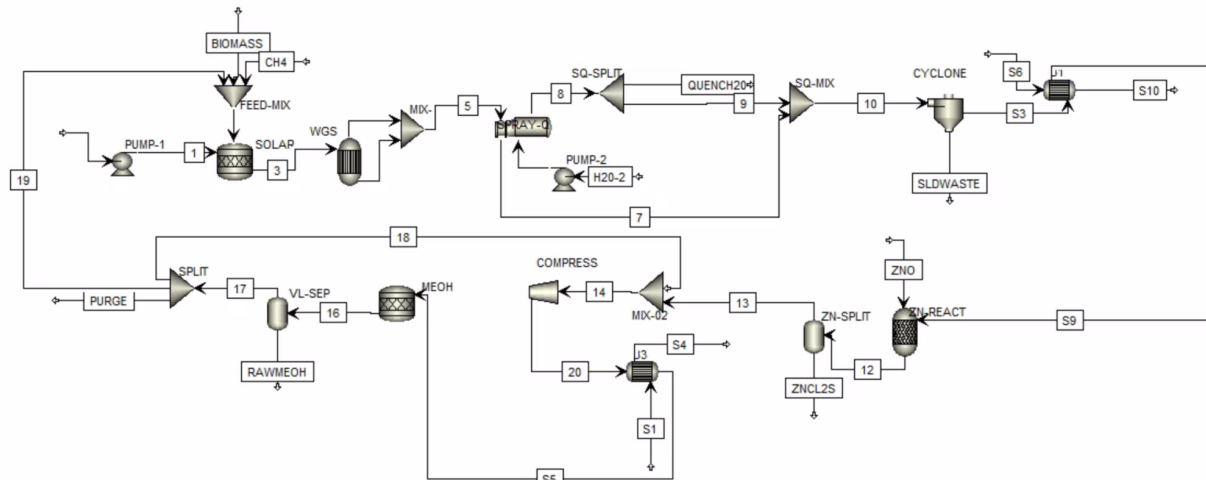


Figure 8: Upstream Aspen Plus Layout

The table below includes stream specifications of important input streams.

Table 17: Important input stream specifications

Input	Biomass Stream	Solid Waste	Recycle to Feed
Temperature (°C)	25	128.264	50
Pressure (bar)	35	35	35
Overall Mass Flow (kg/hr)	10104.7	878	61502.1
Component Mass Flow (kg/hr)	Lignin: 6800 Cellulose: 2175 Ash: 878 N2: 121.859 Cl2: 119.83 S: 9.972	Ash: 878	N2: 8.129 Water: 748.875 CO: 464.198 H2: 51366.5 CO2: 39.54 Methanol: 8874.86

Table 18: Important input stream specifications

Input	Recycle to Mixer	ZnCl2	Raw Methanol
Temperature (°C)	50	210	50
Pressure (bar)	35	35	35
Overall Mass Flow (kg/hr)	582651	97830.2	1.281E+8
Component Mass Flow (kg/hr)	N2: 77.016 Water: 7094.61 CO: 4397.66 H2: 486630 CO2: 374.6 Methanol: 84077.6	ZnO: 97569.5 ZnS: 30.3088 ZnCl2: 230.339	N2: 44.413 Water: 3.058E+7 CO: 2687.82 H2: 33977.8 CO2: 2228.31 Methanol: 9.751E+7

The table below are operation conditions for the reactors.

Table 19: Reactor operation conditions

Input	Solar Reactor	Water Gas Shift	Spray Quench
Temperature (°C)	1450	800	Minimum Temperature Approach: 0.5
Pressure (bar)	30	35	Outlet Pressure: 0

Table 20: Reactor operation conditions

Input	Cyclone	Zn-React	Zn-Split
Temperature (°C)	128.264 (Stream Values)	210	210
Pressure (bar)	35 (Stream Values)	35	35

Table 21: Reactor operation conditions

Input	MeOH Tank	VL-Sep	Compressor
Temperature (°C)	270	50	481.804 (Outlet Temperature)
Pressure (bar)	80	35	115 (Outlet Pressure)

A total of three packages are utilized in this simulation: STEAM-TA, Solids, and UNIQUAC. The Solids package is assigned to processes that involve solid formation. The STEAM-TA package is for the steam table for water. The UNIQUAC package is for vapor-liquid equilibrium properties. The solar reactor, feed mixer, cyclone and input mixer, zinc oxide reactor and splitter, water gas shift equilibrium reactor, spray quench hot side, and solids mixer utilize the solids package. The water pumps, spray quench cold side, and splitter utilizes the STEAM-TA package. The pre-compressor mixer, compressor, methanol reactor, VL-separator, and recycle splitter utilize the UNIQUAC package.

The main difficulty occurred when connecting the recycle streams. This was resolved by resetting the iteration threshold. The stream was reset by increasing the threshold and running the simulation. After, the original threshold was recovered.

4.2. Aspen HYSYS Simulation

The downstream part of the plant is simulated in aspen HYSYS. It consists of a storage tank and a distillation column. Coming out of the upstream from Aspen Plus, the raw methanol stream is fed into a storage tank by which it flows into the distillation column for methanol purification process. The main components of this stream are methanol with a mole fraction of 0.64, water with a mole fraction 0.35, carbon dioxide with a mole fraction of 8.2E-06, carbon monoxide with a mole fraction of 2.1E-05 and hydrogen with a mole fraction of 2.49E-03. Prior to starting the simulation, a component list of the ingredients just discussed were added and a fluid package has been chosen in accordance to the process type; chemical, and therefore UNIQUAC have been implemented. The inlet stream enters the storage tank with a flowrate of 280000 kmol/hr at a pressure of 35 bar, where the components are stored in the downtime of this section of the plant. The operating conditions of the storage tank is 2000 kPa and a vapor outlet of 60 kPa, these conditions were chosen in order to purge out residual gasses from the raw methanol stream as well as some amount of hydrogen to enhance the purification of methanol itself. The flowrate exiting the storage tank amounts to a value of 2.79E+5 kmol/hr which indicates the loss of some material through the purge out stream in the storage tank. The stream enters the distillation column at a temperature of 50 °C. A more detailed description of how a distillation column works is found in the separators section of this report, however for reiteration purposes, this type of separator heavily depends on the physical properties of the materials that

are fed into the system. The volatility of entering ingredients are evaluated and are directed within the column either in an upward flow or downward. The boiling point and K-values are two essential keys in discovering the separation destination, for instance, components with lower boiling points tend to travel in an axial manner towards the distillate. However components with larger boiling points tend to be directed to the bottom part of the column. Mass and heat transfer within the column are also an integral part in the separation process. A condenser is located by the distillate to encourage phase change of the more volatile component, where it re-enters the column and amplifies contact with other flows in other directions and thus mass transfer occurs. A reboiler does the opposite of what a condenser does to less volatile components. Figure x below is a snapshot of the downstream process in Aspen HYSYS.

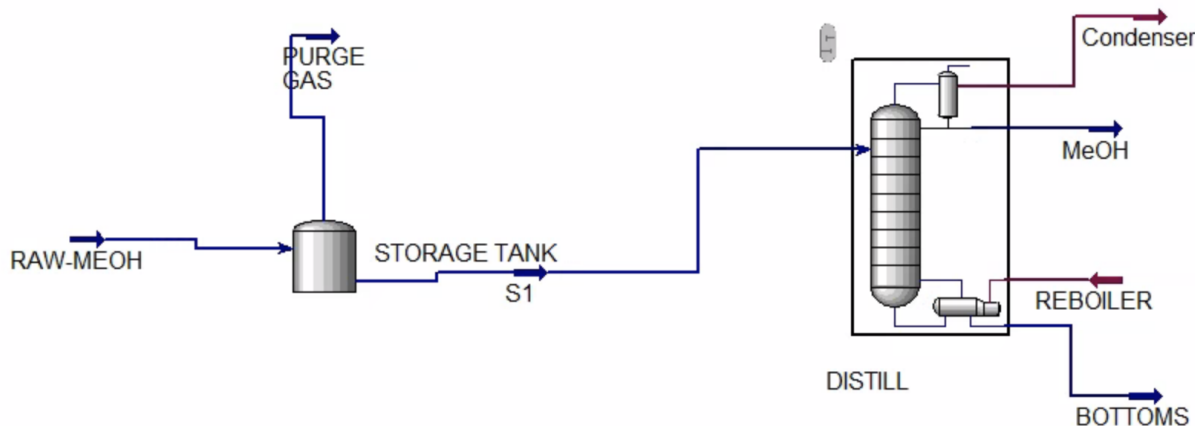


Figure 9: Simulation Snapshot of the Downstream Process in Aspen HYSYS.

Furthermore, design parameters can be changed in accordance to the desired product coming out of the column. For example in this part of the project, a separation of water and methanol is taking place in which methanol is the product that is needed for the consumers and therefore initiative is taken to ensure that all the operating conditions serve a better distillate outcome. An example of these design parameters that have been implemented in the system is to locate the feed stage of the column at the very last stage in order to enhance vapor-liquid contact as methanol travels up the vessel. Also, a high reflux ratio would also be of benefit in terms of the level of purity that is needed for methanol which is 99.97%. The reflux ratio that has been chosen is 4, while keeping in consideration that the larger the reflux ratio; the less cost-effective the process becomes. Following steps and heuristics of column design, a pressure drop and a type of condenser have been chosen and implemented in Aspen HYSYS. Column design was done both by hand calculations and simulation-wise for accuracy purposes, where most of the values were almost identical. The column consists of 16 stages and a pressure drop of 3.447 kPa in the distillate and 10.34 kPa in the bottoms. The specifications that were utilized to get the desired purity were reflux ratio, component fraction of methanol and vent rate, considering that a

partial condenser is implemented. Table 22 below displays the inlet conditions of stream S1 and outlet conditions of the distillate and the bottoms in terms of temperature, pressure, molar flow and mass flow.

Table 22: Operating Conditions of the distillation column.

Property	S1	MeOH	Bottoms
Temperature (°C)	50	-147	89.25
Pressure (kPa)	1500	28.46	70
Molar Flow Rate (kmol/hr)	2.79E+6	1.79E+6	1E+6
Mass Flow Rate (kg/hr)	7.5E+7	5.74E+7	1.8E+7

Moreover, an important factor of this section is how much methanol is being produced. The customer was asking for 56 million gallons per year with a methanol purity of 99.97%. In order to know how much that should be coming out of the distillate, a conversion of gallon per year to kmol per hour have been conducted using both the density and molar mass of methanol, as well as scaling it to the actual amount of hours it would be running at which is eight hours a day and a total of 8000 hours per year. The molar mass of methanol is 32.04 g/mol and the density is 3000 g/gal. A sample calculation of knowing how much flow rate is needed is below:

$$5.6E + 7 \text{ methanol gallon per year} * 3000 \text{ g/gal} = 1.68E + 10 \text{ g/year}$$

$$1.68E + 10 \text{ g/year} \div 32.04 \text{ g/mol} = 5.24E + 09 \text{ mol/year}$$

$$5.24E + 09 \text{ mol per year} / 365 \text{ year} / 24 \text{ hours} = 1.79E + 06 \text{ kmol per year}$$

Meaning that an amount of 1.79E+07 must be produced by the distillate every eight hours of a passing day in each consecutive year. That amount of production requires a feed of 2.79E+6 kmol/hr.

5. Process Details & Equipment Specifications

5.1. Reactors

5.1.1. Solar-Thermal Gasification

The solar reactor is composed of multiple silicon carbide (SiC) tubes, vertically placed within a solar energy absorbing chamber, of which waste biomass enters and undergoes a gasification process to produce syngas. The waste biomass is composed of cellulose (68.25 wt%), lignin (21.75 wt%), ash (8.78 wt%), nitrogen (0.61 wt%), chloride(0.60 wt%), and sulfur (0.01 wt%). Methane is added at high pressure, 35 bar, to aid in biomass transport and gasification. In order for methane to react and produce H₂, the reactor must be operated at high temperatures. In this case, the reactor operates at 1450°C. The H₂ produced by methane can then be used in a water-gas shift reaction, which occurs at cooler temperatures (242.595°C) whilst leaving the reactor. This water-gas shift reaction prevents CO₂ buildup from biomass carbon constituents. As such, CO₂ production is limited, increasing carbon efficiency during biomass conversion and eliminating the need for amine scrubbing. The solar reactor also has a recycle stream from the separator attached to the methanol fixed bed reactor.

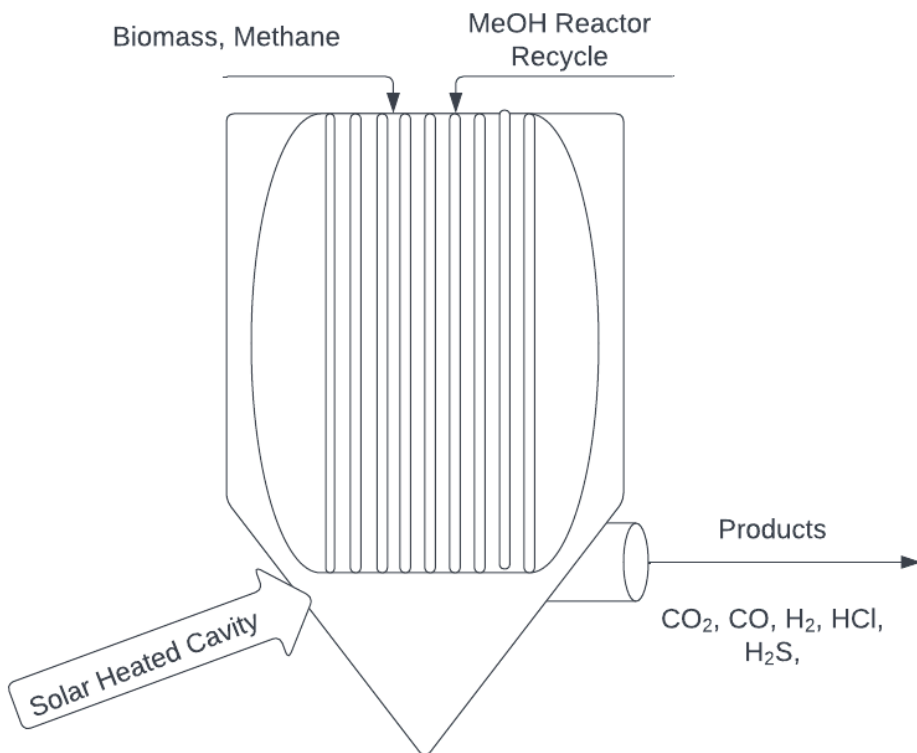
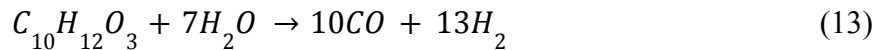
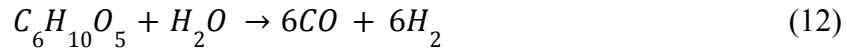


Figure 10: Solar Reactor Diagram

While six reactions take place in this reactor, as shown below, only cellulose, lignin, methane, and water-gas shift equations are utilized to model the reactor. Within these reactions, there is 100% conversion of cellulose, lignin, sulfur, chloride, and methane respectively.



Heats of reactions were calculated in Excel using heat capacity constant integration and the heats of combustion. Cellulose, lignin, and methane reactions are endothermic, while the water-gas shift is exothermic. Results are summarized in the table below.

Table 23: Heats of Reaction for Given Components.

Component	Heats of Reaction
Cellulose	336.791 kJ/mol
Lignin	2459.472 kJ/mol
Methane	175.905 kJ/mol
Water-Gas Shift	-210. 905 kJ/mol

MATLAB was used to model gas and particle temperature differentials using relevant kinetic expressions. All kinetic expressions utilize component partial pressures denoted as P_x , as well as the gas constant (R) and temperature (T) variables. Since very few studies include experimental kinetic data for cellulose and lignin, both components were treated as solid carbon. The kinetic expression for these reactions (r_1) include a conversion factor (X) and geometric factor (ϕ). While the reactor theoretically obtains 100% conversion of these components in their corresponding reactions, this conversion is unrealistic upon application. As such, we assume a conversion factor of 90% (0.9). Based on literature, the geometric factor for char within a temperature range of 900-1160°C is approximately 4.7.

$$r_1 = k_1(1 - X)\sqrt{1 - \phi ln(1 - X)} \quad (5)$$

$$k_1 = \frac{K_A P_{H_2O}}{1 + K_B P_{H_2O} + K_C P_{H_2}} \quad (6)$$

$$K_1 = 2.51 \times 10^3 \exp\left(\frac{-112.6}{R \cdot T}\right) \quad (7)$$

$$K_2 = 6.74 \times 10^{-2} \exp\left(\frac{-37.3}{R \cdot T}\right) \quad (8)$$

$$K_3 = 3.04 \times 10^{-1} \exp\left(\frac{-36.6}{R \cdot T}\right) \quad (9)$$

The water-gas shift reaction is denoted as being reversible, as such there is an kinetic expression for both the forward (r_2) and reverse (r_3) reactions. Kinetics for the methanol reaction (r_4) is also shown below.

$$r_2 = k_2 P_{CO} C_{H_2O} \quad (10)$$

$$k_2 = 2.78 \times 10^3 \exp\left(\frac{-1.26 \times 10^7}{R \cdot T}\right) \quad (11)$$

$$r_3 = k_3 C_{CO_2} C_{H_2} \quad (12)$$

$$k_3 = -9.59 \times 10^4 \exp\left(\frac{-4.66 \times 10^7}{R \cdot T}\right) \quad (13)$$

$$r_4 = k_4 C_{CH_4} C_{H_2O} \quad (14)$$

$$k_4 = 3 \times 10^8 \exp\left(\frac{-1.3 \times 10^8}{R \cdot T}\right) \quad (15)$$

All values within kinetic rate constants are experimentally derived from a hybrid solar/combustive reactor that was operated at high temperature, resembling our solar reactor. Differentials representing the component flow with respect to volume were derived. The ordinary differential equations below represent the change in component flow rate with changes to reactor volume.

$$dF_C = -r_1 \quad (16)$$

$$dF_{H_2O} = -r_1 - r_2 + r_3 - r_4 \quad (17)$$

$$dF_{CO} = r_1 - r_2 + r_3 + r_4 \quad (18)$$

$$dF_{H_2} = r_1 + r_2 - r_3 + 3r_4 \quad (19)$$

$$dF_{CO_2} = r_2 - r_3 \quad (20)$$

$$dF_{CH_4} = -r_4 \quad (21)$$

The biomass and char, referred to as particles, flowing within the silicon carbide tubes of the reactor are primarily heated by radiation, so it is assumed that any conductive or convective

heat forces are negligible. We also assume that the change in particle temperature throughout the reactor can be represented by the change in internal tube temperature, referred to as the microcontainer temperature T_m . The diameter of the particles was approximated to be the size of particles entering a hammer mill. An equation describing the change in biomass and char throughout the reactor can be modified from the Fuel paper written by R. Bryan Woodruff and Alan W. Weimer paper. The first term represents radiative effects between the wall temperature of the reactor (T_w) and the microcontainer (T_m), as seen through the radiative emissivity (ϵ_m), Stefan-Boltzmann constant (σ), outer surface area of the microcontainer (a), and gas viscosity (μ_g) variables. The second terms considers microcontainer cooling via endothermic reactions with microcontainer volume (V_m), density (ρ_m), molecular weight (MW_m), and heat of reaction (ΔH) variables. This term is necessary since cellulose, lignin, and methane all have positive heats of reactions, indicating they are endothermic.

$$\frac{dT_m}{dz} = \frac{\epsilon_m \sigma a (T_w^4 - T_m^4)}{\mu_g} + \frac{V_m \rho_m (-\Delta H)}{MW_m} \quad (22)$$

The temperature differential overtime for the particles was modeled using the Python implementation of Euler's method. As seen in the figure below, the particles within the tubes reach a high temperature within a very short time span. This indicates that heat transfer between the reactor wall and internal particles is rapid, heating the particles almost instantaneously. As such, it can be assumed that the change in temperature of the particles as they travel throughout the reactor is zero (since they reach 1450 K almost immediately).

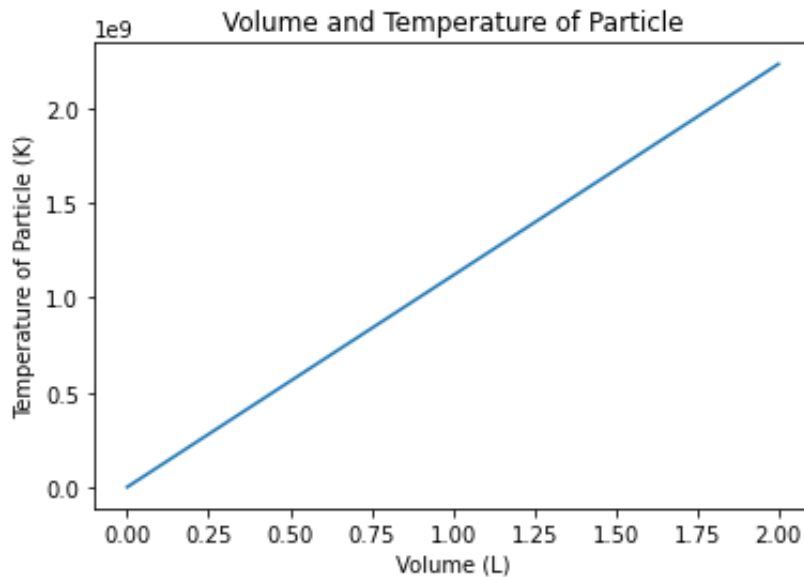


Figure 11: Temperature of Particles Along Reactor Volume

The solar reactor has gas that is heated by convection and conduction. The first term of the gas temperature differential accounts for component generation from reactions. The H_{pg} term reflects convective heat transfer that occurs between the tubes and the gas where h_m is the convection coefficient, a_m is the aggregate surface area, F_i are components flow rates, u_g is gas viscosity, V_m is microcontainer volume, p_c is carbon density, and MW_c is the molecular weight of carbon components. The H_{wg} term reflects convective heat transfer that occurs between the gas and the reactor wall where h_w is the gas-wall convection coefficient, T_w is the wall temperature, and d_i is the internal diameter.

$$\frac{dT_g}{dz} = \frac{A_t \sum_j (\Delta H_{rxn}) r_j - A_t H_{pg} - A_t H_{wg}}{\Sigma F_i C_{pi} A_i} \quad (22)$$

$$H_{pg} = \frac{h_m a_m F_i M W_c}{\mu_g V_m p_c} (T_g - T_m) \quad (23)$$

$$H_{wg} = h_w \pi d_i (T_g - T_w) \quad (24)$$

Plots were generated demonstrating the relationship between the change in component flow rate and the volume of the reactor. The table below represents the initial conditions utilized for the differential equations while Figure x illustrates the component flow rate changes along reactor volume. As volume increases, cellulose and lignin flow rates approach zero since they are acting as carbon sources in these reactions. CO_2 has an increase in flow rate, but decreases as H_2 decreases. This makes sense because H_2 acts as a source for CO_2 removal. Methane is being added into the reactor throughout the process, causing an increase in flow rate over reactor volume. Water and CO are both consumed in this process, decreasing their flow rates. While flow rates appear to be negative in the figure, they are practically zero upon application.

Table 24: Initial Flow Rates of Given Components in kmol/hr.

Component	Initial Flow Rate ($\frac{\text{kmol}}{\text{hr}}$)
CO	2.787×10^6
H_2	5.573×10^6
CO_2	0
H_2O	266380
$\text{C}_6\text{H}_{10}\text{O}_5$	13.414
$\text{C}_{10}\text{H}_{12}\text{O}_3$	37.735
CH_4	259267

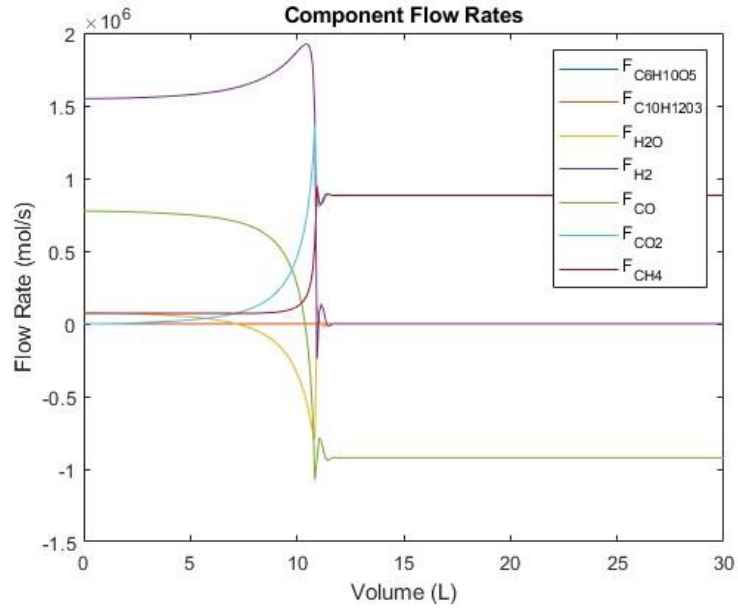


Figure 12: Component Flow Rates Along Reactor Volume

The plot of the gas temperature differential is continuous and logarithmic. As volume increases, gas temperature increases from 298 K and reaches 1450K around a 25 L volume. Temperature is maintained at 1450K for remaining volumes. This high gas temperature allows H₂ to react, reducing carbon dioxide waste. Temperature doesn't decrease, regardless of the endothermic effects of inclosed lignin and cellulose reactions.

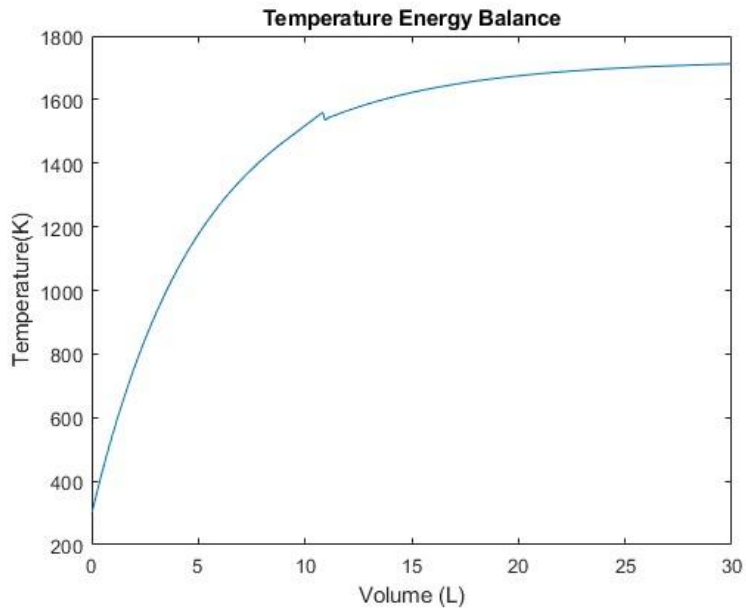


Figure 13: Temperature of Gas Along Reactor Volume

Using flow rates generated by ASPEN Plus, the volumetric flow rate was determined to be 1701.22 L. Assuming a residence time of 1s, it was calculated that 4663 tubes were required for our reactor. These tubes are 20m in length and 6 inches in diameter.

5.1.2. Catalytic Gas Cleaning Bed

A gas cleaning bed of zinc oxide (ZnO) was used to clean sulfur and chlorine out of the gas. The solid ZnO reacts with the hydrogen sulfide (H_2S) gas to produce solid zinc sulfide (ZnS) and water vapor. This reactor was modeled as a plug-flow reactor (PFR), so every component in it moves through the reactor. A model of the ZnO reactor is shown below.

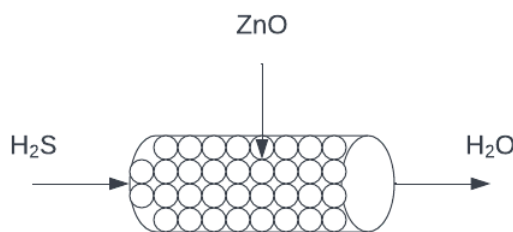
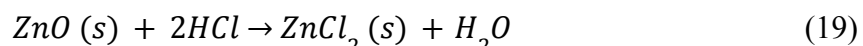
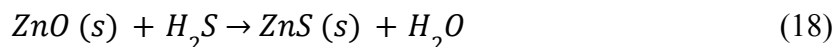


Figure 14. ZnO Reactor Model Diagram.

Hydrogen sulfide enters the reactor and undergoes a sulfidation reaction with ZnO , and the gas that exits the reactor is water.

This reactor was downstream of the spray quench tank and upstream of the methanol reactor, making the methanol more pure in the downstream recovery. There were two reactions that took place in this reactor, shown below.



For this reactor, it was assumed that both reactions went to 100% conversion of H_2S and HCl respectively. In order to model this reactor, the heats of reaction were calculated first, as shown in *3.6 Energy Balances*, and shown again in the table below.

Table 25. Heats of Reaction for ZnO Reactions. Calculated using heats of formation and integrated heat capacity values.

Reaction	Heat of Reaction (kJ/mol)
$ZnO(s) + H_2S \rightarrow ZnS(s) + H_2O$	-105.46
$ZnO(s) + 2HCl \rightarrow ZnCl_2(s) + H_2O$	-162.58

The ZnO reactor was modeled in MATLAB using equations for the energy balance, pressure differentials, and reaction kinetics. In order to simplify calculations, only the desulfurization reaction was considered because the dechlorination reaction is not as significant to the overall reaction design, and kinetics for the desulfurization reaction are more readily available. The reaction kinetics for the desulfurization reaction are shown below.

$$-r = -4\pi R_o^2 C_{H_2S} \left(\frac{R_0 \{ [Z_v + (1-Z_v)(1-x)]^{1/3} - (1-x)^{1/3} \}}{[Z_v + (1-Z_v)(1-x)]^{1/3} (1-x)^{1/3} D_{eff}} \right)^{-1} \quad (25)$$

This was used in the MATLAB code to calculate the consumption or production of each compound in the reaction. This trend was reflected in the flow rates of each component as the reaction progressed through the reactor. A plot of flow rates as a function of reactor volume is shown below.

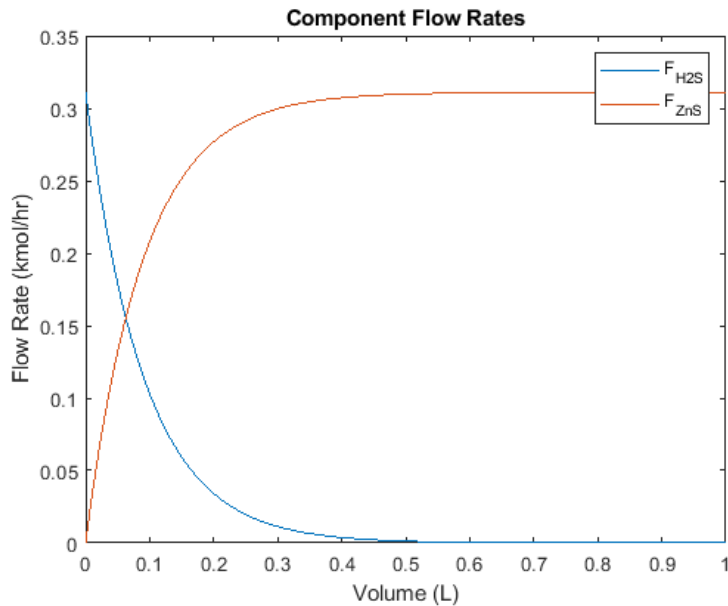


Figure 15. Flow Rates of H₂S and ZnS as a Function of Reactor Volume.

This plot was made using the MATLAB code for the ZnO reactor model. Water and ZnO flow rates were not included as they were orders of magnitude larger than the components containing sulfur, and the stoichiometric ratios of ZnO to H₂S and water to ZnS are 1:1, so the desulfurization reaction can be easily observed in the plot.

This plot shows that the flow rate of hydrogen sulfide decreases as it passes through the reactor and that the flow rate of zinc sulfide increases proportionally as the gas continues through the reactor. This indicates that the reaction is going as expected and that the extent of reaction is very high since the final amount of ZnS is close to the initial amount of H₂S.

In order to model the temperature profile of the zinc oxide reactor, the energy balance below was used. T_g represents the gas temperature, z is the length along the reactor. C_{pg} is the heat capacity of the gas, and this is the only variable besides T_g that varies with temperature.

$$\frac{dT_g}{dz} = \frac{-h_g a_v (T_g - T_s^S)}{mC_{pg}} \quad (26)$$

This energy balance was used to calculate the change in temperature, and the plot generated by the MATLAB code is shown below.

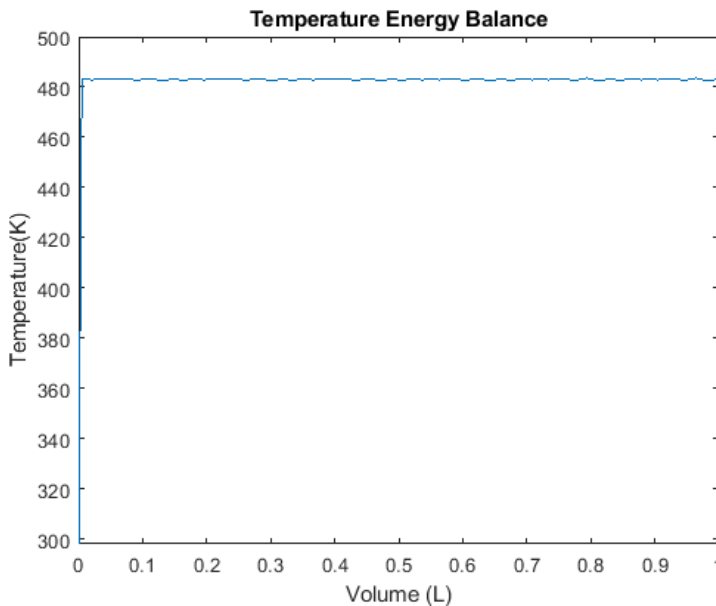


Figure 16. Temperature Profile of Gas in ZnO Reactor.

This plot was made using the MATLAB code for the ZnO reactor model.

This plot shows that the temperature rapidly increased as it entered the reactor, then remained almost constant throughout the remainder of its time in the reactor. This was expected because the desulfurization reaction is exothermic. The last consideration for the MATLAB model of this ZnO reactor was the pressure difference across the reactor that drives the gas through it. The Ergun equation was used to model the pressure, and it is shown below.

$$\frac{dP}{dz} = \frac{-G}{\rho D_p} \left(\frac{1-\phi}{\phi^3} \right) \left[\frac{150(1-\phi)\mu}{D_p} + 1.75G \right] \quad (27)$$

The plot of the pressure across the reactor is shown below.

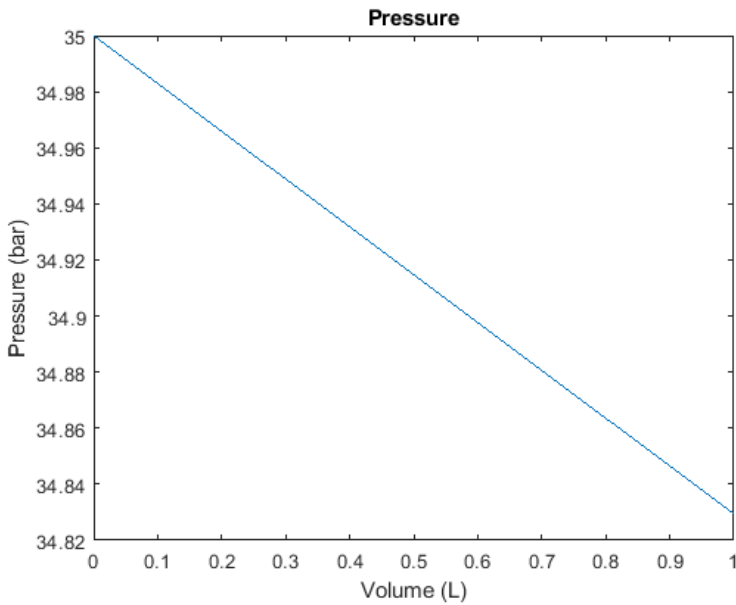


Figure 17. Gas Pressure in the ZnO Reactor.

This plot shows that the pressure decreases across the reactor, which was expected because a pressure gradient is the driving force in the desulfurization reactor. The pressure profile is linear, which would mean steady flow through the reactor.

5.1.3. Methanol Fixed Bed Reactor

Methanol is the key product in this process, in which its production occurs within a multi-tubular fixed bed catalytic reactor. Such a type of a reactor is mostly employed in highly exothermic reactions, for visualization purposes, a multi tubular bed is quite similar to the layout of a shell and tube heat exchanger. Temperature will keep rising due to the continuous release of heat within the reactor which amplifies the necessity of maintaining temperature in a consistent manner to encompass all the reactions that are occurring within the reactor. Therefore, other than actual reaction components, a heat transfer fluid flows through the external parts of the tubes, which can also be referred to as the shell-side for demonstration purposes, to cool down constituents from going above the required temperature. One of the major characteristics that need to be employed in this type of reactor are catalysts; intermediates that help expedite the reaction rate without interfering with the reaction itself. Catalysts are very much needed especially in a large-scale reactor where a huge amount of reactants are incoming and are expected to react with a relatively high conversion and therefore a maximized efficiency. Catalyst pellets are uniformly distributed within the reactor's tube and are activated upon the operating conditions of the reaction. Figure 18 below is an illustration of a general multi-bed tubular reactor, displaying heat inlet and outlet flows, reactants and products flows and baffles that hold the tubes intact.

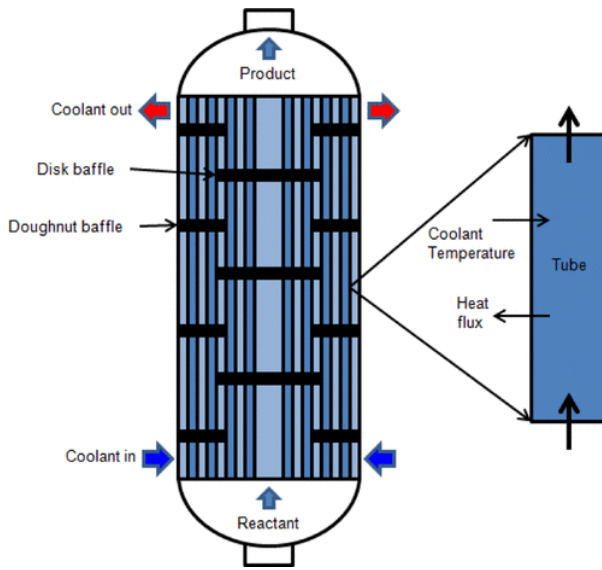
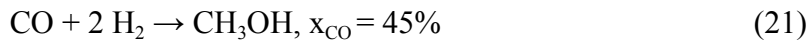
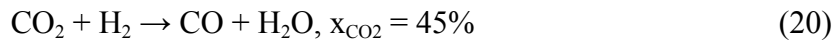


Figure 18: Illustration of a Multi-Tubular Fixed Bed Reactor. (Hukkanen, 2013)

There are three essential reactions that take place in the methanol bed reactor, using products that are extracted from the biomass and natural gas that are fed to the solar reactor. The reactions are as follows, reiterating from material balances:



One of the major aspects that needs to be navigated is reactor design are heats of reactions for they hold a standard parameter of safety and efficiency of the system. In order to calculate heats of reaction, ΔH_{rxn} , heat capacity constants are extracted from Perry's Chemical Engineering Handbook and are integrated from room temperature to reactor operating temperature in order to get a scaled value in accordance with the reactor's operating conditions. Prior to introducing heat capacity constants, the pre integrated heat capacity function is as follows, where C_p is the heat capacity and C_i is the heat capacity constant with a corresponding number.

$$C_p = C_1 + C_2 \left[\frac{C_3}{T \sinh(\frac{C_3}{T})} \right]^2 + C_4 \left[\frac{C_4}{T \cosh(\frac{C_5}{T})} \right]^2 \quad (28)$$

As for the integrated function, it is as shown below,

$$C_1 T + C_2 C_3 \coth(\frac{C_3}{T}) - C_4 C_5 \tanh(\frac{C_5}{T}) \quad (29)$$

Furthermore, the heat of formation, H_f , is utilized to calculate the heats of reaction at 298 K. The equation is exhibited after this sentence.

$$\Delta H_R^\circ = \Sigma H_{f, products} - \Sigma H_{f, reactants} \quad (30)$$

The methodology used to calculate the overall heat of reaction is to find the values acquired by the integrated version of equation (28) and then calculate the heats of reaction obtained by the heats of formation using equation (30). The approach utilizes thermodynamic equilibrium constants which at the end result of this entire formula, which is essentially the summation of the integrated values of products and reactants and heats of formation. The equations for each consecutive reaction are:

$$\left(\int_{298.15 \text{ K}}^{543.15 \text{ K}} C_{p, \text{water}} + C_{p, \text{CO}} \right) + \int_{543.15 \text{ K}}^{298.15 \text{ K}} (C_{p, \text{CO}_2} + C_{p, \text{H}_2}) + \text{Hrxn}_{@ 298.15 \text{ K}} \quad (31)$$

$$\left(\int_{298.15 \text{ K}}^{543.15 \text{ K}} C_{p, \text{CH}_3\text{OH}} \right) + \int_{543.15 \text{ K}}^{298.15 \text{ K}} (C_{p, \text{CO}} + 2C_{p, \text{H}_2}) + \text{Hrxn}_{@ 298.15 \text{ K}} \quad (32)$$

$$\left(\int_{298.15 \text{ K}}^{543.15 \text{ K}} C_{p, \text{CH}_3\text{OH}} \right) + \int_{543.15 \text{ K}}^{298.15 \text{ K}} (C_{p, \text{CO}_2} + 3C_{p, \text{H}_2}) + \text{Hrxn}_{@ 298.15 \text{ K}} \quad (33)$$

The constant values are presented in Table 26 below, and following them is Table 27 where the values of heats of reaction for all three reactions are exhibited.

Table 26: Heat Capacity Constants for All Species.

Name	$C_1 * 1E-05$	$C_2 * 1E-05$	$C_3 * 1E-03$	$C_4 * 1E-05$	C_5
H_2O	33363	26790	2610.5	8896	1169
CO_2	29370	34540	1428	26400	588
CO	29108	8773	3085.1	8455	1538.2
H_2	27617	9560	2466	3760	576.6

CH ₃ OH	39252	87900	37.6	53000	896.7
--------------------	-------	-------	------	-------	-------

Table 27: Heats of Reaction of the First Reaction in the Methanol Bed Reactor.

Reaction 1: CO ₂ + H ₂ → CO + H ₂ O	
ΔH _{rxn} for reactants (kJ/K)	-259.17
ΔH _{rxn} for products (kJ/K)	260.73
ΔH _{rxn} from H _f (kJ/K)	8.66
Actual Overall ΔH _{rxn} (kJ/K)	528.57

Table 28: Heats of Reaction of the Second Reaction in the Methanol Bed Reactor.

Reaction 2: CO + 2 H ₂ → CH ₃ OH	
ΔH _{rxn} for reactants (kJ/K)	-290.69
ΔH _{rxn} for products (kJ/K)	-293.32
ΔH _{rxn} from H _f (kJ/K)	-139.42
Actual Overall ΔH _{rxn} (kJ/K)	-723.40

Table 29: Heats of Reaction of the Third Reaction in the Methanol Bed Reactor.

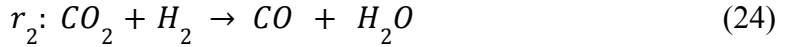
Reaction 3: CO ₂ + 3 H ₂ → CH ₃ OH + H ₂ O	
ΔH _{rxn} for reactants (kJ/K)	-454.37
ΔH _{rxn} for products (kJ/K)	458.60
ΔH _{rxn} from H _f (kJ/K)	-130.76
Actual Overall ΔH _{rxn} (kJ/K)	-126.53

As per Table 27, the heat of reaction of the first reaction is a value of 528.75 kJ/K, which makes sense because it is an endothermic process. As for the other two reactions, the values are -723.40 kJ/K and -126.53 kJ/K, respectively. Both are highly negative due to it being an exothermic process.

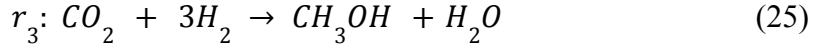
Jean Francois Portha et al. proposed a method for modeling the methanol reactor tank. The following reaction kinetics were adopted from the paper. Rate kinetics are expressed as partial pressures and the parameters k , K , and b .



$$r_1 = k_1 b_{CO} \left[\frac{P_{CO} P_{H_2}^{1/3} - \frac{P_{CH_3OH}}{P_{H_2}^{1/2} K_1}}{(1+b_{CO} P_{CO} + b_{CO_2} P_{CO_2})(P_{H_2}^{1/2} + \frac{b_{H_2O}}{b_{H_2}^{1/2}} P_{H_2O})} \right] \quad (31)$$



$$r_2 = k_2 b_{CO_2} \left[\frac{P_{CO_2} P_{H_2} - \frac{P_{CO} P_{H_2O}}{K_2}}{(1+b_{CO} P_{CO} + b_{CO_2} P_{CO_2})(P_{H_2}^{1/2} + \frac{b_{H_2O}}{b_{H_2}^{1/2}} P_{H_2O})} \right] \quad (32)$$



$$r_3 = k_3 b_{CO_2} \left[\frac{P_{CO_2} P_{H_2}^{3/2} - \frac{P_{CH_3OH} P_{H_2O}}{P_{H_2}^{3/2} K_3}}{(1+b_{CO} P_{CO} + b_{CO_2} P_{CO_2})(P_{H_2}^{1/2} + \frac{b_{H_2O}}{b_{H_2}^{1/2}} P_{H_2O})} \right] \quad (33)$$

The K parameters are presented below. These parameters represent the equilibrium constants. The unit for K_1 is bar^{-2} , K_2 is dimensionless, and K_3 is given in bar^{-2} . Note that the temperature is given in kelvins.

$$\log_{10}(K_1) = \frac{5139}{T} - 12.621 \quad (34)$$

$$\log_{10}(K_2) = \frac{-2073}{T} - 2.029 \quad (35)$$

$$\log_{10}(K_3) = \frac{3066}{T} - 10.592 \quad (36)$$

The b parameters represent the adsorption constants. The units for the b parameter is inverse bars. The gas constant is $8.314 \frac{J}{mol K}$.

$$b_{CO} = -2.16 \times 10^{-5} e^{\left(\frac{46800}{RT}\right)} \quad (37)$$

$$b_{CO_2} = 7.05 \times 10^{-7} e^{\left(\frac{61700}{RT}\right)} \quad (38)$$

$$\frac{b_{H_2O}}{b_{H_2}^{1/2}} = 6.37 \times 10^{-9} e^{\left(\frac{84000}{RT}\right)} \quad (39)$$

The k parameters represent the kinetic constants. The kinetic constant units are $\frac{mol}{s \text{ bar } kg_{cat}}$.

$$k_1 = 4.89 \times 10^6 e^{\left(\frac{-113000}{RT}\right)} \quad (40)$$

$$k_2 = 9.64 \times 10^{11} e^{\left(\frac{-152900}{RT}\right)} \quad (41)$$

$$k_3 = 1.09 \times 10^5 e^{\left(\frac{-87500}{RT}\right)} \quad (42)$$

The above equations were taken into consideration to build the methanol reactor model. Further extending the reaction kinetics, the differential representing the component flow with respect to volume was derived. The ordinary differential equations below represent the change in component flow rate with changes to reactor volume.

$$\frac{dF_{CO}}{dV} = -r_1 + r_2 \quad (43)$$

$$\frac{dF_{H_2}}{dV} = -2r_1 - r_2 - 3r_3 \quad (44)$$

$$\frac{dF_{CH_3OH}}{dV} = r_1 + r_3 \quad (45)$$

$$\frac{dF_{CO_2}}{dV} = -r_2 - r_3 \quad (46)$$

$$\frac{dF_{H_2O}}{dV} = r_2 + r_3 \quad (47)$$

Plots were generated to determine a relationship between the change in component flow rate and the volume of the reactor. The table below represents the initial conditions utilized for the differential equations. Figure 19 illustrates the component flow rate changes. As the volume of the reactor increases, the flow rate of hydrogen decreases in a concave manner. In addition, water and carbon monoxide flow rates decrease to a value close to zero moles per hour. The most important component flow rate to visualize is the methanol flow rate since the process aims to produce pure methanol. In this case, the flow rate of methanol increases as the volume of the reactor increases. Based on visual inspection, hydrogen and methanol are the main components in the reactor after 300L.

Table 30: Initial Feed Conditions

Component	Initial Flow Rate ($\frac{kmol}{hr}$)
CO	537809.040
H ₂	1363146.62
CO ₂	241.87
H ₂ O	535364.100
CH ₃ OH	241.87

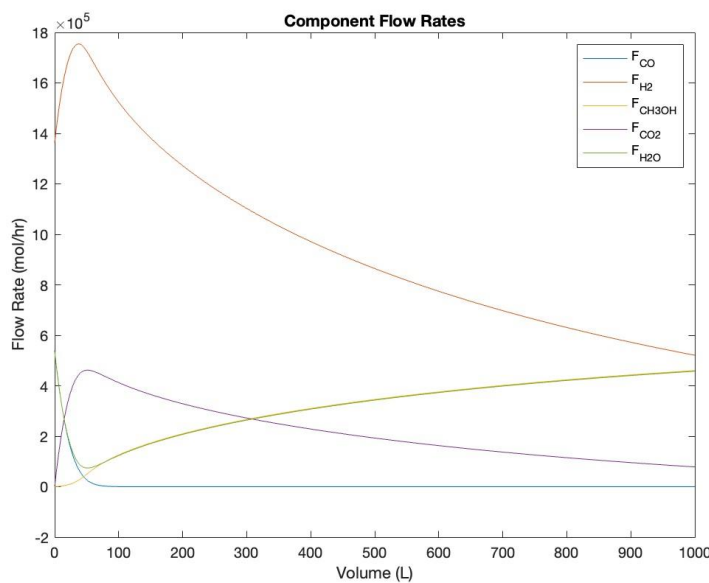


Figure 19: Component Flow Rate and Volume of Reactor.

As for energy balances, an inside-tube and coolant-tube differential balance using the overall transfer coefficient, U_a , density, inlet and outlet temperatures T and T_0 , the summation of the reaction rates multiplied by the corresponding heats of reaction $\sum r_A \Delta H_{rxn}$ and finally the overall flow rate of the system divided by the heat capacity, $\sum F_i C_{pi}$.

$$\frac{dT}{dV} = \frac{\frac{U_a}{\rho}(T - T_0) + \sum r_A \Delta H_{rxn}}{\sum F_i C_{pi}} \quad (48)$$

Equation 48 describes the temperature profile that is occurring within the methanol bed reactor which is displayed in Figure 20 below. There is a peak at the very start of rising volume where an exponential growth relationship between volume and temperature is occurring, however following the dramatic increase there is an instant decline as well. An explanation of such a trend would require a brief understanding of axial flow within a tube. Although heat loss is neglected in the presented calculations, heat transfer with respect to the tube's length in the direction of axial flow causes a condition known as axial flow conduction. The occurrence of such an event causes an instant increase of heat transfer at the very beginning of the entrance region (Kandilakr, 2014) and therefore the instant peak that is occurring in Figure 20 below. Nevertheless, temperature starts to decline steadily and levels off at a reactor volume of 1000 L which could be as a result of an increase of reactor volume that essentially is related to how much cooling is transferred to the constituents of the tube. A correlation between the temperature profile of the reactor and the coolant's temperature have been found, assuming that the system is continuous.

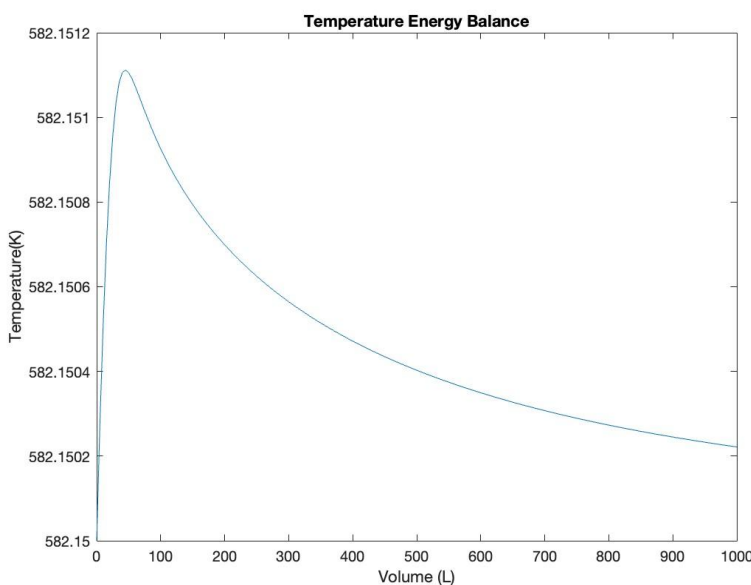


Figure 20: Temperature Profile in the Methanol Bed Reactor vs. Volume of Reactor.

As described above, a multitubular reactor requires a heat transfer fluid to stabilize the temperature profile due to the exothermic reactions. In this system, the chosen utility is boiling water by which condensation occurs and cools down the tubes. Water is widely used in industrial processes as a heat transfer fluid considering how accessible it is, cost-effective and easily manageable in terms of phase changes and temperature control. That being said, the energy balance around the shell-side, where m_c is the coolant mass flow rate and $C_{p,c}$, is:

$$\frac{dT_c}{dV} = \frac{U_a(T - T_0)}{m_c C_{pc}} \quad (49)$$

The expected behavior of such a differential is an increase of the coolant temperature as it cools down the system with respect to reactor volume. However, since the cooling is continuous as the reactor is running, the greater the volume of the reactor the more cooling will be required and therefore an exponential decay relationship between temperature and volume is exhibited in Figure 21 below. The volume domain chosen goes from zero to a thousand liters.

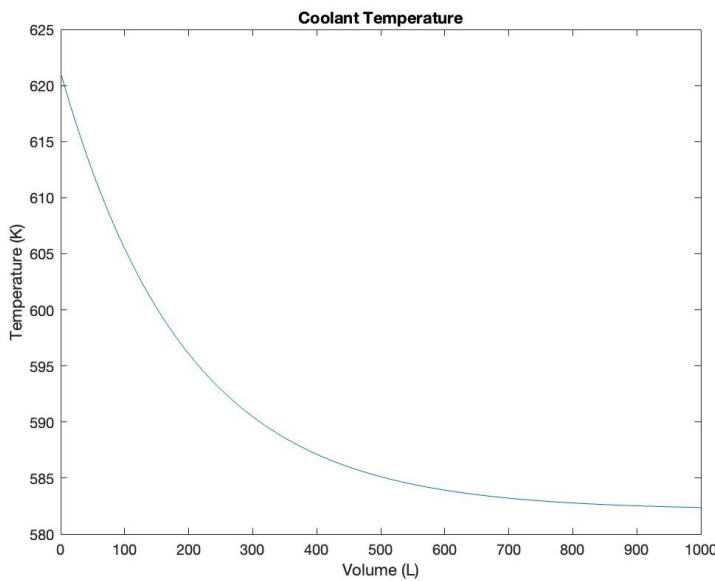


Figure 21: Volume in Liters vs. Temperature of Coolant in Kelvin.

Figures 20 and 21 have been plotted in MATLAB where the entire code can be found in Appendix A. The third navigated differential is pressure drop related. In order to mimic real life situations, the likelihood for a fully developed laminar flow is quite low and it is more likely to have turbulent impulses. As turbulence increases, fluids become more in contact and therefore they become more dependent on velocity which eventually has a major impact on the pressure drop in a system. In other words, the higher the velocity of the flow, the larger pressure drop there is in a tube due to friction factors. In a multi-tube fixed bed reactor, pressure drop is also impacted by catalyst size and temperature gradient. Generally, in such a medium the lower the pressure drop, the more efficient the system is, especially in gas mediums. The methanol bed reactor is running at a highly pressurized and heated system with values of 80 bar and 270°C, meaning that components are expected to be in vapor phase since the least volatile component is water and it has a boiling point of 100 °C. That being said, a pressure differential has been modeled in MATLAB in order to recognize any interesting trends and relationships between different variables within the reactor. The equation employed in a packed bed is known as the Ergun equation. Variables in the formula are ϕ which is the porosity, g_c is the gravity constant, D_p

is the diameter of particle in the bed, μ is the viscosity, z is the length of tube, u is the superficial velocity, ρ is the density and G is the gas superficial velocity.

$$\frac{dP}{dz} = - \frac{G}{\rho g_c D_p} \left[\frac{1-\phi}{\phi^3} \right] \left[\frac{150(1-\phi)\mu}{D_p} + 1.75G \right] \quad (50)$$

Furthermore, the continuity equation is also utilized and is simplified because the reactor is assumed to be at steady state. \dot{m}_0 is the entering mass flow rate and \dot{m} is the general mass flow rate, v_0 is the volumetric flow rate.

$$v = v_0 \frac{\frac{P_0}{P}}{\left(\frac{T}{T_0}\right)} \frac{F_T}{F_{T_0}} \quad (51)$$

An important factor that needs to be considered is that there is a huge correlation between pressure drop in the system and the utilized catalyst. Therefore, the Ergun equation can also be written in terms of catalyst weight. Beta, β_0 , is a parameter that encompasses the variables introduced earlier in Equation 50. W is the weight of the catalyst, A_c is the cross sectional area. The only variation between the following formula and Equation 52, is that the continuity equation is implemented to take into account the flow rates of the system.

$$\frac{dP}{dW} = - \frac{\beta_0}{A_c(1-\phi)\rho_0} \frac{\frac{P_0}{P}}{\left(\frac{T}{T_0}\right)} \frac{F_T}{F_{T_0}} \quad (52)$$

In order to find some constant values, they were obtained from research papers and others were assumed based on reasons that are to be justified. The type of catalyst employed is a copper-zinc catalyst referred to as Cu/Zn/Al₂O₃. The catalyst mass is 135 mg, bed volume is 0.307 cm³, bed height is 0.382 cm, an internal reactor diameter of 1.01 cm and a bed porosity of 0.41 (Portha et al., 2017). In order to choose a value of void fraction, a range was found for zinc oxides with a value of 0.5 (Negri, 2017). The superficial gas velocity is calculated through an iterative process in matlab, considering that it depends on the surface area of the tube. Moreover, pressure in the system is expected to decrease as the volume of the reactor increases. Shown in Figure 22 below is a plot acquired from matlab in which pressure is decreasing with respect to increasing volume.

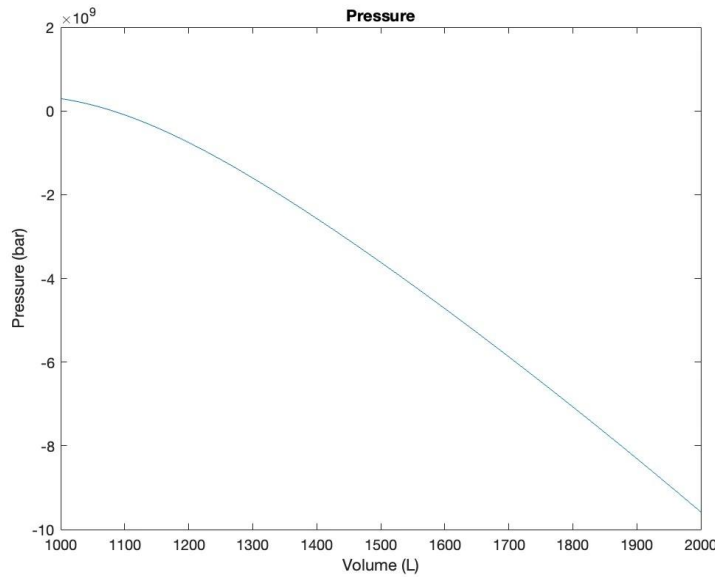


Figure 22: Volume in Liters vs Pressure in Bar, in a Magnified Volume Domain from 1000 L to 2000L

The number of tubes in the reactor are of a value of 16 whereas the inner tubes were assumed to be in between 1 to 1.5 inch as per the design guidelines. A recommendation that could be implemented is to further investigate some of the constants in the system and how much of an impact they have on the efficiency of heat transfer, mass transfer, durability of the system and minimization of pressure drop. In other words, in a less time sensitive option, a sensitivity analysis is to be conducted in order to understand the divergence and convergence of the system.

5.2. Separators

The distillation column is implemented in the downstream section of the plant, where raw methanol is transferred to a storage tank and a column afterwards. The downstream segment runs 24 hours per day every year, resulting in a total of 8000 hours per year. The sole reason for this segment is to separate the constituents of the raw methanol stream in order to reach a purification mole fraction of methanol with a value of 0.9997. As any typical distillation column, the process involves three main streams: feed, distillate and bottoms, the desired outcome of employing such a system is to allow more volatile components to reach out the top and come out the distillate and vice versa for less volatile elements where they are directed to the bottoms. In terms of heat exchange and energy requirements, a total condenser and a reboiler are utilized for both cooling and heating flows that enter back to the column for additional contact and therefore enhanced separation. The first step that needs to be taken in terms of sizing up/ designing a column is categorizing components with respect to volatility, which can be done by looking up the boiling temperatures for each or K values. Ideally, since the column is to be simulated in Aspen HYSYS, the inlet feed K values were noted down after assigning light and heavy keys. In the raw

methanol stream, water, methanol, hydrogen, nitrogen, carbon monoxide and carbon dioxide exited the methanol bed reactor and entered the storage tank in the downstream. Table 31 below displays values of inlet mole fractions, inlet K values and categorization of heavy and light keys.

Table 31: Values of the RAW-MEOH Stream Entering the Storage Tank.

Species	Inlet mole fraction	Inlet K value	H/L
Methanol	0.64	4.03E-02	L
Water	0.35	1.12E-02	H
Hydrogen	0.0025	728.42	L
Nitrogen	3.2E-07	12274.6	L
Carbon Monoxide	1E-05	417.24	L
Carbon Dioxide	2E0-5	112.62	L

Just after setting up a simulation, distillate and bottom flow rate were estimated by hand calculations utilizing inlet flow rates of each species that were obtained from the feed in Aspen HYSYS as well as assuming a non distributing behavior, meaning that all light keys are directed to the distillate and all heavy keys are directed to the bottoms. By assigning assumed recoveries in each stream and utilizing the actual mole fractions desired in each stream, flow rates calculated were pretty close to those automatically calculated by the simulation. An important fact to acknowledge prior to diving into the logistics of designing this separation column, as aforementioned in regards to the flow rate, it is going to be different than the outlet raw methanol stream due to duration difference. The desired specification of this column is a methanol purity of 99.97% and a flow rate limit of 56.5 million gallons per year. In order to apply some recommendations, a short cut column was utilized in order to find a ballpark of some values such as minimum number of trays, recommended number of trays, optimal feed stage and minimum reflux ratio. The outcome values resulted in respective values of 14 trays, 15 trays, 7th stage and 0.715 minimum reflux ratio. When employing such values in the simulation of the full column, some values were changed in accordance to the specification wanted. Nevertheless, the next step was to figure out which type of condenser and reboiler that needs to be utilized in the system. Following heuristics and flow diagram shown in Figure 23, information of such were identified.

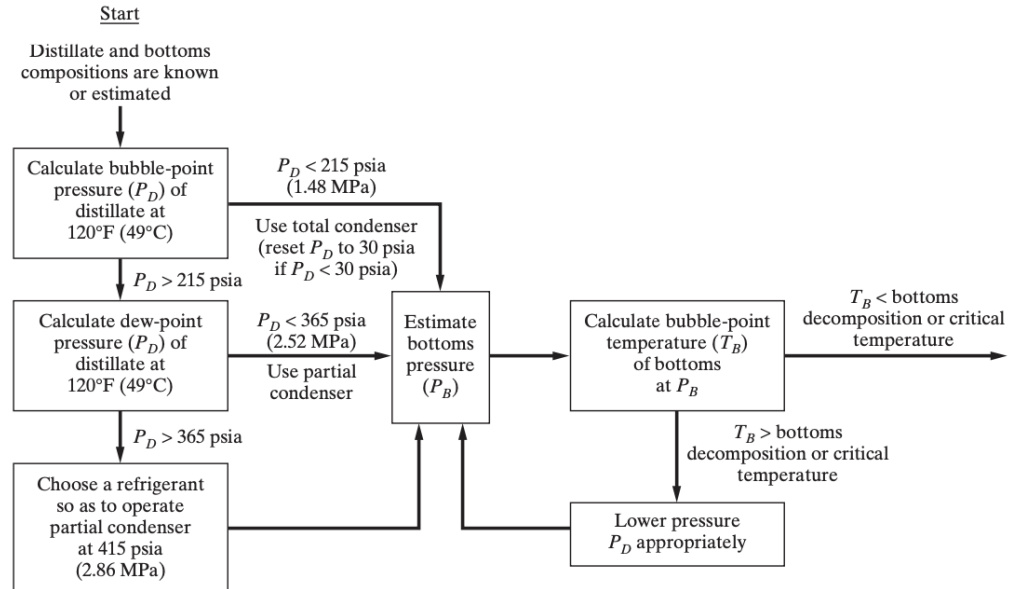


Figure 23: Heuristic Based Algorithm for Utility Type Identification. (Wiley, 246)

In order to calculate the bubble point pressure, P_D , of the distillate, vapor fraction was set at zero in Aspen HYSYS where to give out a value of 403 psi. By following the algorithm, the dew point pressure was calculated by the simulation by setting up the phase fraction as 1 and it resulted with an amount of 4.1 psi, meaning that a partial condenser needs to be used. Considering that the pressure drop in the column needs to be around 10 psi to 12 psi, the bottom pressure, P_B , was estimated in excel by an iterative process and it amounted to a value of 10 psi.

Moving on to the next step which is calculating the minimum number of stages, N_{min} . Using the Fenske equation following a sample calculation, where x_{LK} is the mole fraction of light component, x_{HK} is the mole fraction of heavy key component, D_{LK} is the molar flow rate of the distillate of the light key, D_{HK} is the molar flow rate of the distillate of the light key, B_{LK} and B_{HK} are light key and heavy key molar flow rates in the bottom stream and $\alpha_{LK,HK \text{ AVERAGE}}$ is the average geometric relative volatility.

$$N_{min} = \frac{\log\left[\left(\frac{D_{LK}}{D_{HK}}\right)\left(\frac{B_{HK}}{B_{LK}}\right)\right]}{\log(\alpha_{LK,HK \text{ av}})} = \frac{\log\left[\left(\frac{x_{LK}}{x_{HK}}\right)\left(\frac{x_{HK}}{x_{LK}}\right)\right]}{\log(\alpha_{LK,HK \text{ av}})} \quad (53)$$

$$\alpha_{LK,HK \text{ av}} = \left(\left(\frac{\alpha_{LK,HK D}}{\alpha_{LK,HK D}} \right) \left(\frac{\alpha_{LK,HK B}}{\alpha_{LK,HK B}} \right) \right)^{0.5} \quad (54)$$

Using Equation 53, all values such as flow rates and mole fractions were obtained from Aspen HYSYS,

$$N_{min} = \frac{\log\left[\left(\frac{0.9997}{1.73E-04}\right)\left(\frac{0.9959}{4E-03}\right)\right]}{\log(2.74)} = 13.77 \sim 14 \text{ stages} \quad (55)$$

As per the value obtained from the Fenske equation, it quite matches the value that was obtained from the shortcut column. Subsequently, the minimum reflux ratio needs to be calculated, in which it can be defined as the infinite number of stages that could be attained with respect to a maximum distillate flow rate. As practiced in industry, the reflux ratio is usually 1.1 to 1.5 multiplied by the minimum reflux ratio. For hand calculations that were mainly operated in excel, several equations were used. The standard equation used is known as the underwood equation, in which R_{min} is the minimum reflux ratio, α_i is the average geometric volatility, x_F is the feed mole fraction of a certain component, x_D is the mole fraction of a certain component in the distillate, Θ is theta and it serves as a value that lies between the average volatiles of both the heavy and light keys and lastly q is the moles of saturated liquid on the feed tray.

$$R_{min} + 1 = \sum \frac{(\alpha_i)(x_{D,i})}{(\alpha_i - \Theta)} \quad (56)$$

Even though most variables can be provided through calculations or from the simulation, theta is a parameter needs to be found through an iterative process in excel and it is acquired using the following equation:

$$\sum_{i=1}^n \frac{(\alpha_i)(x_{F,i})}{(\alpha_i - \Theta)} = 1 - q \quad (57)$$

Knowing that q from HSYS, n is the amount of components which is 2, theta was a value of 0.122 and by plugging back variables in the underwood equation, it resulted with an amount of 2.7. Therefore, the minimum reflux ratio was (ADD). Now that minimum reflux ratio and number of stages are obtained, the actual number of stages, N , can be calculated using the following equation:

$$\frac{N-N_{min}}{N+1} = 0.75[1 - (\frac{R-R_{min}}{R+1})]^{0.566} \quad (58)$$

Where a sample calculation using the previous equation is as follows:

$$\frac{N-14}{N+1} = 0.75[1 - (\frac{2.74-4.11}{4.11+1})]^{0.566} = 23 \text{ stages} \quad (59)$$

Moreover, in order to enhance mass transfer alongside vapor and liquid contact within the column, the feed stage was fed at the lowest stage of the column considering that the desired mole fraction of methanol out of the distillate is considered a relatively high purity. Water-alcohol separations are not exceptionally difficult and have been employed in industry for decades, indicating the need for a small to a normal size column for this specific separation.

Moving forward to column internals where other important aspects are investigated such as column diameter, height, type and materials. Some calculations were conducted in order to choose the most efficient type of column that should be utilized for this system. Starting with a trayed column with sieve trays. What makes sieve trays attractive to use in industry is that they're considered to be one of the cheapest options, as well as low required maintenance. They generally operate at a small turn down ratio due to the increased likelihood the column experiencing weeping which can be considered as a disadvantage. The other option is a packed column, either random or structured packing. Regardless, both types are usually utilized when corrosive materials are involved. Nevertheless, the calculations of the trayed column began with column diameter with the following equation, where D_T is the tower diameter, G is the mass flow rate, f is the fraction of the vapor flooding velocity, U_f is the vapor flooding velocity, A_d is the downcomer area, A_T is the tower inside cross sectional area and lastly ρ_G is the vapor density.

$$D_T = \left(\frac{4G}{f U_f \pi (1 - (A_d/A_T)) \rho_G} \right)^{0.5} \quad (60)$$

In order to solve for the vapor flooding velocity, U_f , the following equation is used where C is the empirical capacity parameter and it is also defined in Equation 61 below. C_{SB} is known as the flooding correlation and F_{LG} is the flooding parameter for both liquid and gasses and is also defined in the following equations. F_{ST} is the surface tension factor, F_F is the foam factor and it amounts to a value of 1, F_{HA} is the hole factor.

$$U_f = C [(\rho_L - \rho_G / \rho_G)]^{0.5} \quad (61)$$

$$C = C_{SB} F_{ST} F_F F_{HA} \quad (62)$$

$$F_{ST} = (\sigma/20)^{0.20} \quad (63)$$

$$\frac{A_d}{A_T} = 0.1 + \frac{F_{LG} - 0.1}{9}, \quad 0.1 \leq F_{LG} \leq 1 \quad (64)$$

$$F_{LG} = (L/G)(\rho_G / \rho_L)^{0.5} \quad (65)$$

In order to find correlations of C_{SB} and F_{LG} , Figure 24 below connects them in terms of plate spacing, in which the most suitable value is chosen.

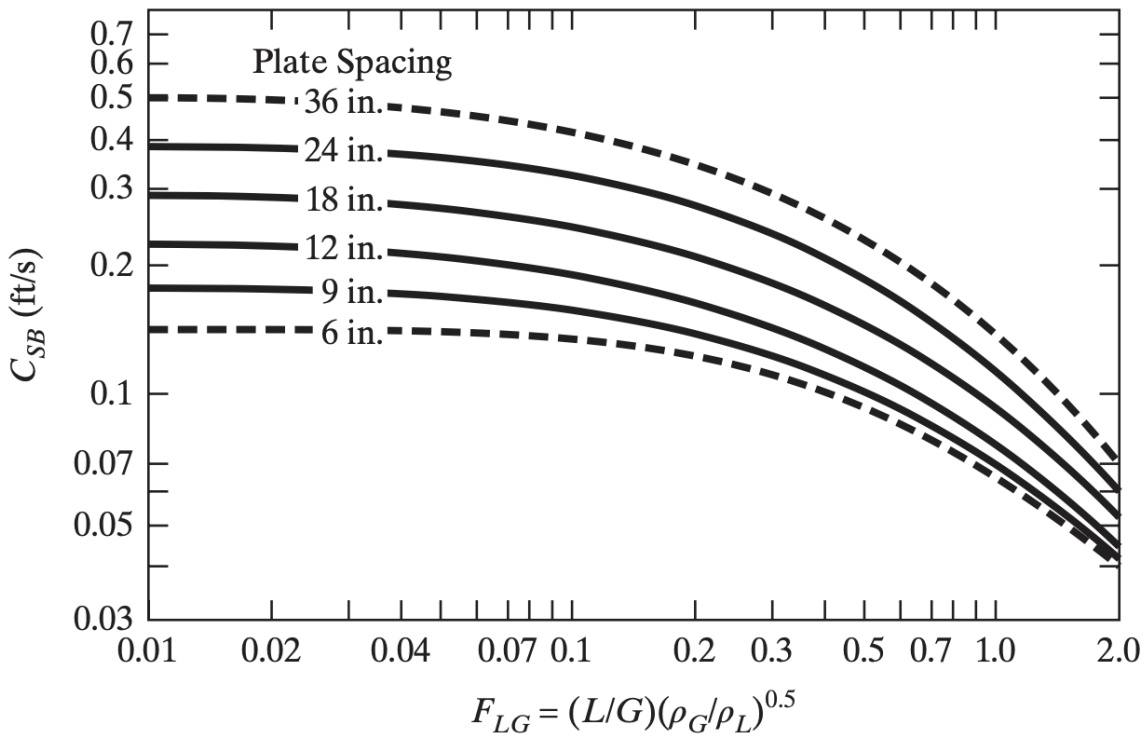


Figure 24: Flooding Correlations for Sieve Trays. (Wiley, 392)

F_{LG} resulted with a value around 0.77, and therefore C_{SB} was in a range of 0.2-0.3 ft/s with a plate spacing of 36 inches. The ratio used for A_d/A_T resulted in a value of 0.175. A sample calculation of vapor flooding velocity U_f and column diameter is shown below.

$$U_f = C[(\rho_L - \rho_G/\rho_G)]^{0.5} \quad (66)$$

$$U_f = 0.132 \text{ m/s} [(954.9 \text{ kg/m}^3 - 781.2 \text{ kg/m}^3/781.2 \text{ kg/m}^3)]^{0.5} = 4.09 \text{ m/s}$$

$$D_T = \left(\frac{4G}{f U_f \pi (1 - (A_d/A_T)) \rho_G} \right)^{0.5} \quad (67)$$

$$D_T = \left(\frac{4G}{0.8 * 4.09 \text{ m/s} \pi (1 - (0.175)) 781.2 \text{ kg/m}^3} \right)^{0.5} = 4.36 \text{ m} = 14.03 \text{ ft}$$

One of the characteristics a trayed sieve column displays is a generally larger diameter than other types of columns such as packed. An important factor to consider in column design is plate efficiency considering that they come hand in hand with column height. Figure 25 below displayed correlation between liquid viscosity and plate efficiency.

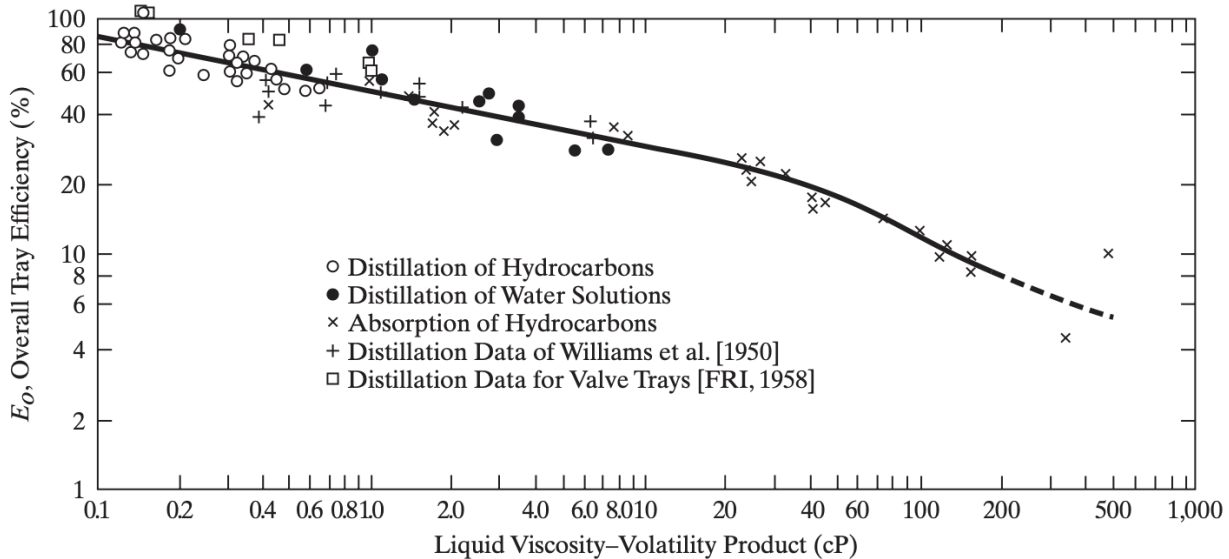


Figure 25: Overall Tray Efficiency, E_0 , versus the Liquid Viscosity.

The liquid viscosity in cP was found in Aspen HYSYS with a value of 0.5 cP. Following the trend in the graph for distillation of hydrocarbons, the efficiency can be estimated to be around 75%. The formula that can be used to get the column height is as follows, where H_{column} is the height of the column, N_{Equil} is the number of equilibrium trays, L_{space} is the tray spacing and E_0 is as described previously as the efficiency, the addition of 10 ft in the bottoms for storage heights and 4 ft for the top disengagement height.

$$H_{\text{Column}} = \frac{N_{\text{equil}}}{E_0} * L_{\text{space}} + 10 \text{ ft} + 4 \text{ ft} \quad (68)$$

$$H_{\text{Column}} = \frac{23 \text{ stages}}{0.75} * 3 \text{ ft} + 10 \text{ ft} + 4 \text{ ft} = 106 \text{ ft}$$

Even though the column is quite large for a considerably simple separation, the level of purity needed is high alongside the desired flow rate which is 56 million gallons per year. The other option that was navigated in terms of which type of column this separation should pertain is a random packing column. One of the reasons why a random packing column would be beneficial for this system is that it provides a very high distribution ratio. However, considering that we're already dealing with a relatively large system and high flow rates, certain expectations need to be met in terms of efficiency that need to be met for the separation to occur. In order to ensure that the choice of a trayed column is valid, other calculations for a packed column, where the vapor flooding velocity exhibited a value of 7 ft/s, whereas the column diameter was a value of 19 ft, with a choice of ceramic Raschig rings to enhance column durability with respect to

column's temperature gradient. The column height was of a value of 24 ft using the HETP methodology. The ending recommendation would depend on the resources available, where the efficiency is maximized while maintaining an economically feasible system. However, considering that the simulation was run as a trayed column with sieve trays, that is the ending choice for this system for consistency purposes, keeping in mind that it does not limit exploration of other types of columns in future projects.

5.2.2 Cyclone

A Cyclone separator is placed after stream ten that is exiting the spray quench and mixer to get rid of solid waste. The flowrate exiting the cyclone was a value of 14.6 kmol/hr with a temperature of 128 C with a mole fraction of one for ash. At that point of the process, liquid needs to be isolated and therefore solid particulates are discharged. Coming out of the mixer and into the cyclones, components enter tangentially and undergo centrifugal force. Subsequently, they exit the cyclone almost axially alongside the trajectory of gravity. Shown in figure below is a sketch that describes the behavior of materials coming in and out of a cyclone.

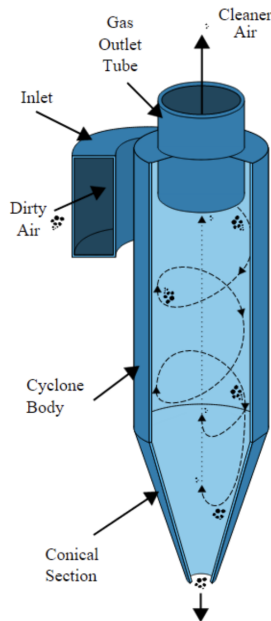


Figure 26: A Schematic of a Cyclone Separator. (Energy Education, n.d.)

Ash solid particulates size range from $2 \mu\text{m}$ to $300 \mu\text{m}$ (Yu et al., 2013), cyclones are generally equipped to remove solids larger than $10 \mu\text{m}$ in size. The efficiency of a cyclone is maximized with particles of a size around $2 \mu\text{m}$ to $2.5 \mu\text{m}$. However, considering that the flow rate and mole fraction coming out are almost a hundred percent, it means that the employed cyclone is effective enough for the system.

5.2.3 ZN-Split

A flash separator is added in the simulation after the ZnO cleaning bed, to get rid of the solid ZnCl₂ solid particulates. The main two phases that are in the separator are vapor and solid, where the vapor stream (stream 13) exits and enters a mixer where it merges with the recycling stream, and the solid waste is discharged in stream ZNCL2-S. A regular flash separator uses the concept of equilibrium between vapor and liquid phases; it can also be referred to as condensate stabilization, however that is not the case in the modeled separator. The particulate size distribution of ZnCl₂ is 0.1 weight fraction. In industry, the concept of flash separator is already embedded within the ZnO cleaning bed.

5.2.4 VL-SEP

Exiting the methanol bed reactor, stream 16 enters at a very high pressure and temperature, therefore a knock out drum has been employed to cool down and decompress constituents. The utilization of a knockout drum is to extract liquid from gas systems, liquid condenses and is collected out of the raw methanol stream. The components that are in the raw methanol stream are methanol, water, hydrogen, nitrogen, carbon monoxide and carbon dioxide. The main two components are methanol and water, other materials are deemed as residuals. At that point of the simulation, exiting the knock drum materials are sent to a storage tank to the downstream segment of the plant.

5.3. Heat Exchangers

5.3.1. Spray Quench Tank

Spray quenching allows for optimal control of flow temperature. As the name suggests, cooling is done by spraying the incoming flow with a liquid medium. The liquid medium can be water, oil, or brine. Since this is a heat exchanger, it is important to examine the heat and mass transfer during the cooling process. The efficiency and performance of the spray quench tank depend on the drop surface area, the drop motion, and the tank's geometry. It is key to understand the spray patterns as they impact the rate of evaporation and heat exchange. The spray quench geometry can be divided into a horizontal or vertical configuration. In addition, it can further be divided into a wet wall or a drywall process. As the name implies, a wet wall tank will use an excess liquid medium, causing a wet tank. The excess use of liquid ensures no residue is left on the tank; however, it also indicates that the process requires additional optimization of recirculating the liquid and gas streams. On the other hand, drywall will use a smaller drop size, eventually evaporating everything at the end of the process. Generally, a drywall configuration is utilized for a larger scale process since the wet wall configuration requires additional maintenance. However, it is important to note that a wet wall can be desirable in some processes because it is efficient. In addition to the tank configuration, the spray nozzle configuration impacts the tank's heat transfer rate and efficiency. The quenching process can change dramatically depending on the droplet's angle, flow, pressure, and size. Spray nozzles can be

divided into a single fluid flat fan, single fluid, and two fluid. A single fluid flat fan controls the accumulation of water and gas on the wall. Single and two-fluid configurations are generally used in drywall configurations since both produce fine atomization.

During the initial drop of the spray quench, the large temperature difference is a driving force for heat transfer. Since there is heat exchange between the drop and the gas, the droplet temperature will increase, decreasing the change in temperature at the outlet conditions. The diameter of the droplet is proportionally related to the drop size. Equation 69 is the formulation of residence time in relation to the drop size provided by BETE.

$$\theta = \frac{\rho_l \lambda D_0^2}{8k_g \Delta T} \quad (69)$$

In the above equation, let θ represent the residence time in seconds, ρ_l the density of the drop liquid in $\frac{kg}{m^3}$, λ the heat of vaporization of the liquid in $\frac{J}{kg}$, D_0 the drop diameter in m , k_g the thermal conductivity in $\frac{W}{mK}$, and ΔT the log mean temperature difference of the tank in K .

$$\Delta T_m = \frac{\Delta T_1 - \Delta T_2}{\ln(\frac{\Delta T_1}{\Delta T_2})} \quad (70)$$

$$\Delta T_1 = T_{h,in} - T_{c,in} \quad (71)$$

$$\Delta T_2 = T_{h,out} - T_{c,out} \quad (72)$$

The log mean temperature difference formula is presented above. Note that $T_{h,in}$ represents the inlet temperature of the hot side, $T_{c,in}$ represents the inlet temperature of the cold side, $T_{h,out}$ represents the outlet temperature of the hot side, and $T_{c,out}$ represents the temperature of the outlet temperature of the cold side.

$$\tau = \frac{V_R}{V_0} \quad (73)$$

The residence time equation above is the ratio between the volume of the reactor and the volumetric flow rate.

In this process, water will be pumped into the spray quench tank which is utilized to cool down the incoming vapor stream. The mixed stream is then sent out to the cyclone processor. The spray quench is operated using a hot/cold medium approach temperature of $0.5^\circ C$. The cold medium is supplied through a water stream which is pumped using a 35 bar pump. The cold side

of the heat exchanger has an exit temperature of 210°C. Ideally, the mixed stream after the spray quench process should have a composition of 64 mol% H₂, 34 mol% CO, and some contaminants.

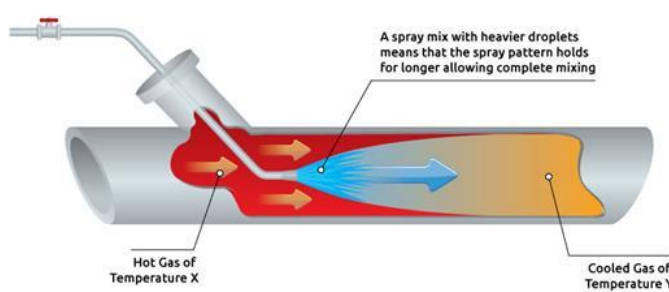


Figure 27: Horizontal Spray Quench Tank Diagram (The Spray Nozzle People, n.d.)

The table below lists important parameters of the spray quench tank.

Table 32: Spray Quench Tank Parameters

Parameter	Process Values	Units
Hot Stream Inlet Temperature (Stream 5)	800	°C
Hot Stream Outlet Temperature (Stream 7)	579.98	°C
Cold Stream Inlet Temperature (Stream 6)	25.20	°C
Cold Stream Outlet Temperature (Stream 8)	369.98	°C
Density of Water	997	kg/m ³
Heat of Vaporization of Water	2260000	J/kg
Thermal Conductivity of Water	0.598	J/SmK

Using the parameters above, the formula proposed by BETE was tested to relate reactor volume and diameter of droplet. The log mean temperature difference calculation is presented below.

$$\Delta T = \frac{(1073.15K - 298.35K) - (853.13K - 643.12K)}{\ln(\frac{1073K - 298.35K}{853.13K - 643.12K})} = 432.63K \quad (74)$$

$$\theta = \frac{(997 \frac{kg}{m^3})(2260000 \frac{J}{kg})(D_0)^2}{8(0.598 \frac{J}{smK})(432.63K)} \quad (75)$$

A range of droplet diameters from 0.01m to 1m were utilized to calculate and plot the residence time in hours. Figure 28 illustrates the relationship between drop diameter and residence time.

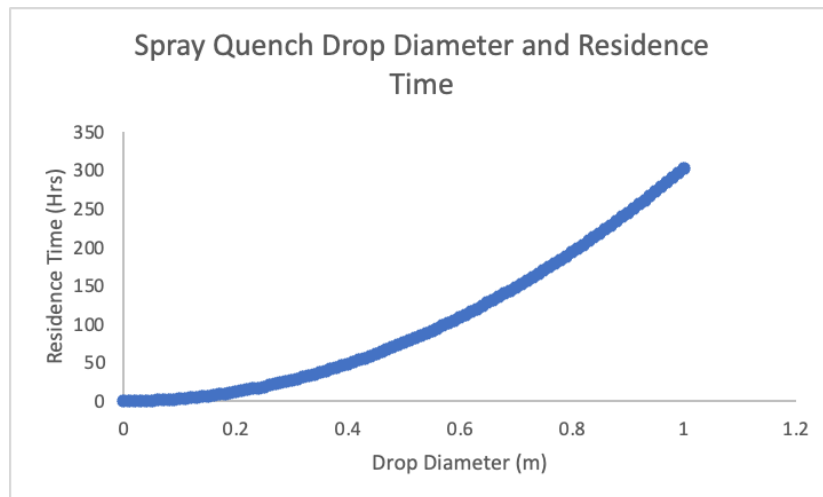


Figure 28: Change in Residence Time and Drop Diameter

Figure 28 shows that the residence time and drop diameter has a concave pattern due to the squared diameter. Since the residence time is proportional to the reactor volume, as the diameter of the droplet increases, the residence time increases, thus, causing an increase in tank volume given that the volumetric flow rate stays constant. On the other hand, the relationship between the volumetric flow rate and the diameter of the droplet is inversely proportional. As a result, if the diameter of the droplet increases, the volumetric flow rate decreases, given that the tank volume stays constant.

When designing the spray quench for this specific process, the goal is to increase the efficiency of the cooling process and limit residue left on the spray quench tank. Since some solids are present during the quenching process, it is important to maintain the majority of the solids even after the process. As a result, a horizontal spray quench with a wet wall configuration would be the best fit since it reduces the number of residuals. Since a wet wall configuration fits the desired goal, a single fluid flat fan spray nozzle would be appropriate. BETE, a spray nozzle specialization company, has a standard flat fan nozzle called their NF line. Spray angles go from 0 to 120 degrees providing a flow rate range from 0.103 to 130 gpm. The process deals with high

temperatures and liquids. Therefore, the material of the fan nozzle should be corrosion-resistant and heat-resistant. As a result, metals such as stainless steel, chrome, and iron fit the requirements. BETE's flat fan nozzle is made of stainless steel, which is desired in this process.

5.3.2. Shell-and-Tube

In any chemical process synthesis, more often than not there will be the need for temperature changes and sometimes phase changes as a result of it. This is where the concept of heat transfer comes into play when it comes to a chemical plant. The main type of heat transfer that is occurring in this system is known as forced convection, where a heated or a cooled fluid flows through a solid medium by which heat transfer occurs. In this section, the type of heat exchanger is shell-and-tube. Either cooling or heating, heat transfer occurs through circulation where utility moves through the shell side or the tube side. Generally, corrosive materials are to pass through the tube side.

The first heat exchanger employed is located after the cyclone; inlets contain water, hydrogen, nitrogen, carbon monoxide, carbon dioxide and methanol residuals. Prior to entering the ZnO bed, it needs to be cooled to reach a temperature of 210 °C. There are certain steps to be taken in order to design a shell and tube heat exchanger starting with choosing a utility, specifying components in tube and shell, pressure drops, heat transfer surface area and geometry. Considering that we are looking to decrease the temperature of the stream that is passing through the cyclone, the utility chosen is cooling water. It is an attractive heat transfer medium due to its high level of stability and easy access. Moreover, constituents entering the heat exchanger into the tube side are mostly vapor, following heuristic 31 a pressure drop of 3 psi has been employed. As for the shell side, considering that the utility will be passing through, a pressure drop of 6 psi has been chosen for liquid cooling water. In accordance with heuristic 55, corrosive and high pressure materials are to pass through tubes, and other stable materials through the shell side. A shell-and-tube heat exchanger has been simulated in Aspen HYSYS in order to understand the variations of the system by comparing hand calculated values vs. simulation values. Table 33 below provides information in regards to the inlet and outlet conditions of the first shell-and-tube heat exchanger.

Table 33: Shell and Tube Flows Operating Conditions.

	Hot in	Cold out	Cold in	Hot out
Temperature (°C)	488.2	210.6	10	15
Pressure (kPa)	3.50E+03	3.48E+03	101.34	41
Molar Flow (kmol/hr)	1.09E+07	1.09E+07	6.3E+07	6.3E+07

The duty obtained from Aspen HYSYS is a value of 9.35E+10, the overall heat transfer coefficient per area is 2.943E+10 kJ/hr. The correction factor, F_T , is 0.99, and the uncorrected logarithmic mean temperature difference, LMTD, is 317.65 °C. Chilled water ranges from 45 °F to 90 °F. The desired specification is to set the outlet temperature of the tube to decrease from 488.2 °C to 210 °C. As for hand calculations, LMTD was calculated by the following equation, where ΔT_1 and ΔT_2 represent the temperature difference of the hot and cold streams.

$$\Delta T_{LM} = \frac{\Delta T_1 - \Delta T_2}{\ln(\Delta T_1 / \Delta T_2)} \quad (76)$$

The hand calculated LMTD is almost identical to the one calculated in Aspen HYSYS with a value of 317.67°C. In order to find the correction factor, parameters known as R and S need to be calculated for multiple passes in a shell-and-tube heat exchanger. The equations to calculate both factors are as follows.

$$R = \frac{T_{H,in} - T_{H,out}}{T_{C,out} - T_{C,in}} \quad (77)$$

$$S = \frac{T_{H,in} - T_{H,out}}{T_{C,out} - T_{C,in}} \quad (78)$$

R and S resulted with consecutive values of 2.3 and 0.42. Considering that the chosen heat exchanger type is a 4-8, the following Figure 29 was obtained from product and process design principles by Sieder et al.

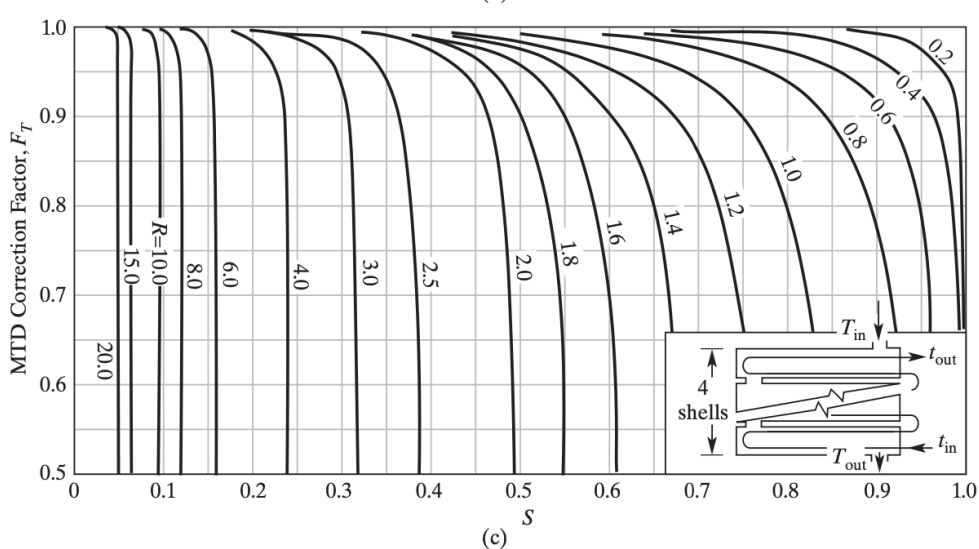


Figure 29: F_T correction Factor vs the S Factor. (Wiley, 373)

The corresponding F_T with the S value is 0.99 which gives a low margin of error between hand calculated values and simulation values. As for the overall heat transfer coefficient, following heuristics, is a value of 225 Btu/ft²-hr. The heat duty was determined by the simulation with a value of 6.2E+10 kJ/hr. The next important step to take is to figure out the heat transfer surface area in which heat transfer would occur. Using the following equation, the heat exchanger area was calculated, where Q is the heat duty, F_T is the correction factor, U is the overall heat transfer coefficient, A is the heat exchanger area and as mentioned earlier ΔT_{LM} is the log mean temperature.

$$A = \frac{Q}{U * F_T * \Delta T_{LM}} \quad (79)$$

The area amounted to a value of 8348.4 ft². As per the textbook and the lectures, the area cannot exceed 8000 ft² and a new configuration of the heat exchanger must be executed in parallel using equal areas. That being said, it is proposed that two heat exchangers in parallel are to be utilized, giving out a consecutive value of 4174.24 ft². Figure 30 below demonstrates two heat exchangers in parallel.

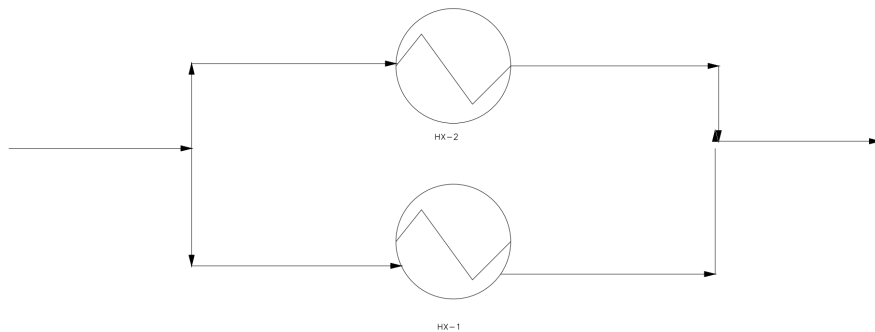


Figure 30: Two Heat Exchangers in Parallel.

The next step taken was to figure out the volumetric flow rate of both the tube and shell side. Where once again Q is the heat duty, ρ_{tube} and ρ_{shell} are the respective densities for the tube and shell side, $C_{p,shell}$ and $C_{p,tube}$ are the respective mass heat capacities for both the tube side and the shell side. Considering that the simulation gives out values that correspond with each stream, values for density and heat capacities were the average of the inlet and outlets with respect to their side in the heat exchanger.

$$Volumetric\ Flow = \frac{Q}{\rho * C_p * \Delta T} \quad (80)$$

Refer to Appendix A for sample calculations. The volumetric flow rate of the tube side amounted to a value of 586392.86 ft³/hr, whereas the volumetric flow rate of the shell resulted in a value of 497827.90 ft³/hr. Proceeding with the geometry of the heat exchanger, heuristic 54 states that shell and tube heat exchangers employ a 3/4 inch O.D gauge, 16 ft long tubes and a shell of 1 ft diameter (Wiley, 365). The chosen flow area per tube was a value of 0.015 ft from table 12.5 in the textbook. The calculated tube surface area is 2.01 ft², knowing that the inner diameter is 0.04 ft. In order to solve for the number of tubes, A_{HX} is the heat exchanger area, $A_{tube\ surface}$ is the tube surface area and N is the number of tubes.

$$N = A_{HX} / A_{tube\ surface} / N \quad (81)$$

The number of tubes is 258.43 for both heat exchangers. As for tube velocity, there is a certain range that the value should be between depending on the phase of the components, in this presented case the materials are mostly vapor with some residual liquid resulting in a tube velocity 42 ft/s using the following equation. Velocity of the tube is v_{tube} and A_{cross} is the flow area per tube and N is the number of tubes.

$$v_{tube} = \text{Volumetric Flow Rate of Tube} / A_{cross} / N \quad (82)$$

As for shell inner diameter and spacing, heuristics were followed and they were values of 1 ft and 1 inch triangular spacing, respectively. In heat exchangers, baffles are implemented in order to support tubes to stay in place as well as assisting in directing flow of both tube and shell sections of the heat exchanger. Redirecting flow rates to the correct route aids in enhancing heat transfer that is occurring between the tube and shell sides. That being said, a lower pressure drop is generally more preferred in a shell and tube heat exchanger and vertical baffles provide a minimized pressure drop (Enerquip, n.d.). Therefore, a vertical baffle has been chosen for this system. On the contrary, horizontal baffles maximize the pressure drop in a system which in return has an impact on the leakage flow. Figure 34 below illustrates the difference between a vertical and a horizontal baffle.

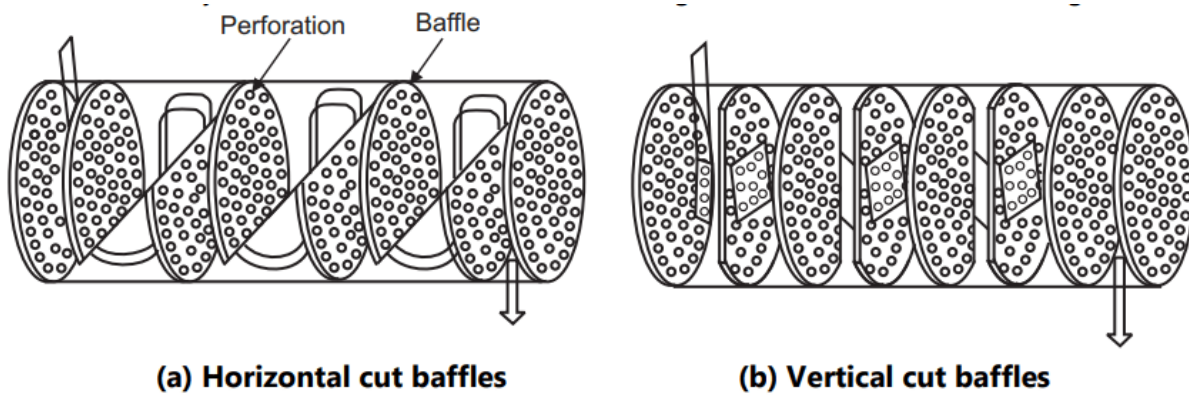


Figure 31: The Difference Between Horizontal and Vertical Baffles. (Rajibray, 2021)

The final thing that could be looked into is the type of materials that should be used in both shell and tube sides. In order to maximize heat transfer, materials should be conductive especially in the tube section of the heat exchanger. Typical materials that are used range from nickel, copper, brass and carbon. However, the key is to find a material that would augment the efficiency of heat transfer and is cost-effective simultaneously. Copper-nickel alloys possess a relatively high conductivity of 50 W/mK (Nickel Institute, n.d.), and are relatively cost effective in comparison to carbon based materials.

The second heat exchanger is located after the compressor and before the methanol bed reactor. The compressor increases the temperature of the materials to a value of 481°C and it needs to be 270 °C entering the methanol. Therefore a chosen utility should be able to cool down the stream. As widely utilized in industry, water is the first choice for a coolant and hence it is the chosen utility for this system. Components coming out of the compressor are gaseous, and therefore a pressure drop of 3 psi is occurring in the tubes, as for the shell-side, it is liquid water and so a pressure drop of 6 psi has been chosen. The temperature range that has to be used for water as a coolant ranges from 90 °F to 120 °F. The following table presents the operating conditions of the second shell and tube exchanger in terms of temperature, pressure and molar flows.

Table 34: Operating conditions of inlets and outlets of the second head exchanger.

	Hot in	Cold out	Cold in	Hot out
Temperature (°C)	481.2	270	32	48
Pressure (kPa)	1.15E+04	1.15E+04	101.34	41
Molar Flow (kmol/hr)	1.15E+07	1.15E+04	6.3E+07	6.3E+07

The same methodology has been followed in regards to calculations and simulation values. The extracted heat duty, Q, is a value of 7.33E+10 kJ/hr, overall heat transfer coefficient per area, UA, is 2.25E+08 kJ/°C-hr, correction factor is one and an uncorrected log mean temperature is an amount of 326.2 °C. As for hand calculated values, the log mean temperature was also 326.2 °C, and the R and S factors are 1.8 and 0.53. In order to achieve a correction factor that is larger than 0.85, a 4-8 heat exchanger has also been chosen for this system in which Figure 29 was employed in order to get the correction factor and it was a value of 0.88. The required surface area in which heat transfer occurs was calculated to be a value of 21754 ft² which is larger than 8000 ft² and therefore a configuration of 3 heat exchangers in parallel have been implemented with an area of 7251.2 ft² for each piece of equipment. Furthermore, the

volumetric flow rate of the tube side is 606788 ft³/hr, whereas the shell side is 121972.6 ft³/hr. The geometry chosen for the previous heat exchanger can also be used for this system considering that the resulting specifications are within the accepted range. All things considered, the number of tubes are 449 as well, however the tube velocity was a value of 24 ft/s which is within the desired range. Finally, spacing is one inch and triangular, whereas the shell inner diameter is 1 ft. The materials that are used in the first heat exchanger will also be used in this system considering that the components are almost identical in terms of inlets and outlets. Therefore copper-nickel will also be utilized, as well as a vertical baffle.

5.4. Pumps & Compressors

5.4.1. Pumps

There are a total of three pumps: two upstream and one downstream. The very first pump is used to pump out feed water into the solar reaction at a pressure of 35 bar to accommodate the relatively high conditions of temperature and pressure the reactor is to be run at. Water will arrive at a pressure of 1 bar and 25 °C and is fed to the pump with an outlet pressure of 35 bar and 25 °C. In order to size/ design the pump system some assumptions/ and or arbitrary values of control valve distance, reactor distance and height increase were calculated with respective values of 10 psi, 1.64 psi and 6.56 psi. The total required pressure change amounted to a value of 33.2 psi, whereas required head was of a value of 1215 ft. Some important values such as capacity and net positive suction head available were obtained from Aspen Plus and Aspen HYSYS, depending on the pump's location. It was observed that the system possesses quite a large capacity and a required head. Following certain expectations of how the system needs to be operated, centrifugal pumps have been chosen due to easy maintenance. A configuration of eight pumps in series and nine pumps in parallel is used to maximize efficiency. The process of finding important values such as brake horsepower, speed in rpm, impeller diameter, and net positive suction required entitles the utilization of a pump curve where capacity is plotted against total required head, and it is almost always provided by the manufacturer. The company that is manufacturing pumps for this system is called AIPU solids control and has provided the needed curves for sizing. Below is a step-by-step equation flow alongside a calculation sample for sizing the first water pump, refer to Appendix A for further calculations in regards to other pumps in the system.

Equation 83 is used to calculate the total pressure difference in the system, where $P_{reactor}$ is the pressure of the solar reactor and P_{in} is the pressure of water in the pump and P_{out} is the pressure change that is entering the solar reactor.

$$P_{reactor} - P_{in} = P_{out} \quad (83)$$

Equations 84 and 85 are based on heuristics to calculate the pressure drop of a control valve where for each 10 ft rise in elevation, a pressure drop of 4 psi is assumed. $D_{control\ valve}$ is the distance of a control valve in accordance to the pressure drop occurring, $D_{reactor}$ is the reactor's distance, $H_{control\ valve}$ is the height of the control valve.

$$2 \text{ psi}/100 \text{ ft} * D_{control\ valve} = D_{reactor} \quad (84)$$

$$4 \text{ psi}/10 \text{ ft} * H_{control\ valve} = H_{increase} \quad (85)$$

The next step is to calculate the total required pressure of the system which is simply the summation of pressure change obtained in equation (83) alongside control valve, reactor distance and height increase which is exhibited in the following equation:

$$H = P_{out} + D_{reactor} + H_{increase} + D_{control\ valve} \quad (86)$$

As discussed previously, some constant values were obtained from ASPEN PLUS/HYSYS and are the capacity, Q, in gpm with a value of 21189 and net positive suction available, NPSH_A, with a value of 32 ft. The very next step is to extract information from the pump curve provided by the manufacturer which is shown in Figures 32 and 33..

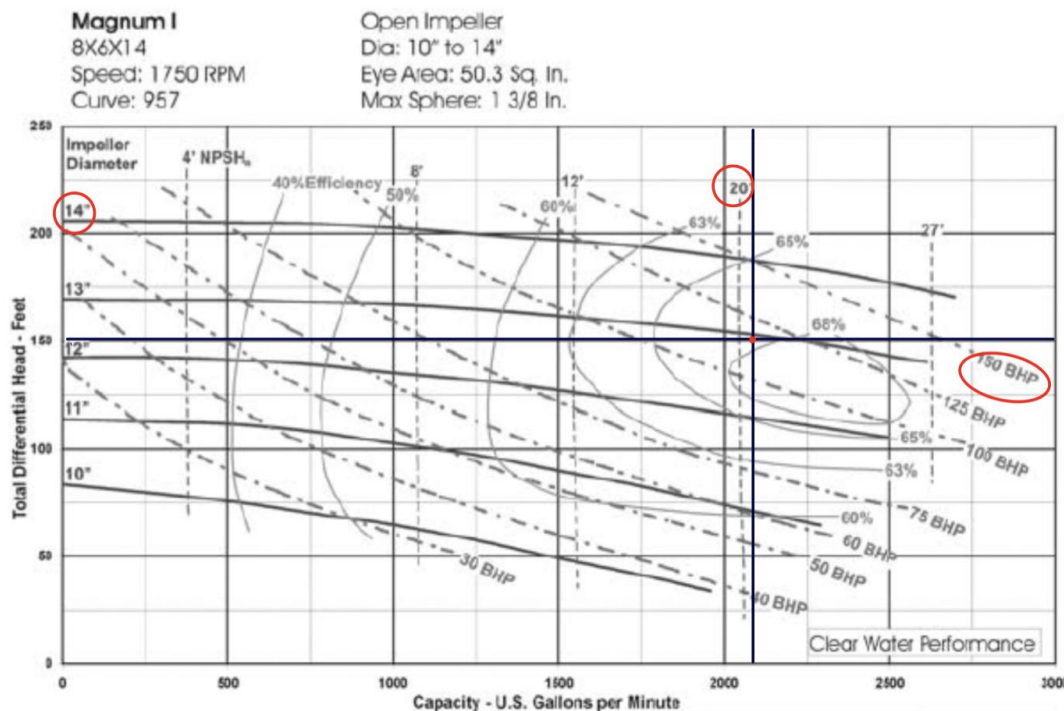


Figure 32: Pump Flow Performance Curve by AIPU with the Operating Point.

As illustrated in Figure 32, the capacity is around 2354.3 gpm considering that there are nine pumps in parallel, whereas the feet of head required is 150 ft knowing that we need eight pumps in series. The procedure requires choosing the brake horsepower, BH_p, that is above the intersection of the operating point. BH_p at this stage is the minimum that can be used for the system, meaning that in another system an even above value can be utilized which is not available for this system and thus a value of 150 hp was chosen. A similar concept applies to the speed, S_{shaft}, in RPM where a value of 1750 RPM has been chosen. The impeller diameter is provided alongside the curve and it amounts to 14". In addition, the net positive suction required was determined to be of a value of 20 ft.

The next step in terms of equation flow is to calculate the theoretical horsepower, TH_p, for the system to determine the margin of error in comparison to BH_p. Equation (87) below is provided by heuristics:

$$TH_p = \frac{Q * (\text{pressure increase})}{1714} \quad (87)$$

$$\text{Error \%} = \frac{BH_p - TH_p}{BH_p} * 100 \quad (88)$$

The subsequent step is to calculate the efficiency of the pump system sized where the capacity per pump, head ft required per pump, brake horsepower are employed and demonstrated in the following equation:

$$\text{Pump Efficiency} = \frac{Q * H}{3960 * BH_p} \quad (89)$$

For other systems where the components are other than water, specific gravity is used to scale the efficiency, considering that most curves are for water. The calculation sample of sizing the pump with the chosen configuration is shown below:

$$P_{\text{reactor}} - P_{in} = P_{out} \rightarrow 522 \text{ psi} - 14 \text{ psi} = 526 \text{ psi} \quad (90)$$

$$\frac{2 \text{ psi}}{100 \text{ ft}} * D_{\text{control valve}} = D_{\text{reactor}} \rightarrow 25 \text{ m} * 3.28 \frac{\text{ft}}{\text{m}} * \frac{2 \text{ psi}}{100 \text{ ft}} = 1.64 \text{ psi} \quad (91)$$

$$\frac{4 \text{ psi}}{10 \text{ ft}} * H_{\text{control valve}} = H_{\text{increase}} \rightarrow \frac{4 \text{ psi}}{10 \text{ ft}} * 5 \text{ m} * 3.28 \frac{\text{ft}}{\text{m}} = 6.56 \text{ psi} \quad (92)$$

$$H = 526 \text{ psi} + 1.64 \text{ psi} + 6.56 \text{ psi} + 10 \text{ psi} = 33.2 \text{ psi} \rightarrow 33.2 \text{ psi} * \frac{2.31 \text{ ft}}{\text{psi}} = 1215 \text{ ft} \quad (93)$$

$$THp = \frac{Q * (\text{pressure increase})}{1714} \rightarrow \frac{41247 \text{ GPM} * (80 \text{ psi})}{1714} = 109 \text{ hp} \quad (94)$$

$$\text{Pump Efficiency} = \frac{Q * H}{3960 * BHp} \rightarrow \frac{2354 \text{ gpm} * 152 \text{ ft}}{3960 * 150 \text{ hp}} = 61\% \quad (95)$$

In terms of safety, prevention of corrosion and prolonging the lifespan of the pump, the process design must determine if cavitation will be avoided. Cavitation can be defined as the event where the pressure of liquids is lower than saturated vapor pressure (Zhu et al., 2015), which results in the formation of air bubbles at very low pressures and as liquid feed is transferred from suction side of the impeller to the outlet, the bubbles collapse and cause damage to the materials as well as the mechanics of the overall pump system. Luckily, there are ways to steer clear from such a matter in terms of designing a system, the variable is known net positive suction head, NPSH, as stated previously in the text. The net positive suction head available, $NPSH_A$, must be greater than the net positive suction head required, $NPSH_R$. In this system, $NPSH_A$ is 32 ft whereas $NPSH_R$ is 20 ft, meaning that cavitation will be avoided.

The second pump in the system is located in the heat exchange section of the process, where pumped water is utilized as a utility to enter a spray quench and cool the constituents of the flowrate incoming from the solar reactor. This pump system has the same assumptions applied in terms of reactor and control valve distance, meaning they require the same value of total pressure. The overall capacity (Q) was 119316.32 gpm, theoretical horsepower (THp) was 140 hp, brake horsepower (BHp) was 150 hp. The configuration system is forty pumps in parallel and eight in series, which resulted in an efficiency of 76%. As for the net positive suction available was also a value of 32 ft and the extracted net positive suction required from the performance curve provided amounted to a value of 27 ft, which fortunately means that cavitation will be avoided.

An implementation of a large number of pumps in the system might not be economically feasible, however since we're feeding a large amount of water to cool down the stream coming out the water-gas shift reactor from 800 °C to 210 °C. The water is pumped at room temperature which requires a larger flow rate to be able to cool it down, which resulted in a great capacity. It is acknowledged that such an approach would have some economic implications and therefore a recommendation that can be implemented is to find the optimum amount of water that has the ability to lower the temperature of the stream in accordance with the required value. Another proposal would be to look for larger-scale pumps in industry and size it with correspondence of cavitation avoidance. Moreover, in terms of construction materials, water is the least abrasive component that could be used in a pump which expands the available choices of materials. Stainless steel has a prolonged life expectancy in comparison to other materials such as cast iron and bronze, and can be utilized in most if not all components of the pump such as: casing, impeller, column, shaft, bolting and collet.

5.4.2. Compressors

Compressors can generally be divided into positive displacement and dynamic compressors. Positive displacement compressors will capture air in the compression chamber and reduce the volume. This will cause an increase in pressure which is then going to discharge. Dynamic compressors generate power by bringing air into the rotating blade, causing restriction. Examples of positive displacement compressors include rotary screw, vane, and reciprocating air compressors. Generally, positive displacement compressors are utilized in small to medium-sized processes. On the other hand, centrifugal and axial are examples of dynamic compressors. Dynamic compressors are utilized in large process plants. In this case, a centrifugal compressor will be utilized in the upstream process after the zinc oxide reactor. The outlet stream of the zinc split reactor is fed through a mixer which is then fed through a compressor. The compressor will operate isentropically to 80 bar. It is important to note that during this process, the pressure will increase ideally from 35 bar to 115 bar. In addition to the pressure increase, the temperature of the outlet stream will increase. The table below illustrates important design parameters taken into consideration during the calculation process.

Table 35: Compressor Parameters

Parameter	Process Values	Units
Compressor Input Pressure	35	bar
Compressor Output Pressure	115	bar
Outlet Temperature	477.365	°C
Inlet Temperature	210	°C
Mass Density	0.0820193	lb/gal
Volumetric Flow	544149500	gal/hr
Mass Flow	12397.43363	lb/min
$\frac{c_p}{c_v}$	1.37	None

When examining the properties of a compressor, it is important to calculate pressure ratio, corrected mass flow, and temperature ratio. Equation 96 represents pressure ratio. Equation X represents the corrected mass flow. The discharge pressure is the pressure at the outlet of the compressor and the suction pressure is the pressure at the inlet of the compressor. The temperature ratio is calculated using the pressure ratio. Note that the compressor operates isentropically so the temperature equation is derived from the isentropic flow equations. In the

temperature ratio, the gamma parameter is present, which is the ratio between the specific heats. The corrected mass flow takes in the actual flow rate of the compressor and adds a parameter to transform the mass flow rate. In this case, the square root of the temperature ratio divided by the ratio of the pressure represents the correction parameter. It is important to note that temperature is taken in kelvins and pressure units have to be in psi.

$$\text{Pressure Ratio} = \frac{P_{\text{Discharge}}}{P_{\text{Suction}}} \quad (96)$$

$$\text{Temperature Ratio} = \left(\frac{P_{\text{Discharge}}}{P_{\text{Suction}}} \right)^{\frac{\gamma-1}{\gamma}} \quad (97)$$

$$\gamma = \frac{c_p}{c_v} \quad (98)$$

$$\text{Corrected Mass Flow} = \frac{W \sqrt{\frac{T_1}{545}}}{\frac{P_1}{28.4}} \quad (99)$$

Taking the above process values into consideration, the following process values were calculated.

$$\text{Pressure Ratio} = \frac{115 \text{ bar}}{35 \text{ bar}} = 3.29$$

$$\text{Temperature Ratio} = (2.4)^{\frac{1.37-1}{1.37}} = 1.27$$

$$\text{Corrected Mass Flow} = \frac{12397.43 \sqrt{\frac{410 \text{ F}}{545 \text{ F}}}}{\frac{507.632 \text{ psi}}{28.4 \text{ psi}}} = 601.58 \frac{\text{lb}}{\text{min}}$$

The pressure ratio and corrected mass flow equations are from the company Turbonetics so the values have been standardized to match their T-106 product line. When reviewing the required mass flow rate and the horse power, the T-106 line at Turbonetics fits the required parameters of a compressor. The Thumper 91-106 Turbo has a 91mm and larger compression wheel meaning that a range of 900-2400Hp can be produced. The pressure ratio and corrected mass flow are taken into consideration when calculating the efficiency and the number of compressors required for the process. A compressor performance map will be utilized to determine these values. The figure below is the compression performance map from Turbonetics. When reading a compression map, it is important to recognize the choke line, surge line, and efficiency island. Generally, the choke line is present near the right side of the graph and the surge line is near the left. The efficiency island is the middle of the graph with the highest efficiency rate. When designing compressors, it is desirable to land at the highest efficiency.

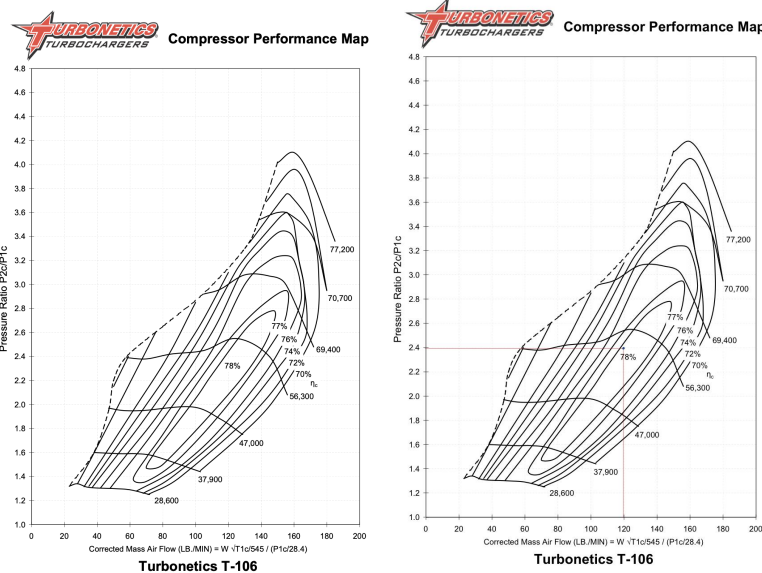


Figure 33: (a) Compressor Performance Map for T-106, (b) Compressor Performance Map Specifications

After the scaling process of the compressor performance map, it was determined that around one compressor in series and five compressors in parallel would produce the optimal performance. Figure xa represents the original compressor performance map for T-106. Figure xb represents the compressor performance map for the compressor utilized in this process. The scaled pressure ratio is around 2.4. The corrected mass air flow is around 120.31 lb/min. The efficiency of this configuration is at the highest efficiency island, which is around 78%.

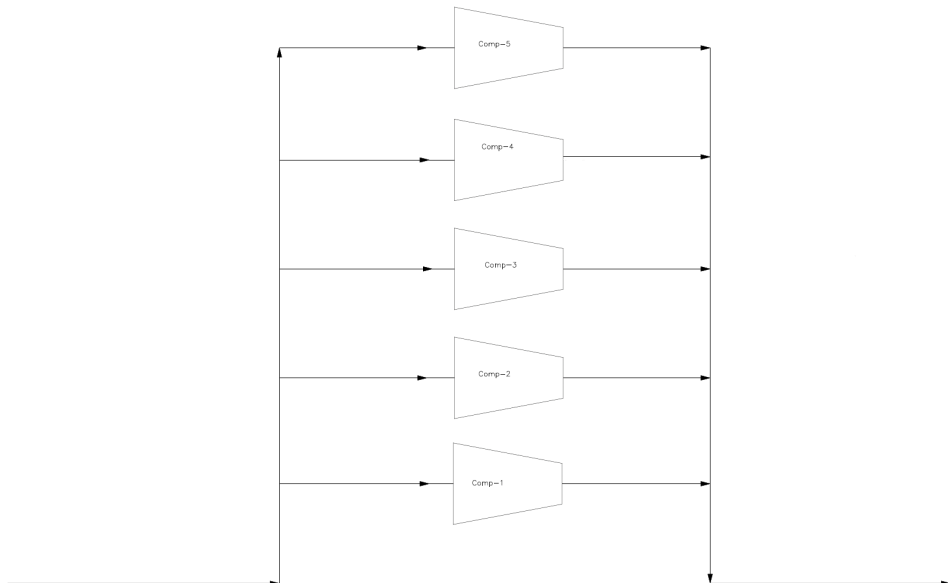


Figure 34: Compressor Configuration for Process

5.5 Heliostat Design

The first step in designing the heliostat field was to determine the energy requirement. A theoretical value was calculated by hand using the hand-calculated heat capacities, heats of reaction, and flow rates. The flow rates of each component were multiplied by the corresponding heat capacity to get the heat required to keep the temperature at 1450°C. The heats of reaction were multiplied by the flow rates of each component to get the energy required for the reactants to completely react. These two energy values were summed to get the total energy requirement of the solar reactor. These values and calculations are shown below.

Table 36. Hand Calculation of Heliostat Energy Requirement. The Energy Required to Heat Components was added to the Energy Required for Reactions to get the total Energy Requirement for the heliostat, shown in green.

Component	Energy Required to Heat Components (MW)	Energy Required for Reactions (MW)
Cellulose	11.0903	3.9267
Lignin	7.1446	28.6751
Methane	0.1917	0.0020
Ash	0.0007	0.0717
Water	1.0521	165.3090
Sum	217.4640 MW	

This value was used to determine the number and size of the heliostats with three different solar concentrations by using the Lewendowski Excel files. The final spreadsheets are shown in Appendix B. The heliostat design was determined for solar concentrations of 2000, 4000, and 8000 times the energy requirement. For each design, the goal was to find a tower height and the number of towers that would produce the amount of energy required. Some considerations for this design were keeping the number of towers to a minimum while also keeping the height of each tower below 200 m. The total energy from the tower also needed to be within 1% of the energy requirement of the solar reactor design in order to meet the energy requirement. In the Excel files used, the energy requirement used was determined from the input energy requirement of 217000 kWh/hour and the assumption that the heliostat was working for eight hours a day, 365 days per year. This calculated that the annual net energy required for the solar reactor was 633.6 GWhr, so the heliostat needed to produce between 627.0 GWhr and 640.0 GWhr.

In order to determine the cost of each heliostat design, the base cost was \$125 per square meter of mirror, and the base cost of a secondary concentrator is \$1250 per square meter. Likewise, the base cost of each tower is $[\$600,000 + 17.72 * (m)^{2.392}] * 1.41$ where m represents the height of each tower in meters. These calculations are shown for each heliostat design.

The first solar concentration that was considered was 2000 times solar concentration. In this design, there were two towers that were each 163.7 meters tall. This heliostat design would produce 633.4 GWhr of energy, and a diagram is shown below.

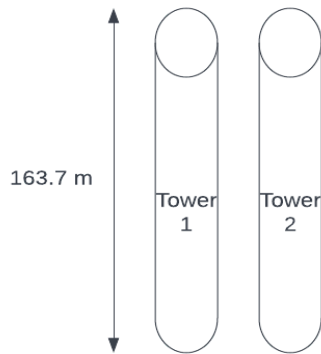


Figure 35. Heliostat Design for 2000 Times Solar Concentration.

For this heliostat design, the total heliostat area is 726,351 square meters. The base cost of the heliostat alone is \$90.79 million, and the base cost for the secondary concentrator alone is \$907.9 million. The cost of each tower in this design is \$3.56 million, which would make the total cost for both towers \$7.12 million. The total cost for this heliostat design would be \$1.0 billion.

The second solar concentration that was considered was 4000 times solar concentration, for which there were also two towers. In this design, however, each tower was 195.4 meters tall. This design would give 633.4 GWhr, and the tower design is shown below.

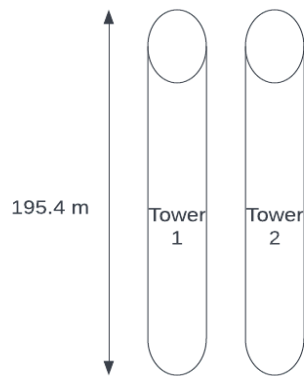


Figure 36. Heliostat Design for 4000 Times Solar Concentration.

In this heliostat design, there is a total heliostat area of 534,918 square meters. This would make the base cost of the heliostat \$66.86 million, and the base cost of the secondary concentrator \$668.65 million. The base cost of each tower in this design would be \$5.41 million, and the total cost of both towers would be \$10.82 million. The total base cost would be \$746.3 million.

The last heliostat design was for 8000 times solar concentration. In this design, there were five towers that were 184.8 meters tall each. This configuration of towers would give 633.8 GWhr, and it is shown below.

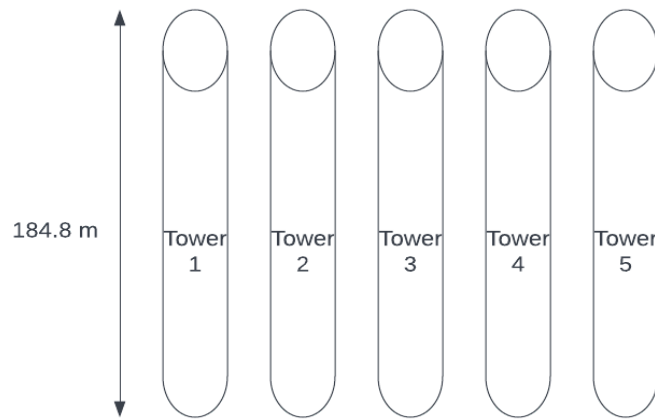


Figure 37. Heliostat Design for 8000 Times Solar Concentration.

In this heliostat design, the total heliostat area is 458,478 square meters, which would make the base cost of the heliostat alone \$57.3 million, and the base cost of the secondary concentrator \$573.1 million. The cost of each tower in this design would be \$4.72 million, and the total cost of all five towers would be \$23.59 million. This would make the total cost of both the heliostat and the secondary concentrator \$654.0 million.

As the solar concentration of the heliostat increases, the height of each tower as well as the number of towers increases, but the heliostat area decreases as solar concentration increases. This means that the total cost of the base case heliostat and the secondary concentrator also decreases as solar concentration increases because cost is proportional to the total area of the heliostat.

6. Utilities Summary & Heat Integration

As per the description of heat exchangers earlier in the report, there are three heat exchangers in the whole process. One after the cyclone to cool down the stream to a temperature of 210 °C prior to entering the ZnO bed, the second one is located after the compressor prior to entering the methanol bed reactor to scale the temperature to a value of 270 °C. Both these heat exchangers are shell-and-tube heat exchangers, and are employed to cool down the streams to meet the operating conditions of each reactor. The chosen utility for both equipment was cooling water, in which its temperature ranged from 90 °F to 120 °F. The second type of heat exchanger is known as a spray quench and has also been defined in previous sections in the report. The utilization of a spray quench is quite essential because it cools down components coming out of the solar reactor, which operates at a very large temperature of 1450 °C, even though the outlet stream of the solar reactor goes through a water-gas-shift reaction which cools down the reaction in some sense to a temperature of 800 °C. Another factor that makes an employment of a spray quench quite important is due to the fact that the inlets are a mixture of vapor, liquid and solid, resulting in a viscous sludge-like consistency, once again it is a cooling process in hopes to reduce the temperature from around 780 °C to 210 °C, however while taking into account some constraints, the temperature was only able to get to around 488 °C. Hence the addition of the shell-and-tube after the cyclone. Nevertheless, cooling water was also chosen in the spray quench as a cooling utility. Moreover, even though no other heat exchangers were utilized, the methanol bed reactor is a multi-tubular fixed bed, and one of its main characteristics is to use a heat transfer fluid to flow through the shell-side of the reactor to sustain temperature levels in a highly exothermic medium.

Aspen Energy Analyzer was used for heat integration purposes. The base-case simulation scenario resulted in the following values presented in table 37. As for table 38, it presents utilities in aspen plus alongside inlet and outlet temperatures, and target flow rates in kg/hr.

Table 37: Base Case Scenario of Heat Integration.

	HEN	% of Target
Heating (kJ/h)	7.831E+10	287.7
Cooling (kJ/h)	2.957E+10	363.5
Number of units	9	52.94
Total Area (m ²)	2.412E+6	9.24E-8

Table 38: Utilities, Temperature Inlets and Outlets, and Targeted Flow Rate.

Name	Inlet temperature (°C)	Outlet temperature (°C)	Target flow rate (kg/h)
MP Steam Generation	174	175	1606784.8
HP Stream Generation	249	250	0.00
Air	30	35	8.17E+8

Figures 38 and 39 are a demonstration of the base case scenario heat integration showing a general outline and pinch temperatures.

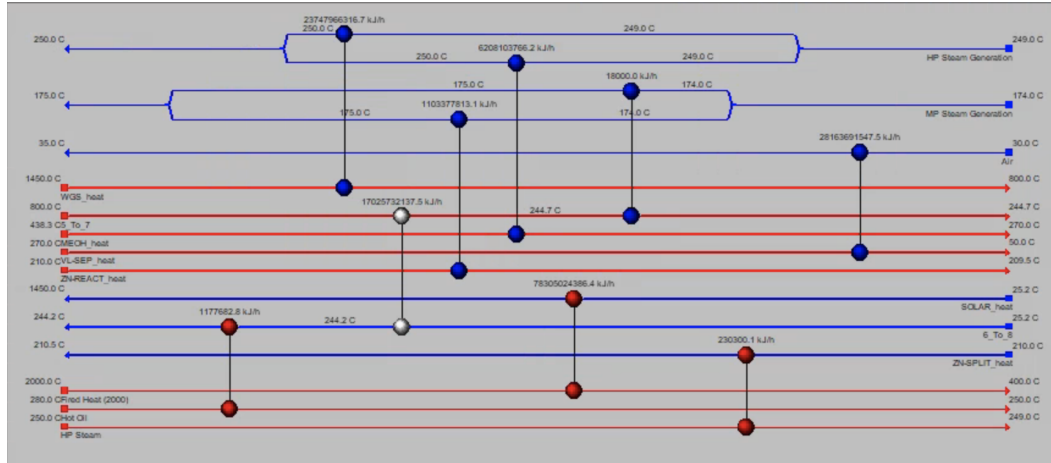


Figure 38: Heat Integration Network of Simulation Base Case.

Pinch temperatures represent the amount of temperature in which no heat transfer is occurring between cold and hot streams. Figure 39 shows the cross over between some streams and where they are located and how they affect the desired utility target.

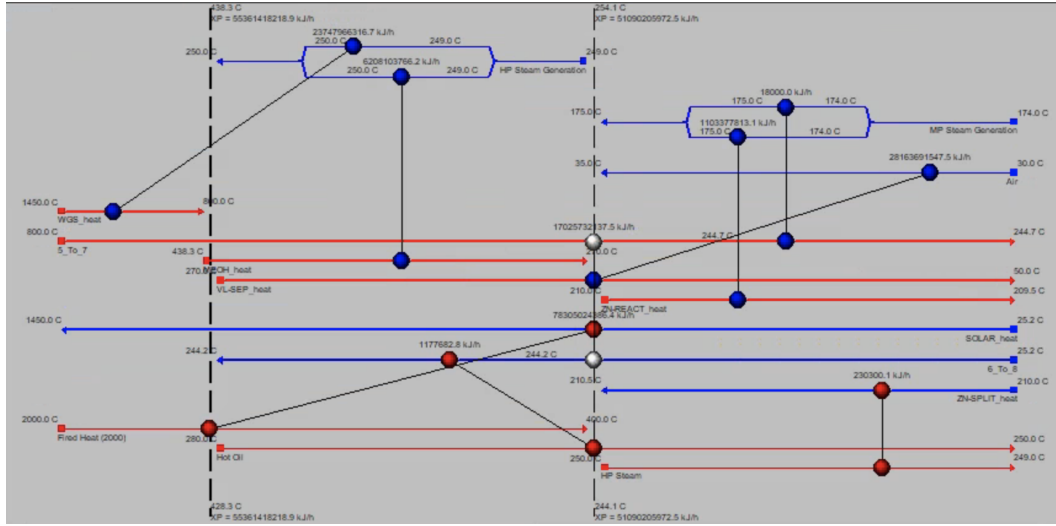


Figure 39: Pinch Temperature Crossover.

In order to get a converged HEN in energy analyzer, an iterative process is executed in which it recommends a number of designs that has the potential to minimize the amount of energy used in the process. For this system, it took four iterations for a converged proposal. Shown in table 39 below are the values in one of the recommended designs.

Table 39: Recommended Design Scenario of Heat Integration.

	HEN	% of Target
Heating (kJ/h)	2.977E+10	109.4
Cooling (kJ/h)	1.102E+10	135.5
Number of units	15	88.24
Total Area (m ²)	7E+6	2.56E-7

As per Table 39, the values of the percentage target are clearly less than the base case scenario. Where the targeted % of heating of the base case is 287.7, as for the recommended design it is a value of 109.4. Vice versa for cooling. Figure 40 and 41 below represent the general outline of the design and the pinch temperature cross over. Generally, the less crossover there is, the better the system in terms of energy savings.

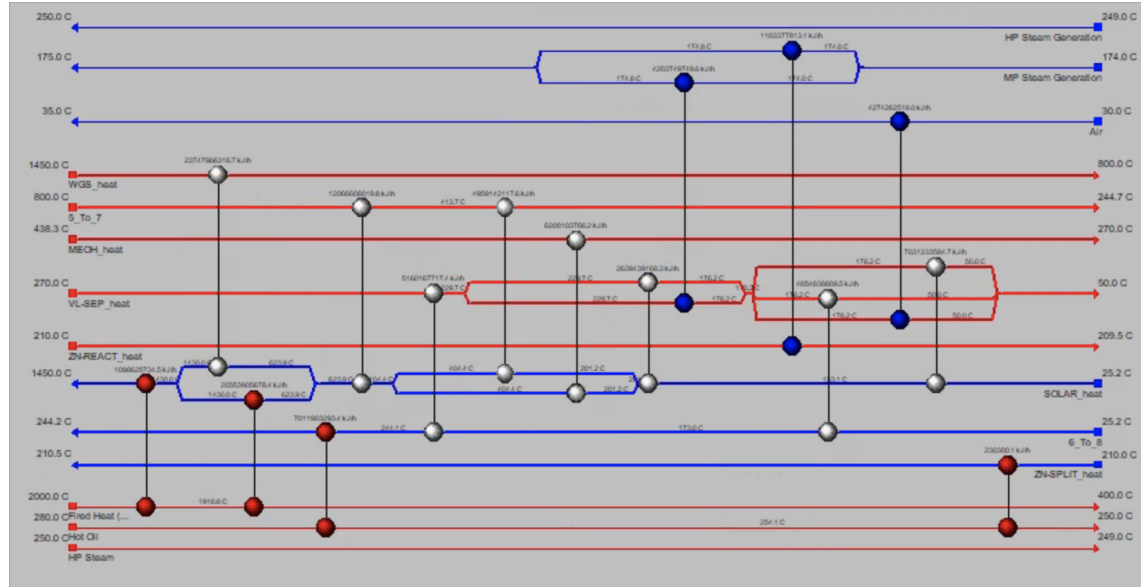


Figure 40: Heat Integration Network from a Recommended Design for Energy Savings.

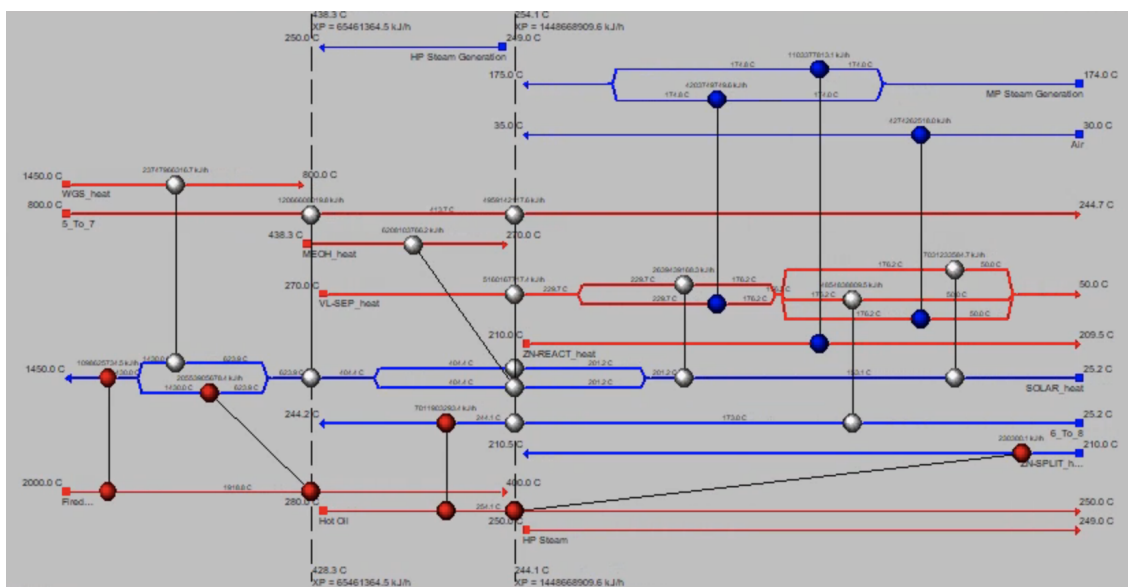


Figure 41: Pinch Temperature Crossover for Recommended Design.

Acquired from Aspen Plus, bar plots that can illustrate the difference between the actual utility energies and the targeted value when energy savings are employed for total, cooling and heating utilities.

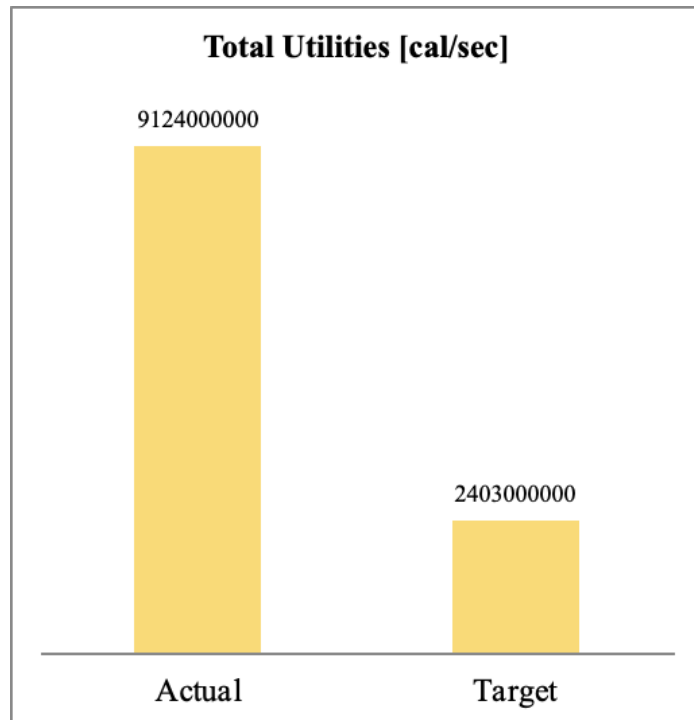


Figure 42: Actual Utilities vs Target Utilities.

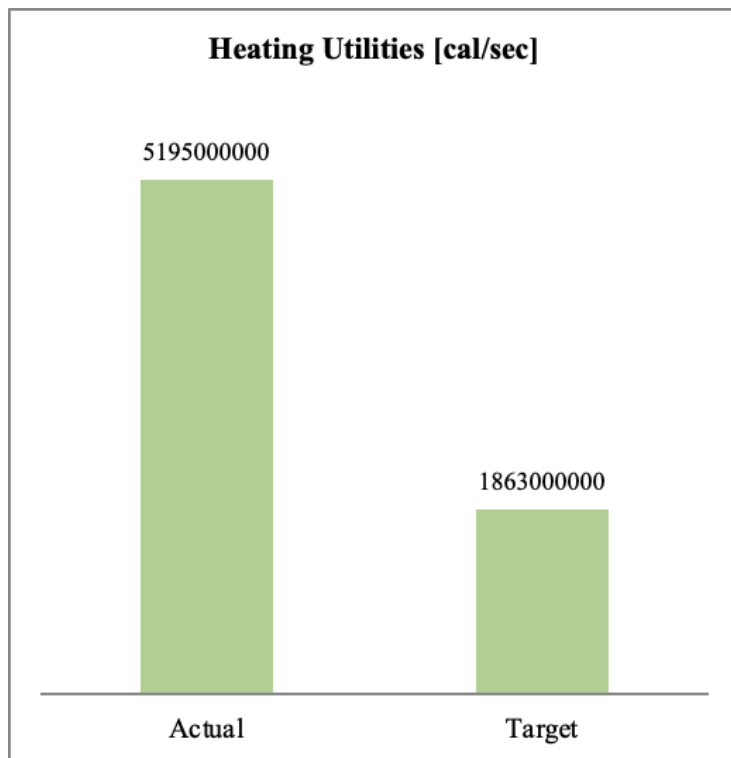


Figure 43: Actual Utilities vs Target Heating Utilities.

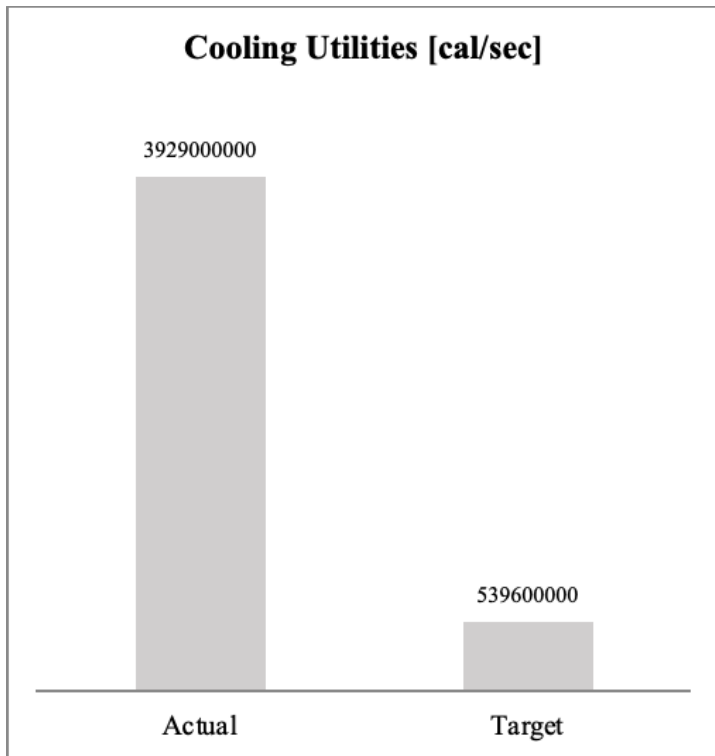


Figure 44: Actual Utilities vs Target Cooling Utilities.

As for cost analysis, energy savings would decrease in accordance with the amount of energy consumed. In other words, both variables are proportional and are sensitive to each other's variations. In the following table, a comparison of actual and targeted costs, as well as available savings and how many percentages of the actual price.

Table 40: The Cost of Actual and Target Utilities in the System.

Property	Actual	Target	% of Actual
Total Utilities (\$ Millions/Yr)	3679	1325	64
Heating Utilities (\$ Millions/Yr)	4353	1403	67
Cooling Utilities (\$ Millions/Yr)	674.8	77.65	88

The final thing that can be discussed in terms of energy is electricity. As per the information provided by aspen plus, the first pump in the system utilizes an amount of 5444 kW of electricity by pumping water into the solar reactor. The second pump in the system also pumps

water into the system, however into the spray quench as a utility. The amount of electricity the pump utilizes is 34745.9 kW.

7. Estimation of Capital Investment, Cash Flow, & Profitability Analysis

All equipment costs, barring the solar reactor, were determined from Matches with inputs of material and overall area. Tube cost for a given diameter was provided for the solar reactor. This cost was scaled to fit our modeled tube diameter, then multiplied by the length of each tube and the total number of tubes. All equipment costs were also adjusted with a CE index to account for inflation over time. Raw materials were determined by multiplying the ASPEN derived flow rates (in kg/hr) by the number of plant operational hours per year (hr/year), converted to gallons, and divided by the capacity of methanol in gallons per year. This quantity was multiplied by the cost of material to obtain the cost of raw material per gallon of methanol. Carbon credit was also included as one of the raw materials, reflecting the profit from reducing carbon production.

Table 41: Calculation of Number of Operators Required

Operation Unit	Elements	Process Classification	Number of Operators Required
Solar Reactor	Solids and fluids	Continuous	2
Spray Quench	Fluids	Continuous	1
Zinc Reactor	Solids and fluids	Semi-Batch	3
Methanol Reactor	Fluids	Continuous	1
Cyclone	Solids and fluids	Continuous	2
Distillation Column	Fluids	Continuous	1
Storage Tank	Fluids	Continuous	1
Pumps	Fluids	Continuous	1
Total Number of Operators Required	12		

This process plant produces 56 million gallons of methanol per year and operates 365 days per year. In total, approximately 153425 gallons of methanol are produced per day, which equates to 205 tons per day. The estimation of the number of operators required applies to processes that produce 10-100 tons of product per day. As such, the total number of operators

required is multiplied by a factor of 1.25 to be 15. The distillation column and storage tank are incorporated in the methanol purification plant, which runs 24 hr/day for 333 days per year. Assume 8 hours shifts where 4 workers are required for each shift, 12 workers are required per day. Since the solar plant runs 8 hours per day it also requires 12 workers per day. Taking into account weekends and replacement (due to vacation or sickness) days, an extra 24 workers should be employed.

The base case scenario was explored using the parameters provided. The IRR for the base case is 12.5%. The table below summarizes values such as selling price, NPV cash flow at the end of the period, NPV cash flow at the beginning of the period, capital investment, ROI, and payback period. It is important to note that the first year is spent designing the process plant, and two years are spent constructing it. The cash flow will be plotted for 27 years, but the plant is only fully running for 25 years.

Table 42: Base Case Important Financial Figures.

Financial Information	
Selling Price	\$ 2.49
NPV Cash Flow at the End of Period	\$ 9,713
NPV Cash Flow at the Beginning of Period	\$ 10,538
Capital Investment	\$ 35,265
ROI	18.9%
Payback Period	5.3 Years

Based on the table presented above, the payback period of the process plant is 5.3 years which is relatively fast. This indicates that the selling price of methanol balances out with the investments made. Figure 45 below is the cash flow throughout the process plant operation period.

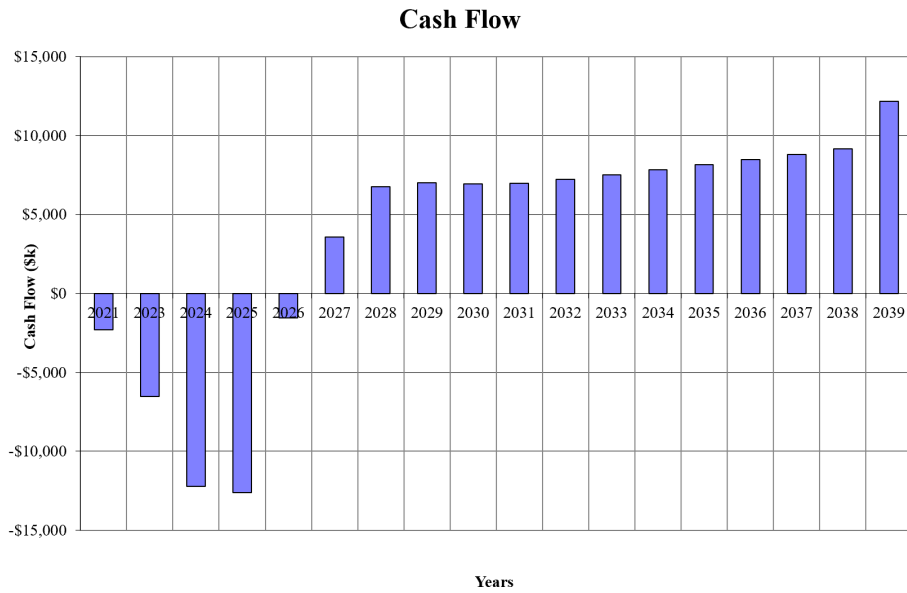
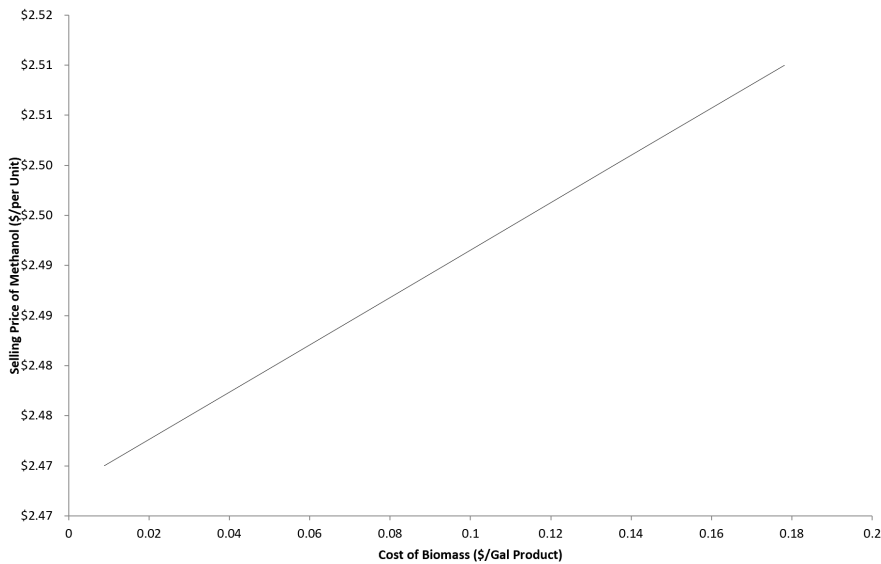


Figure 45: Base Case Cash Flow

The first five years (2021-2026) have a negative cash flow since time is spent building the process plant. In addition, working capital has to be paid, which further adds to the negative values. As the process plant gains stability in selling the methanol and investments are all paid back, cash flows start to increase, indicating an increase in profit. The relationship between cash flow and years is nonlinear and presents some concave functions. The max cash flow occurs in the year 2039, which is the end of the operation period.

After the base case was explored, multiple sensitivity analyses were performed to explore the relationship with the selling price of methanol. Parameters such as capital investment, cost of biomass/methane, number of operators, and IRR were varied. Figure 46 below is the sensitivity analysis between biomass and methanol selling prices. The relationship between these two variables is linear. As the cost of biomass increases, the selling price increases. This is an expected observation since increased biomass increases the expenses. In addition, Figure 46 shows a linear relationship between methane and selling price of methanol. Similar to biomass, as the cost of methane increases, the expenses increase causing an increase in selling price of methanol.

Biomass Price and Methanol Selling Price



Methane Cost and Methanol Selling Price

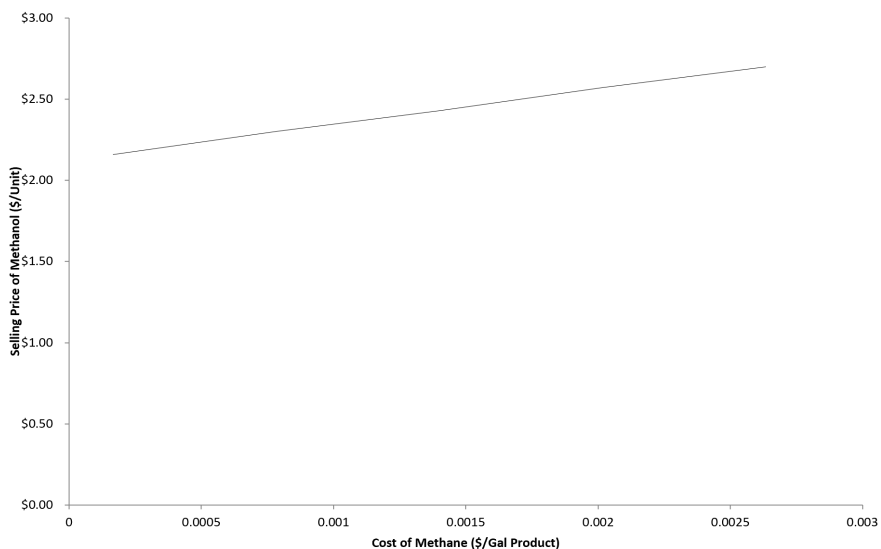


Figure 46: Biomass Price and Methanol Selling Price

Figure 47 below shows the relationship between the number of operators and the selling price of methanol. As the number of operators increases, the selling price of methanol increases linearly. This is also an expected behavior since an increase in the number of operators increases salary expenses.

Operators and Methanol Selling Price

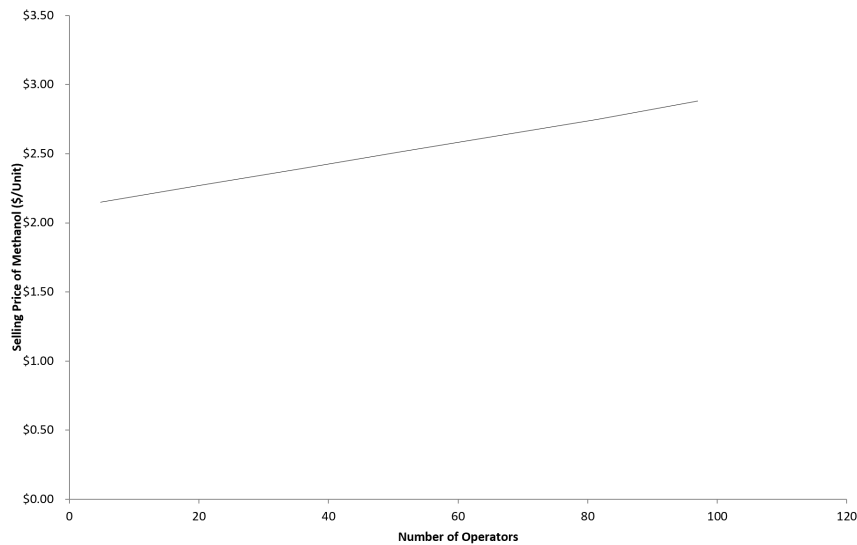


Figure 47: Number of Operators and Selling Price

Figure 48 below displays the change in the selling price of methanol with respect to the change in IRR. Unlike the other sensitivity analyses, the relationship between IRR and the selling price of methanol is some concave function indicating that the changes in IRR and selling price of methanol are not constant. Generally, as the IRR increases, the selling price of methanol increases. An increase in IRR indicates an increase in profitability which is reflected by the increase in the selling price of methanol.

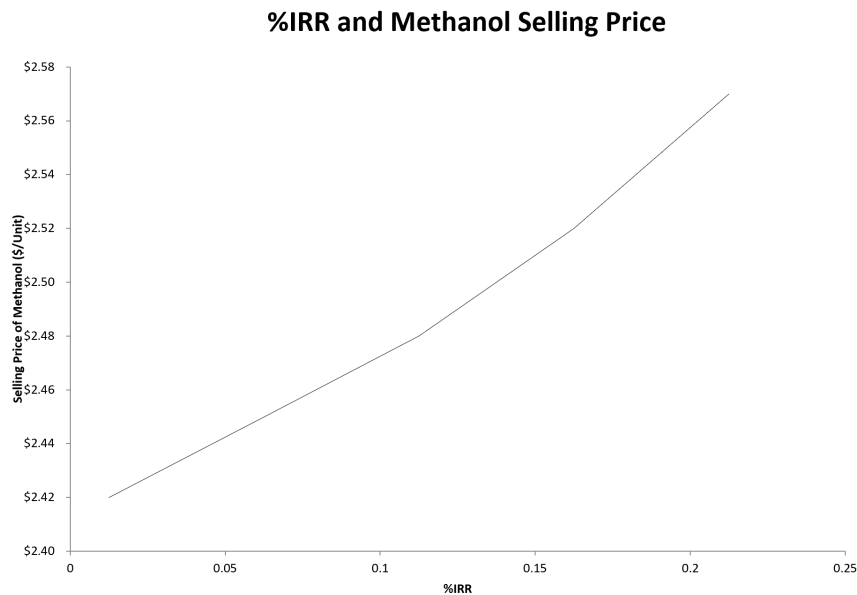


Figure 48: IRR and Methanol Selling Price

References

1. A review of the water gas shift reaction kinetics - researchgate. (n.d.). Retrieved November 23 2022 from
https://www.researchgate.net/publication/228506095_A_Review_of_the_Water_Gas_Shift_Reaction_Kinetics
2. Arab A. Marc Commenge Portha Falk Zamaniyan A. Tomašić V. . . Bussche K. (2014 March 15). Methanol synthesis from CO₂ and H₂ in multi-tubular fixed-bed reactor and multi-tubular reactor filled with monoliths. Retrieved December 7 2022 from
<https://reader.elsevier.com/reader/sd/pii/S0263876214001324?token=E452A1B7F76AB8F3BD33D4D3C2F81639275A82075BC7604C657BAF782FDCFFFFC91BD160D4119B63B49052E2779C18BD&originRegion=us-east-1&originCreation=20221207000935>
3. AIPU solid control. (n.d.). Retrieved December 8, 2022, from
<https://www.aipusolidcontrol.com/>
4. Axial flow curves - mwi pumps - moving water industries. MWI Pumps - Moving Water Industries - High Volume Water Pumps Accessories Repair Service and Rentals. (2020 October 5). Retrieved November 15 2022 from <https://mwipumps.com/axial-flow-curves/>
5. Ayodele B. Mustapa S. Tuan Abdullah T. & Salleh S. (2019 October 07). A Mini-Review on hydrogen-rich syngas production by thermo-catalytic and bioconversion of biomass and its environmental implications. Retrieved December 8 2022 from
<https://www.frontiersin.org/articles/10.3389/fenrg.2019.00118/full>
6. Boujjat H. Rodat S. & Abanades S. (n.d.). 1-10. In AIP Conference Proceedings 2126 180005 (2019).
7. Chemical synthesis of single atomic site catalysts. (n.d.). Retrieved December 7 2022 from
<https://pubs.acs.org/doi/10.1021/acs.chemrev.9b00818>
8. Cyclone Separator. (n.d.). Retrieved December 3 2022 from
https://energyeducation.ca/encyclopedia/Cyclone_separator
9. Cyclone Separator. (n.d.). Retrieved December 2 2022 from
<https://energyeducation.ca/encyclopedia/Energy>
10. Department of Labor Logo United States Department of Labor. OSHA Worker Rights and Protections | Occupational Safety and Health Administration. (n.d.). Retrieved December 8 2022 from <https://www.osha.gov/workers>

- 11.** Elsevier. (n.d.). Intensified convective heat transfer using ZnO nanofluids in heat exchanger with helical coiled geometry at constant wall temperature. In Materials science for energy technologies (pp. 161–170). essay.
- 12.** Environmental Protection Agency. (n.d.). EPA. Retrieved December 8 2022 from <https://www.epa.gov/ghgreporting>
- 13.** Environmental Protection Agency. (n.d.). EPA. Retrieved December 8 2022 from <https://www.epa.gov/hwpermitting>
- 14.** Felder R. M. Rousseau R. W. & Bullard L. G. (2020). Elementary Principles of Chemical Processes. Wiley.
- 15.** Feng W. & Qian Z. (2016 June 2). Simulation of cavitation performance of an axial flow-sage journals. Retrieved November 23 2022 from <https://journals.sagepub.com/doi/10.1177/1687814016651583>
- 16.** Frilund C. Simell P. Kaisalo N. Kurkela E. & Koskinen-Soivi M.-L. (2020). Desulfurization of biomass syngas using zno-based adsorbents: Long-term hydrogen sulfide breakthrough experiments. Energy & Fuels 34(3) 3316–3325. <https://doi.org/10.1021/acs.energyfuels.9b04276>
- 17.** G. Kandlikar S. (2013 October 31). Single-phase liquid flow in minichannels and microchannels. Retrieved December 7 2022 from <https://www.sciencedirect.com/science/article/pii/B978008098346200003X>
- 18.** Garbis P. Kern C. & Jess A. (2019). Kinetics and reactor design aspects of selective methanation of CO over a Ru/ γ -al₂O₃ catalyst in CO₂/H₂ Rich Gases. Energies 12(3) 469. <https://doi.org/10.3390/en12030469>
- 19.** Gas cooling nozzles. Spray Nozzles for Gas Cooling. (n.d.). Retrieved December 1 2022 from <https://www.spray-nozzle.co.uk/spray-nozzle-applications/gas-cooling>
- 20.** Gunugunuri K. R. & Smirniotis P. G. (2015). Chapter 1 - Introduction About WGS Reaction. In Water gas shift reaction: Research Developments and Applications (pp. 1–20). essay Elsevier.
- 21.** Heat transfer from a cylinder in axial turbulent flows. (2004 December 22). Retrieved December 7 2022 from <https://www.seas.upenn.edu/~lior/>
- 22.** Institute H. (2021 November 03). Materials for circulating water pumps at power plants. Retrieved November 23 2022 from <https://www.pumpsandsystems.com/materials-circulating-water-pumps-power-plants>

- 23.** Johnson J. A. Hrenya C. M. & Weimer A. W. (2002). Intrinsic reaction and self-diffusion kinetics for silicon carbide synthesis by rapid carbothermal reduction. *Journal of the American Ceramic Society* 85(9) 2273–2280. <https://doi.org/10.1111/j.1151-2916.2002.tb00447.x>
- 24.** K.Reddy G. (2015 July 17). Introduction about WGS reaction. Retrieved November 22 2022 from <https://www.sciencedirect.com/science/article/pii/B9780124201545000012>
- 25.** Kitchin J. (n.d.). The Kitchin Research Group. Water gas shift equilibrium via the NIST Webbook. Retrieved December 1 2022 from <https://kitchingroup.cheme.cmu.edu/blog/2013/02/01/Water-gas-shift-equilibria-via-the-NIST-Webbook/>
- 26.** Leiviskä Mayara & Leiviskä. (2017 November 17). Modeling in methanol synthesis. Retrieved December 7 2022 from <https://reader.elsevier.com/reader/sd/pii/B9780444639035000170?token=826480E9A4C2456A8CBF9671439F09F3EEF71CBFEB0CAD9590C9DF8C874FFF8BA18FD7AA0CB3964CA916C3E254DD99A4&originRegion=us-east-1&originCreation=20221207000835>
- 27.** Liza P. (2020 November 11). Perry's Chemical Engineers' handbook. Retrieved December 8 2022 from https://www.academia.edu/44481513/Perrys_Chemical_Engineers_Handbook
- 28.** Mechanical properties of copper-nickel alloys. (n.d.). Retrieved December 6 2022 from <https://nickelinstitute.org/en/about-nickel-and-its-applications/copper-nickel-alloys/mechanical-properties-of-copper-nickel-alloys/>
- 29.** Methanol synthesis. (n.d.). Retrieved December 8 2022 from <https://www.sciencedirect.com/topics/engineering/methanol-synthesis>
- 30.** Morin M. Pécate S. & Hémati M. (2018). Experimental study and modeling of the kinetic of biomass char gasification in a fluidized bed reactor. *Chemical Engineering Research and Design* 131 488–505. <https://doi.org/10.1016/j.cherd.2017.09.030>
- 31.** Negri M. (2018 April 5). New technologies for ammonium dinitramide based monopropellant thrusters.
- 32.** Physical and chemical characterization of ashes. (n.d.). Retrieved December 4 2022 from https://www.researchgate.net/publication/236338043_Physical_and_chemical_characterization_of_ashes_from_municipal_solid_waste_incinerator_in_China
- 33.** Portha J.-F. Parkhomenko K. Kobl K. Roger A.-C. Arab S. Commengé J.-M. & Falk L. (2017). Kinetics of methanol synthesis from carbon dioxide hydrogenation over copper-zinc oxide catalysts. *Industrial & Engineering Chemistry Research* 56(45) 13133–13145. <https://doi.org/10.1021/acs.iecr.7b01323>

- 34.** Publisher of open access journals. (n.d.). Retrieved December 6 2022 from <https://www.mdpi.com/>
- 35.** Radkara. (2019 February 13). Intensified convective heat transfer using zno nanofluids in heat exchanger with helical coiled geometry at constant wall temperature. Retrieved December 4 2022 from <https://www.sciencedirect.com/science/article/pii/S2589299118301678>
- 36.** Rajibray. (2021 November 27). Heat interchangers. Retrieved December 6 2022 from <https://pharmacygyan.com/heat-interchangers/>
- 37.** Review of mass-transfer correlations for packed columns. (n.d.). Retrieved December 4 2022 from <https://pubs.acs.org/doi/10.1021/ie050017w>
- 38.** Rumbino Y. Purwono S. & Hidayat M. (n.d.). 1-10. In AIP Conference Proceedings 2014 020086.
- 39.** Sadeghbeigi R. (2012 January 27). Process and mechanical design guidelines for FCC Equipment. Retrieved December 2 2022 from <https://www.sciencedirect.com/science/article/pii/B9780123869654000112>
- 40.** Sadhwani N. S. (2017). Conversion of Carbon Dioxide and Biomass for Fuels and Chemicals Precursor through Gasification: Experimental and Modeling Approach (dissertation).
- 41.** SDS Search. (n.d.). Retrieved December 8 2022 from <https://www.fishersci.com/us/en/catalog/search/sdshome.html>
- 42.** SDS Search. Airgas. (n.d.). Retrieved December 8 2022 from <https://www.airgas.com/sds-search>
- 43.** Seider W. D. (2010). Product and process design principles: Synthesis analysis and evaluation. Hoboken: Wiley.
- 44.** Smith R. J. Muruganandam L. & Murthy S. S. (2010). Cheminform Abstract: A review of the water gas shift reaction kinetics. ChemInform 41(38). <https://doi.org/10.1002/chin.201038231>
- 45.** Spray nozzles & systems. BETE Spray Technology. (2022 November 7). Retrieved December 8 2022 from <https://bete.com/>
- 46.** Turbochargers. Turbonetics. (n.d.). Retrieved December 8 2022 from <https://www.turboneticsinc.com/industrial/product/turbochargers-0>
- 47.** Turton R. Berry D. A. Gardner T. H. & Miltz A. (2004). Evaluation of zinc oxide sorbents in a pilot-scale transport reactor: sulfidation kinetics and reactor modeling. Industrial & Engineering Chemistry Research 43(5) 1235–1243. <https://doi.org/10.1021/ie030364a>

- 48.** Turton R. Berry D. A. Gardner T. H. & Miltz A. (2004). Evaluation of zinc oxide sorbents in a pilot-scale transport reactor: sulfidation kinetics and reactor modeling. *Industrial & Engineering Chemistry Research* 43(5) 1235–1243. <https://doi.org/10.1021/ie030364a>
- 49.** Wang C.-P. (1989). Dynamic models of the high temperature desulfurization process in a fixed-bed reactor (dissertation). University Microfilms Int. Ann Arbor.
- 50.** Woodruff R. & W. Weimer A. (2012 October 04). A novel technique for measuring the kinetics of high-temperature gasification of biomass char with steam. Retrieved December 8 2022 from <https://www.sciencedirect.com/science/article/pii/S001623611200748X>
- 51.** Zhang Y. Xiao J. & Shen L. (n.d.). Simulation of methanol production from biomass ... - ACS publications. Retrieved December 8 2022 from <https://pubs.acs.org/doi/10.1021/ie801983z>
- 52.** Zhu H. Qiu N. Wang C. Si Q. Wu J. Deng F. & Liu X. (2021 November 15). Prediction of cavitation evolution and cavitation erosion on centrifugal pump blades by the DCM-RNG method. Retrieved November 22 2022 from <https://www.ncbi.nlm.nih.gov/pmc/articles/PMC8608526/>

Table of Nomenclature

Symbol	Definition	Units
C_p	Heat Capacity	kJ/hr
C_i	Heat Capacity Constant	kJ/hr
ΔH_R	Heats of reaction	kJ/K
H_f	Heats of formation	kJ/K
r_i	Rate of reaction	M/min
k	Kinetic rate constant	1/M s
K	Kinetic equilibrium constant	Unitless
T	Temperature	K
b	Adsorption parameter constant	$\frac{mol}{s \text{ bar } kg_{cat}}$
R	Ideal gas constant	J/mol-K
T_0	Inlet Temperature	C/K/F
r_A	Rate of reaction of A	M/min
F_i	Flow rate of species i	kmol/hr
T_c	Coolant temperature	C/K/F
U_a	Overall heat transfer coefficient	W/m ² -K
P	Pressure	kPa/bar/psi
P_0	Inlet pressure	kPa/bar/psi
V_0	Inlet volumetric flow rate	m ³ /hr
F_{T0}	Inlet molar flow rate	kmol/hr
F_T	Molar flow rate	kmol/hr
W	Weight of catalyst	g

A_c	Cross sectional area	m^2
A_s	Surface area	m^2
ρ	Density	kg/m^3
ϕ	Void fraction	Unitless
N_{min}	Minimum number of stages	Unitless
N	Actual number of stages	Unitless
D_i	Distillate flow rate	$kmol/hr$
B	Bottoms flow rate	$kmol/hr$
x_i	Mole fraction	Unitless
α	Volatility	Unitless
R_{min}	Minimum reflux ratio	Unitless
R	Reflux ratio	Unitless
Θ	Theta	Unitless
q	Saturated amount of liquid moles	mol
D_T	Column diameter	ft^2/m^2
U_f	Flooding velocity	m/s
G	Gas flow rate	kg/hr
L	Liquid flow rate	kg/hr
f	Vapor flooding fraction	Unitless
A_d	Downcomer Area	m^2
A_T	Tower cross sectional area	m^2
F_{LG}	Flooding parameter	m/s
F_{ST}	Surface tension factor	N

F_F	Foam factor	Unitless
F_{HA}	Hole factor	Unitless
C_{SB}	Flooding correlation	ft/s
C	Empirical capacity	ft/s
H_i	Height of a certain equipment	m/ft
ΔT_{lm}	Log mean temperature	C/K/F
R	Heat transfer parameter	Unitless
S	Heat transfer parameter	
θ	Residence Time	sec
ρ_l	Density of Drop	kg/m ³
λ	Heat of Vaporization	J/kg
D_0	Drop Diameter	m
k_g	Thermal Conductivity	J/(s m K)
ΔT	Log Mean Temperature Difference	K
$P_{Discharge}$	Discharge Pressure	bar
$P_{Suction}$	Suction Pressure	bar
c_p	Specific Heat Capacity	J/(mol K)
c_v	Specific Heat Capacity	J/(mol K)
m	Mass Flow Rate	kg/hr
C_{pg}	Heat Capacity of Gas	kJ/mol K
T_g	Temperature of Gas	K

z	Length of ZnO Reactor	m
h_g	Gas-solid Heat Transfer Coefficient	W/m ² K
a_v	Gas-Solid Interfacial Area per Unit Volume	m
T_s^s	Solid Surface Temperature	K
R_0	Initial Radius of Grains	m
C_{H2S}	Concentration of H ₂ S at Surface	mol/L
Z_v	Ratio of the Molar Volume of the Product to That of the Reactant	Unitless
x	Conversion	Unitless
D_{eff}	Effective Diffusivity through the Product Layer	m ² /s
G	Superficial Mass Velocity	mol/cm ² s
ρ	Gas Density	mol/L
D_p	Diameter of ZnO Particle	μm
ϕ	Porosity	Unitless
μ	Viscosity of Gas Passing Through the Bed	kg/m s
k_g	Gas thermal Conductivity	W/mK
h_w	Gas-wall convection coefficient	W/m ² K
μ_g	Gas viscosity	Pas
V_m	Total microcontainer volume	m ³
ρ_c	Density of carbon	kg/m ³

d_i	Internal diameter	m
H_{pg}	Heating between particles and gas	Calculated from equation 23
H_{wg}	Heating between wall and gas	Calculated from equation 24
h_m	Gas microcontainer convection coefficient	W/m ² K
T_m	Temperature of microcontainer	K
MW_c	Molecular weight of carbon	kg/mol
T_w	Wall temperature	K
A_m	Aggregate surface	m ³
F_c	Initial molar flow rate of carbon	mol/s
p_m	Density of microcontainer	kg/m ³
MW_m	Molecular weight of microcontainer	g/mol
ϵ_m	Radiative emissivity	Unitless

Appendices

Appendix A (Sample Calculations)

3.6 Energy Balances

A sample calculation of the heat capacity of methanol is shown below. Heat capacity constants were found in Perry's Chemical Engineer's Handbook are shown and the equation used to calculate the integrated heat capacity from room temperature to the reactor temperature of 1450°C.

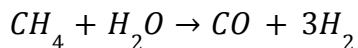
Table 43: Heat Capacity Constants for Methanol for C_p in kJ/mol K.

C ₁	C ₂	C ₃	C ₄	C ₅
0.033298	0.079933	0.0020869	0.041602	0.00099196

$$\Delta H = C_1 \Delta T + C_2 C_3 \cosh(C_3 / \Delta T) - C_4 C_5 \tanh(C_5 / T)$$

Inputting the heat capacity constants gives $\Delta H = 161.35 \text{ kJ/mol}$.

Likewise, the heats of reaction at room temperature were calculated for each reaction occurring in this process. A sample reaction is as follows:



The heats of formation were used to determine the heat of reaction at room temperature, and they are shown in the table below.

Table 44: Heats of Formation of Sample Calculation.

Component	Heat of Formation (kJ/mol)
CH ₄	-74.85
H ₂ O	-285.83
CO	-110.52
H ₂	0

The heat of reaction at room temperature was calculated by subtracting the heat of formation of the reactants from the heat of formation of the products. This is shown below.

$$\Delta H_{rxn} = (-110.52 + 3 * 0) - (-74.85 - 285.83) = 250.16 \text{ kJ/mol}$$

In a similar fashion, the heats of combustion of each reaction were calculated by using those of the components. A sample reaction is shown below, followed by the heats of reaction for each component.

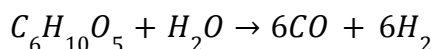


Table 45: Heats of Combustion for Sample Reaction.

Component	Heat of Combustion (kJ/mol)
C ₆ H ₁₀ O ₅	-2811.64
H ₂ O	0
CO	-282.99
H ₂	-285.84

The heat of combustion for this sample reaction was determined by subtracting the heats of combustion of the reactants from that of the products, as shown below.

$$\Delta H_{combustion} = (-282.99 - 285.84) - (-2811.64 + 0) = 601.34 \text{ kJ/mol}$$

Finally, the overall heat of reaction of each reaction was determined by adding the heat of reaction of the products, reactants, the heat of combustion, and the heat of vaporization of water was subtracted if necessary. A sample calculation of this is shown below for the reaction of cellulose.

Table 46: Heat of Reaction Calculation for Sample Reaction.

Heat of Reaction of Reactants	-865.49 kJ/mol
Heat of Reaction of Products	641.75 kJ/mol
Heat of Reaction at Room Temperature	601.34 kJ/mol
Heat of Vaporization of Water	40.8 kJ/mol
Overall Heat of Reaction	336.79 kJ/mol

These values were used in the energy balances on the corresponding reactors that they occurred in.

Sample calculations for determining gas temperature energy balance values for the solar reactor can be found below:

$$F_c = 51.1489 \frac{\text{kmol}}{\text{hr}} \times \frac{1000\text{mol}}{1 \text{kmol}} \times \frac{1\text{hr}}{3600\text{s}}$$

$$A_m = \frac{6V_m}{d_m} = \frac{6(0.365m^3)}{0.02m} = 109.5 m^3$$

Assuming particles in the solar reactor are constant throughout the length:

$$A_m = \frac{6V_m}{d_m} = \frac{6(0.001853)}{0.02m} = 0.556 m^3$$

$$MW_c = \frac{162.1406 \text{ g/mol} + 180.2045 \text{ g/mol}}{2} = 171.172 \frac{\text{g}}{\text{mol}} \times \frac{0.001 \text{ kg}}{1\text{g}} = 0.1711725 \text{ kg/mol}$$

$$h_m = \frac{k_g}{R_o} = \frac{0.05478}{0.0762 \text{ m}} = 0.7189 \frac{\text{W}}{\text{m}^2 \text{K}}$$

$$\rho_c = 1.41157 \frac{\text{mol}}{\text{L}}, 15270.1 \frac{\text{mg}}{\text{L}} \times \frac{1 \times 10^{-6} \text{ kg}}{1 \text{ mg}} \times \frac{1\text{L}}{0.001 \text{ m}^3} = 15.2701 \frac{\text{kg}}{\text{m}^3}$$

5.2 Separators

5.3 Heat Exchangers

For the first heat exchanger located after the cyclone, the following sample calculations were conducted, starting with calculating the log mean temperature:

$$\Delta T_{LM} = \frac{\Delta T_1 - \Delta T_2}{\ln(\Delta T_1 / \Delta T_2)} \quad (100)$$

$$\Delta T_{LM} = \frac{433.2 \text{ C} - 238.8 \text{ C}}{\ln(433.2/238.8)} = 326.4 \text{ C}$$

The heat transfer parameters R and S:

$$R = \frac{T_{H,in} - T_{H,out}}{T_{C,out} - T_{C,in}} = \frac{481.2 \text{ C} - 48 \text{ C}}{270 \text{ C} - 32 \text{ C}} = 1.8 \quad (101)$$

$$S = \frac{T_{H,in} - T_{H,out}}{T_{C,out} - T_{C,in}} = \frac{270 \text{ C} - 32 \text{ C}}{481.2 \text{ C} - 32 \text{ C}} = 0.53 \quad (102)$$

Area in which heat transfer occurs upon:

$$A = \frac{Q}{U^* F_r * \Delta T_{LM}} = \frac{2.44E+8 \text{ kJ/hr}}{1277 \text{ W/m}^2 \text{ C} * 0.87 * 326 \text{ C}} = 673.6 \text{ m}^2 \quad (103)$$

Volumetric flow rate of tube side:

$$Vol\ flow\ tube = \frac{Q}{\rho * C_p * \Delta T} = \frac{2.44E+8\ kJ/hr}{24\ kg/m^3 * 2.7\ kJ/kg-C*210\ C} = 17336.7\ m^3/hr = 606797\ ft^3/hr \quad (104)$$

Number of tubes:

$$N = 7251\ ft^2 / 2.5\ ft^2 / 8 = 359 \quad (105)$$

Velocity of tubes:

$$v_{tube} = 606797\ ft^3/hr / 0.015\ ft^2 / 359 / 3600 = 31\ ft/s \quad (106)$$

5.4 Pumps and Compressors

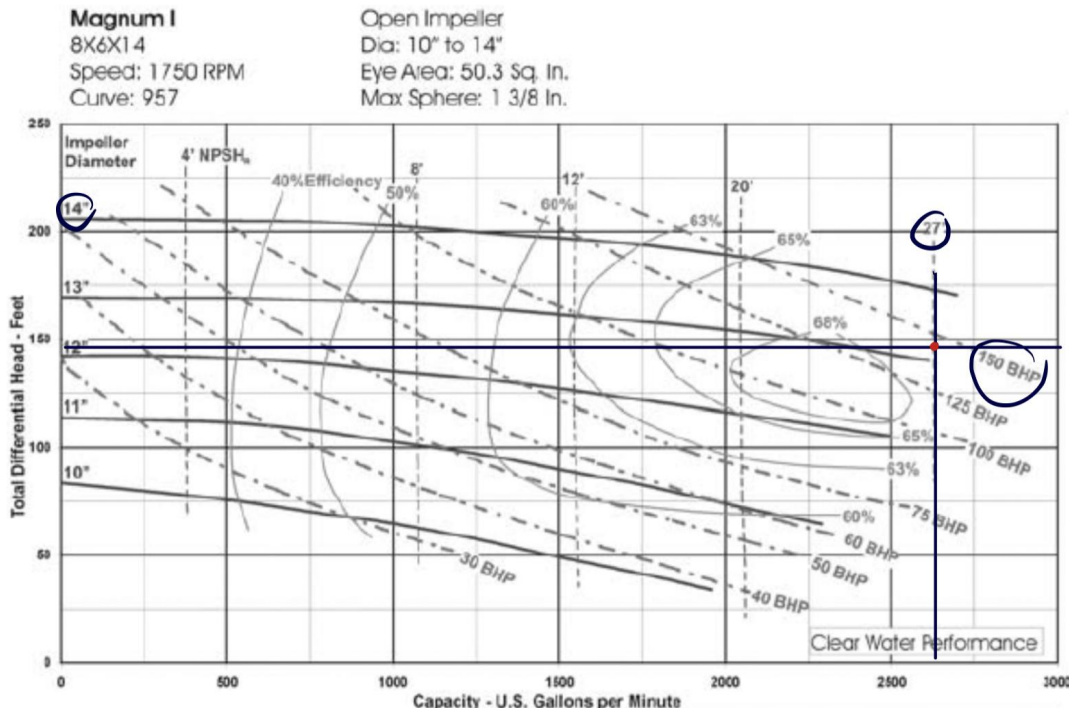


Figure 49: Second Pump Performance Curve with Operating Point.

The calculations of sizing the second pump in the system is as follows:

$$P_{reactor} - P_{in} = P_{out} \rightarrow 522\ psi - 14\ psi = 526\ psi \quad (107)$$

$$\frac{2 \text{ psi}}{100 \text{ ft}} * D_{control \text{ valve}} = D_{reactor} \rightarrow 25 \text{ m} * 3.28 \frac{\text{ft}}{\text{m}} * \frac{2 \text{ psi}}{100 \text{ ft}} = 1.64 \text{ psi} \quad (108)$$

$$\frac{4 \text{ psi}}{10 \text{ ft}} * H_{control \text{ valve}} = H_{increase} \rightarrow \frac{4 \text{ psi}}{10 \text{ ft}} * 5 \text{ m} * 3.28 \frac{\text{ft}}{\text{m}} = 6.56 \text{ psi} \quad (109)$$

$$H = 526 \text{ psi} + 1.64 \text{ psi} + 6.56 \text{ psi} + 10 \text{ psi} = 33.2 \text{ psi} \rightarrow 33.2 \text{ psi} * \frac{2.31 \text{ ft}}{\text{psi}} = 1215 \text{ ft} \quad (110)$$

$$THp = \frac{Q * (pressure \text{ increase})}{1714} \rightarrow \frac{2982 \text{ GPM} * (80 \text{ psi})}{1714} = 140 \text{ hp} \quad (111)$$

$$Pump \text{ Efficiency} = \frac{Q * H}{3960 * BHp} \rightarrow \frac{2982 \text{ gpm} * 152 \text{ ft}}{3960 * 150 \text{ hp}} = 76\% \quad (112)$$

5.5 Heliostat Design

In the heliostat design, an Excel spreadsheet was used to do most of the calculations as it used the Solver tool, but other calculations were done to determine the cost of each design. Sample calculations here are for the 8000 times solar concentration design, in which there were five towers that were each 184.8 meters tall. This gave a total heliostat area of 458,478 square meters. The base cost of each heliostat design was \$125 per square meter. This would give a base cost for the 8000 times solar concentration as shown below.

$$Base \text{ Cost} = (\$125/\text{m}^2)(458,478 \text{ m}^2) = \$57.3 \text{ million} \quad (113)$$

Likewise, the base cost of the secondary concentrator for each heliostat design was \$1250 per square meter. For the 8000 times solar concentration, the secondary concentrator cost is shown below.

$$Base \text{ Cost} = (\$1250/\text{m}^2)(458,478 \text{ m}^2) = \$573.1 \text{ million} \quad (114)$$

Similarly, the cost of each tower was determined by the following equation. The sample calculation for the 8000 times solar concentration is shown below this equation.

$$Base \text{ Cost} = 1.41[\$600 + 17.72(tower \text{ height})^{2.392}] \quad (115)$$

$$(Base \text{ Cost})_{single \text{ tower}} = 1.41[\$600 + 17.72 * (184.8 \text{ m})^{2.392}] = \$4.72 \text{ million/tower} \quad (116)$$

$$(Base \text{ Cost})_{all \text{ towers}} = (\$4.72 \text{ million/tower})(5 \text{ towers}) = \$23.6 \text{ million} \quad (117)$$

Bringing this all together, the total cost of this heliostat design is the sum of each component. This is shown below.

$$\text{Cost of Heliostat Field} = \$57.3 \text{ million} + \$573.1 \text{ million} + \$23.6 \text{ million} = \$654.0 \text{ million}$$

Thus, we have the final total cost of the heliostat design for 8000 times solar concentration as \$654.0 million.

Appendix B: Excel

Gantt Chart, Energy Balances, and Material Balances: Pages 114-120

Reactor and Component Design: Pages 121-127

Finances: Pages 128-131

Task Name	Week 1: November 1	Week 2: November 8	Week 3: November 15 - Including Thanksgiving Break	Week 4: November 26	Week 5: December 3																																	
Cover Page & Table of Contents					All																																	
Executive Summary					All																																	
1. Project Definition, Scope & Background					All																																	
2. Environmental, Health & Safety Considerations					All																																	
3.1. Overview of Project					All																																	
3.2. Project Management					All																																	
3.3. Process Flow Diagram					All																																	
3.4. Battery Limits and Design & Economic Premises					All																																	
3.5. Material Balance (overall hand MB to provide starting point for simulation)		Teeb and Sam Ally and Abby			All																																	
3.6. Energy Balances (incl. using heat capacity, etc. to determine heats of rxn)					All																																	
4.1. Aspen HYSYS Simulation			Teeb		All																																	
4.2. Aspen HYSYS Simulation				Abby	All																																	
5.1. Reactor (math models should be developed and solved with Matlab or other solver)				Abby	All																																	
5.2. Solar-Thermal Specification				Abby	All																																	
5.3.1. Methanol Fixed Bed				Abby	All																																	
5.3.2. Methanol Fixed Bed Reactor				Abby	All																																	
5.2 Separators				Abby	All																																	
5.3 Heat Exchangers				Abby	All																																	
5.4 Heliotest Commission				Abby	All																																	
5.5 Heliotest Design (design based on lowest cost considering 2000, 4000, and 8000 suns)				Abby	All																																	
6. Utilities Summary & Heat Integration including Energy Analyzer Analysis				Abby	All																																	
7. Estimation of Capital Investment & Cash Flow, and Profitability Analysis				Abby	All																																	
Milestones					All																																	
Table of Nomenclature					All																																	
Appendices					All																																	
Formatting & Presentation					All																																	
Mechanics of Writing, Grammar, Types					All																																	
Day of Project	1	2	3	4	5	6	7	8	9	10	11	12	13	14	15	16	17	18	19	20	21	22	23	24	25	26	27	28	29	30	31	32	33	34	35	36	37	38
Date	11/1	11/2	11/3	11/4	11/5	11/6	11/7	11/8	11/9	11/10	11/11	11/12	11/13	11/14	11/15	11/16	11/17	11/18	11/19	11/20	11/21	11/22	11/23	11/24	11/25	11/26	11/27	11/28	11/29	11/30	11/31	11/32	11/33	11/34	11/35	11/36	11/37	11/38
Day	Tue	Wed	Thu	Fri	Sat	Sun	Mon	Tue	Wed	Thu	Fri	Sat	Sun	Mon	Tue	Wed	Thu	Fri	Sat	Sun	Mon	Tue	Wed	Thu	Fri	Sat	Sun	Mon	Tue	Wed	Thu	Fri	Sat	Sun	Mon	Tue	Wed	Thu

Name	Heats of Formation (kJ/mol) [Pg 201 of perry handbook]	kJ/mol
ZOO	-348.7734	T ₁
ZAS	-389.552	T ₂
H ₂ O	-385.82	T ₂ -T ₁
H ₂ S	-19.9277	48.15
ZEO ₁₂	-411.9816	18.15
HCl	92.31	

C1	C2	C3	C4	C5	H2S
HCl	0.029157	0.099243	0.000238	-0.000107	0.039742 J/mole K
HS	0.033388	0.050862	0.0069134	-0.017799	0.0009494 J/mole K
H ₂ O	0.023363	0.026793	0.00062605	0.008896	6.013368 kJ/mol K
Integrated from 288 to 483.15					5.9763568 kJ/mol K
HCl	C1*(T2-T3)	C2*C3*COTH(C3,T)	C4*C5*TANH(C5,T)	sum kJ/mol	
H ₂ S	5.3981855	1.6722372	8.3319151	2.0736558	
H ₂ O	6.352232	4.829828	8.52566151	10.93395	
	6.1773545	4.9601885	6.65995151	11.133238	
ZOO	Specific heat	MW	40.20177	0.0402017 / 433345	
ZAS	0.494	81.38	45.15366	0.0451535 / 434189	
ZEO ₁₂	0.73954	97.174	100.7889184	0.1007885 / 18.661074	

$$\text{COp} = \text{C1} + \text{C2}[\text{C3}/(\text{sum}(\text{C3}, \text{T})^2 + \text{C4}[\text{C5}/(\text{sum}(\text{C5}, \text{T})^2)]^2)]^{\frac{1}{2}}$$

5.9374468 kJ/mol K
0.06115 J/mole K
6.013368 kJ/mol K
5.9763568 kJ/mol K

Rxn # 1 ZOO + H ₂ S → ZAS + H ₂ O	18.3504456
H r R	19.6015166
H r P	-1.06562326
H rxn 1	-0.4618177
Atrial Hrx	

Rxn # 2 ZOO + 2HCl → ZEO ₁₂ + H ₂ O	21.36035267
H r R	25.39840175
H r P	-1.704135
H rxn 2	-1.62573309
Atrial Hrx	

Component	Integrated Cp (kJ/mol)
Cellulose	951.2211
Lignin	612.7957
Ash	60.3639
Methane	161.3542
Water	126.5270
Sum	1912.2619

Component	Flow rate *Cp	kJ/hr	MW
Cellulose	39893321.55	11.09034	11
Lignin	25700078.09	7.144622	7
Ash	2531.605432	0.000704	0.000704
Methane	689480.0208	0.191675	0.191675
Water	3784625.354	1.052126	1.052126
Sum	70070036.63		

Component Heat of Reaction (kJ/mol)

Cellulose	336.7906648
Lignin	2459.472233
Methane	175.1808771
Ash	60.36389775
Water	2760.539137

Component Flow Rate (mol/hr)

Cellulose	41939.06501
Lignin	41939.06501
Methane	41.93906501
Ash	4213.084479
Water	29911.59136

Component Flow Rate *Hrxn

Component	Flow Rate *Hrxn	kJ/hr	MW
Cellulose	14124685.58	3.926663	11
Lignin	103147966.7	7.144622	7
Methane	7346.922191	0.000704	0.000704
Ash	257940.0346	0.071707	0.071707
Water	594636647.7	165.309	165.309
Sum	712174587	2.78E-07	

Component Flow Rate *Hrxn

Cellulose	41939.06501
Lignin	41939.06501
Methane	41.93906501
Ash	4213.084479
Water	29911.59136

Component Flow Rate *Hrxn

Component	Flow Rate *Hrxn	kJ/hr	MW
Cellulose	14124685.58	3.926663	11
Lignin	103147966.7	7.144622	7
Methane	7346.922191	0.000704	0.000704
Ash	257940.0346	0.071707	0.071707
Water	594636647.7	165.309	165.309
Sum	712174587	2.78E-07	

Component Flow Rate *Hrxn

Cellulose	41939.06501
Lignin	41939.06501
Methane	41.93906501
Ash	4213.084479
Water	29911.59136

Component Flow Rate *Hrxn

Component	Flow Rate *Hrxn	kJ/hr	MW
Cellulose	14124685.58	3.926663	11
Lignin	103147966.7	7.144622	7
Methane	7346.922191	0.000704	0.000704
Ash	257940.0346	0.071707	0.071707
Water	594636647.7	165.309	165.309
Sum	712174587	2.78E-07	

Component Flow Rate *Hrxn

Cellulose	41939.06501
Lignin	41939.06501
Methane	41.93906501
Ash	4213.084479
Water	29911.59136

Component Flow Rate *Hrxn

Component	Flow Rate *Hrxn	kJ/hr	MW
Cellulose	14124685.58	3.926663	11
Lignin	103147966.7	7.144622	7
Methane	7346.922191	0.000704	0.000704
Ash	257940.0346	0.071707	0.071707
Water	594636647.7	165.309	165.309
Sum	712174587	2.78E-07	

Component Flow Rate *Hrxn

Cellulose	41939.06501
Lignin	41939.06501
Methane	41.93906501
Ash	4213.084479
Water	29911.59136

Component Flow Rate *Hrxn

Component	Flow Rate *Hrxn	kJ/hr	MW
Cellulose	14124685.58	3.926663	11
Lignin	103147966.7	7.144622	7
Methane	7346.922191	0.000704	0.000704
Ash	257940.0346	0.071707	0.071707
Water	594636647.7	165.309	165.309
Sum	712174587	2.78E-07	

Component Flow Rate *Hrxn

Cellulose	41939.06501
Lignin	41939.06501
Methane	41.93906501
Ash	4213.084479
Water	29911.59136

Component Flow Rate *Hrxn

Component	Flow Rate *Hrxn	kJ/hr	MW
Cellulose	14124685.58	3.926663	11
Lignin	103147966.7	7.144622	7
Methane	7346.922191	0.000704	0.000704
Ash	257940.0346	0.071707	0.071707
Water	594636647.7	165.309	165.309
Sum	712174587	2.78E-07	

Component Flow Rate *Hrxn

Cellulose	41939.06501
Lignin	41939.06501
Methane	41.93906501
Ash	4213.084479
Water	29911.59136

Component Flow Rate *Hrxn

Component	Flow Rate *Hrxn	kJ/hr	MW
Cellulose	14124685.58	3.926663	11
Lignin	103147966.7	7.144622	7
Methane	7346.922191	0.000704	0.000704
Ash	257940.0346	0.071707	0.071707
Water	594636647.7	165.309	165.309
Sum	712174587	2.78E-07	

Component Flow Rate *Hrxn

Cellulose	41939.06501
Lignin	41939.06501
Methane	41.93906501
Ash	4213.084479
Water	29911.59136

Component Flow Rate *Hrxn

Component	Flow Rate *Hrxn	kJ/hr	MW
Cellulose	14124685.58	3.926663	11
Lignin	103147966.7	7.144622	7
Methane	7346.922191	0.000704	0.000704
Ash	257940.0346	0.071707	0.071707
Water	594636647.7	165.309	165.309
Sum	712174587	2.78E-07	

Component Flow Rate *Hrxn

Cellulose	41939.06501
Lignin	41939.06501
Methane	41.93906501
Ash	4213.084479
Water	29911.59136

Component Flow Rate *Hrxn

Component	Flow Rate *Hrxn	kJ/hr	MW
Cellulose	14124685.58	3.926663	11
Lignin	103147966.7	7.144622	7
Methane	7346.922191	0.000704	0.000704
Ash	257940.0346	0.071707	0.071707
Water	594636647.7	165.309	165.309
Sum	712174587	2.78E-07	

Component Flow Rate *Hrxn

Cellulose	41939.06501
Lignin	41939.06501
Methane	41.93906501
Ash	4213.084479
Water	29911.59136

Component Flow Rate *Hrxn

| THERM | | C | | C₂ | | C₃ | | C₄ | | C₅ | | C₆ | | C₇ | | C₈ | | C₉ | | C₁₀ | | C₁₁ | | C₁₂ | | C₁₃ | | C₁₄ | | C₁₅ | | C₁₆ | | C₁₇ | | C₁₈ | | C₁₉ | | C₂₀ | | C₂₁ | | C₂₂ | | C₂₃ | | C₂₄ | | C₂₅ | | C₂₆ | | C₂₇ | | C₂₈ | | C₂₉ | | C₃₀ | | C₃₁ | | C₃₂ | | C₃₃ | | C₃₄ | | C₃₅ | | C₃₆ | | C₃₇ | | C₃₈ | | C₃₉ | | C₄₀ | | C₄₁ | | C₄₂ | | C₄₃ | | C₄₄ | | C₄₅ | | C₄₆ | | C₄₇ | | C₄₈ | | C₄₉ | | C₅₀ | | C₅₁ | | C₅₂ | | C₅₃ | | C₅₄ | | C₅₅ | | C₅₆ | | C₅₇ | | C₅₈ | | C₅₉ | | C₆₀ | | C₆₁ | | C₆₂ | | C₆₃ | | C₆₄ | | C₆₅ | | C₆₆ | | C₆₇ | | C₆₈ | | C₆₉ | | C₇₀ | | C₇₁ | | C₇₂ | | C₇₃ | | C₇₄ | | C₇₅ | | C₇₆ | | C₇₇ | | C₇₈ | | C₇₉ | | C₈₀ | | C₈₁ | | C₈₂ | | C₈₃ | | C₈₄ | | C₈₅ | | C₈₆ | | C₈₇ | | C₈₈ | | C₈₉ | | C₉₀ | | C₉₁ | | C₉₂ | | C₉₃ | | C₉₄ | | C₉₅ | | C₉₆ | | C₉₇ | | C₉₈ | | C₉₉ | | C₁₀₀ | | C₁₀₁ | | C₁₀₂ | | C₁₀₃ | | C₁₀₄ | | C₁₀₅ | | C₁₀₆ | | C₁₀₇ | | C₁₀₈ | | C₁₀₉ | | C₁₁₀ | | C₁₁₁ | | C₁₁₂ | | C₁₁₃ | | C₁₁₄ | | C₁₁₅ | | C₁₁₆ | | C₁₁₇ | | C₁₁₈ | | C₁₁₉ | | C₁₂₀ | | C₁₂₁ | | C₁₂₂ | | C₁₂₃ | | C₁₂₄ | | C₁₂₅ | | C₁₂₆ | | C₁₂₇ | | C₁₂₈ | | C₁₂₉ | | C₁₃₀ | | C₁₃₁ | | C₁₃₂ | | C₁₃₃ | | C₁₃₄ | | C₁₃₅ | | C₁₃₆ | | C₁₃₇ | | C₁₃₈ | | C₁₃₉ | | C₁₄₀ | | C₁₄₁ | | C₁₄₂ | | C₁₄₃ | | C₁₄₄ | | C₁₄₅ | | C₁₄₆ | | C₁₄₇ | | C₁₄₈ | | C₁₄₉ | | C₁₅₀ | | C₁₅₁ | | C₁₅₂ | | C₁₅₃ | | C₁₅₄ | | C₁₅₅ | | C₁₅₆ | | C₁₅₇ | | C₁₅₈ | | C₁₅₉ | | C₁₆₀ | | C₁₆₁ | | C₁₆₂ | | C₁₆₃ | | C₁₆₄ | | C₁₆₅ | | C₁₆₆ | | C₁₆₇ | | C₁₆₈ | | C₁₆₉ | | C₁₇₀ | | C₁₇₁ | | C₁₇₂ | | C₁₇₃ | | C₁₇₄ | | C₁₇₅ | | C₁₇₆ | | C₁₇₇ | | C₁₇₈ | | C₁₇₉ | | C₁₈₀ | | C₁₈₁ | | C₁₈₂ | | C₁₈₃ | | C₁₈₄ | | C₁₈₅ | | C₁₈₆ | | C₁₈₇ | | C₁₈₈ | | C₁₈₉ | | C₁₉₀ | | C₁₉₁ | | C₁₉₂ | | C₁₉₃ | | C₁₉₄ | | C₁₉₅ | | C₁₉₆ | | C₁₉₇ | | C₁₉₈ | | C₁₉₉ | | C₂₀₀ | | C₂₀₁ | | C₂₀₂ | | C₂₀₃ | | C₂₀₄ | | C₂₀₅ | | C₂₀₆ | | C₂₀₇ | | C₂₀₈ | | C₂₀₉ | | C₂₁₀ | | C₂₁₁ | | C₂₁₂ | | C₂₁₃ | | C₂₁₄ | | C₂₁₅ | | C₂₁₆ | | C₂₁₇ | | C₂₁₈ | | C₂₁₉ | | C₂₂₀ | | C₂₂₁ | | C₂₂₂ | | C₂₂₃ | | C₂₂₄ | | C₂₂₅ | | C₂₂₆ | | C₂₂₇ | | C₂₂₈ | | C₂₂₉ | | C₂₃₀ | | C₂₃₁ | | C₂₃₂ | | C₂₃₃ | | C₂₃₄ | | C₂₃₅ | | C₂₃₆ | | C₂₃₇ | | C₂₃₈ | | C₂₃₉ | | C₂₄₀ | | C₂₄₁ | | C₂₄₂ | | C₂₄₃ | | C₂₄₄ | | C₂₄₅ | | C₂₄₆ | | C₂₄₇ | | C₂₄₈ | | C₂₄₉ | | C₂₅₀ | | C₂₅₁ | | C₂₅₂ | | C₂₅₃ | | C₂₅₄ | | C₂₅₅ | | C₂₅₆ | | C₂₅₇ | | C₂₅₈ | | C₂₅₉ | | C₂₆₀ | | C₂₆₁ | | C₂₆₂ | | C₂₆₃ | | C₂₆₄ | | C₂₆₅ | | C₂₆₆ | | C₂₆₇ | | C₂₆₈ | | C₂₆₉ | | C₂₇₀ | | C₂₇₁ | | C₂₇₂ | | C₂₇₃ | | C₂₇₄ | | C₂₇₅ | | C₂₇₆ | | C₂₇₇ | | C₂₇₈ | | C₂₇₉ | | C₂₈₀ | | C₂₈₁ | | C₂₈₂ | | C₂₈₃ | | C₂₈₄ | | C₂₈₅ | | C₂₈₆ | | C₂₈₇ | | C₂₈₈ | | C₂₈₉ | | C₂₉₀ | | C₂₉₁ | | C₂₉₂ | | C₂₉₃ | | C₂₉₄ | | C₂₉₅ | | C₂₉₆ | | C₂₉₇ | | C₂₉₈ | | C₂₉₉ | | C₃₀₀ | | C₃₀₁ | | C₃₀₂ | | C₃₀₃ | | C₃₀₄ | | C₃₀₅ | | C₃₀₆ | | C₃₀₇ | | C₃₀₈ | | C₃₀₉ | | C₃₁₀ | | C₃₁₁ | | C₃₁₂ | | C₃₁₃ | | C₃₁₄ | | C₃₁₅ | | C₃₁₆ | | C₃₁₇ | | C₃₁₈ | | C₃₁₉ | | C₃₂₀ | | C₃₂₁ | | C₃₂₂ | | C₃₂₃ | | C₃₂₄ | | C₃₂₅ | | C₃₂₆ | | C₃₂₇ | | C₃₂₈ | | C₃₂₉ | | C₃₃₀ | | C₃₃₁ | | C₃₃₂ | | C₃₃₃ | | C₃₃₄ | | C₃₃₅ | | C₃₃₆ | | C₃₃₇ | | C₃₃₈ | | C₃₃₉ | | C₃₄₀ | | C₃₄₁ | | C₃₄₂ | | C₃₄₃ | | C₃₄₄ | | C₃₄₅ | | C₃₄₆ | | C₃₄₇ | | C₃₄₈ | | C₃₄₉ | | C₃₅₀ | | C₃₅₁ | | C₃₅₂ | | C₃₅₃ | | C₃₅₄ | | C₃₅₅ | | C₃₅₆ | | C₃₅₇ | | C₃₅₈ | | C₃₅₉ | | C₃₆₀ | | C₃₆₁ | | C₃₆₂ | | C₃₆₃ | | C₃₆₄ | | C₃₆₅ | | C₃₆₆ | | C₃₆₇ | | C₃₆₈ | | C₃₆₉ | | C₃₇₀ | | C₃₇₁ | | C₃₇₂ | | C₃₇₃ | | C₃₇₄ | | C₃₇₅ | | C₃₇₆ | | C₃₇₇ | | C₃₇₈ | | C₃₇₉ | | C₃₈₀ | | C₃₈₁ | | C₃₈₂ | | C₃₈₃ | | C₃₈₄ | | C₃₈₅ | | C₃₈₆ | | C₃₈₇ | | C₃₈₈ | | C₃₈₉ | | C₃₉₀ | | C₃₉₁ | | C₃₉₂ | | C₃₉₃ | | C₃₉₄ | | C₃₉₅ | | C₃₉₆ | | C₃₉₇ | | C₃₉₈ | | C₃₉₉ | | C₄₀₀ | | C₄₀₁ | | C₄₀₂ | | C₄₀₃ | | C₄₀₄ | | C₄₀₅ | | C₄₀₆ | | C₄₀₇ | | C₄₀₈ | | C₄₀₉ | | C₄₁₀ | | C₄₁₁ | | C₄₁₂ | | C₄₁₃ | | C₄₁₄ | | C₄₁₅ | | C₄₁₆ | | C₄₁₇ | | C₄₁₈ | | C₄₁₉ | | C₄₂₀ | | C₄₂₁ | | C₄₂₂ | | C₄₂₃ | | C₄₂₄ | | C₄₂₅ | | C₄₂₆ | | C₄₂₇ | | C₄₂₈ | | C₄₂₉ | | C₄₃₀ | | C₄₃₁ | | C₄₃₂ | | C₄₃₃ | | C₄₃₄ | | C₄₃₅ | | C₄₃₆ | | C₄₃₇ | | C₄₃₈ | | C₄₃₉ | | C₄₄₀ | | C₄₄₁ | | C₄₄₂ | | C₄₄₃ | | C₄₄₄ | | C₄₄₅ | | C₄₄₆ | | C₄₄₇ | | C₄₄₈ | | C₄₄₉ | | C₄₅₀ | | C₄₅₁ | | C₄₅₂ | | C₄₅₃ | | C₄₅₄ | | C₄₅₅ | | C₄₅₆ | | C₄₅₇ | | C₄₅₈ | | C₄₅₉ | | C₄₆₀ | | C₄₆₁ | | C₄₆₂ | | C₄₆₃ | | C₄₆₄ | | C₄₆₅ | | C₄₆₆ | | C₄₆₇ | | C₄₆₈ | | C₄₆₉ | | C₄₇₀ | | C₄₇₁ | | C₄₇₂ | | C₄₇₃ | | C₄₇₄ | | C₄₇₅ | | C₄₇₆ | | C₄₇₇ | | C₄₇₈ | | C₄₇₉ | | C₄₈₀ | | C₄₈₁ | | C₄₈₂ | | C₄₈₃ | | C₄₈₄ | | C₄₈₅ | | C₄₈₆ | | C₄₈₇ | | C₄₈₈ | | C₄₈₉ | | C₄₉₀ | | C₄₉₁ | | C₄₉₂ | | C₄₉₃ | | C₄₉₄ | | C₄₉₅ | | C₄₉₆ | | C₄₉₇ | | C₄₉₈ | | C₄₉₉ | | C₅₀₀ | | C₅₀₁ | | C₅₀₂ | | C₅₀₃ | | C₅₀₄ | | C₅₀₅ | | C₅₀₆ | | C₅₀₇ | | C₅₀₈ | | C₅₀₉ | | C₅₁₀ | | C₅₁₁ | | C₅₁₂ | | C₅₁₃ | | C₅₁₄ | | C₅₁₅ | | C₅₁₆ | | C₅₁₇ | | C₅₁₈ | | C₅₁₉ | | C₅₂₀ | | C₅₂₁ | | C₅₂₂ | | C₅₂₃ | | C₅₂₄ | | C₅₂₅ | | C₅₂₆ | | C₅₂₇ | | C₅₂₈ | | C₅₂₉ | | C₅₃₀ | | C₅₃₁ | | C₅₃₂ | | C₅₃₃ | | C₅₃₄ | | C₅₃₅ | | C₅₃₆ | | C₅₃₇ | | C₅₃₈ | | C₅₃₉ | | C₅₄₀ | | C₅₄₁ | | C₅₄₂ | | C₅₄₃ | | C₅₄₄ | | C₅₄₅ | | C₅₄₆ | | C₅₄₇ | | C₅₄₈ | | C₅₄₉ | | C₅₅₀ | | C₅₅₁ | | C₅₅₂ | | C₅₅₃ | | C₅₅₄ | | C₅₅₅ | | C₅₅₆ | | C₅₅₇ | | C₅₅₈ | | C₅₅₉ | | C₅₆₀ | | C₅₆₁ | | C₅₆₂ | | C₅₆₃ | | C₅₆₄ | | C₅₆₅ | | C₅₆₆ | | C₅₆₇ | | C₅₆₈ | | C₅₆₉ | | C₅₇₀ | | C₅₇₁ | | C₅₇₂ | | C₅₇₃ | | C₅₇₄ | | C₅₇₅ | | C₅₇₆ | | C₅₇₇ | | C₅₇₈ | | C₅₇₉ | | C₅₈₀ | | C₅₈₁ | | C₅₈₂ | | C₅₈₃ | | C₅₈₄ | | C₅₈₅ | | C₅₈₆ | | C₅₈₇ | | C₅₈₈ | | C₅₈₉ | | C₅₉₀ | | C₅₉₁ | | C₅₉₂ | | C₅₉₃ | | C₅₉₄ | | C₅₉₅ | | C₅₉₆ | | C₅₉₇ | | C₅₉₈ | | C₅₉₉ | | C₆₀₀ | | C₆₀₁ | | C₆₀₂ | | C₆₀₃ | | C₆₀₄ | | C₆₀₅ | | C₆₀₆ | | C₆₀₇ | | C₆₀₈ | | C₆₀₉ | | C₆₁₀ | | C₆₁₁ | | C₆₁₂ | | C₆₁₃ | | C₆₁₄ | | C₆₁₅ | | C₆₁₆ | | C₆₁₇ | | C₆₁₈ | | C₆₁₉ | | C₆₂₀ | | C₆₂₁ | | C₆₂₂ | | C₆₂₃ | | C₆₂₄ | | C₆₂₅ | | C₆₂₆ | | C₆₂₇ | | C₆₂₈ | | C₆₂₉ | | C₆₃₀ | | C₆₃₁ | | C₆₃₂ | | C₆₃₃ | | C₆₃₄ | | C₆₃₅ | | C₆₃₆ | | C₆₃₇ | | C₆₃₈ | | C₆₃₉ | | C₆₄₀ | | C₆₄₁ | | C₆₄₂ | | C₆₄₃ | | C₆₄₄ | | C₆₄₅ | | C₆₄₆ | | C₆₄₇ | | C₆₄₈ | | C₆₄₉ | | C₆₅₀ | | C₆₅₁ | | C₆₅₂ | | C₆₅₃ | | C₆₅₄ | | C₆₅₅ | | C₆₅₆ | | C₆₅₇ | | C₆₅₈ | | C₆₅₉ | | C₆₆₀ | | C₆₆₁ | | C₆₆₂ | | C₆₆₃ | | C₆₆₄ | | C₆₆₅ | | C₆₆₆ | | C₆₆₇ | | C₆₆₈ | | C₆₆₉ | | C₆₇₀ | | C₆₇₁ | | C₆₇₂ | | C₆₇₃ | | C₆₇₄ | |<th
| --- | --- | --- | --- | --- | --- | --- | --- | --- | --- | --- | --- | --- | --- | --- | --- | --- | --- | --- | --- | --- | --- | --- | --- | --- | --- | --- | --- | --- | --- | --- | --- | --- | --- | --- | --- | --- | --- | --- | --- | --- | --- | --- | --- | --- | --- | --- | --- | --- | --- | --- | --- | --- | --- | --- | --- | --- | --- | --- | --- | --- | --- | --- | --- | --- | --- | --- | --- | --- | --- | --- | --- | --- | --- | --- | --- | --- | --- | --- | --- | --- | --- | --- | --- | --- | --- | --- | --- | --- | --- | --- | --- | --- | --- | --- | --- | --- | --- | --- | --- | --- | --- | --- | --- | --- | --- | --- | --- | --- | --- | --- | --- | --- | --- | --- | --- | --- | --- | --- | --- | --- | --- | --- | --- | --- | --- | --- | --- | --- | --- | --- | --- | --- | --- | --- | --- | --- | --- | --- | --- | --- | --- | --- | --- | --- | --- | --- | --- | --- | --- | --- | --- | --- | --- | --- | --- | --- | --- | --- | --- | --- | --- | --- | --- | --- | --- | --- | --- | --- | --- | --- | --- | --- | --- | --- | --- | --- | --- | --- | --- | --- | --- | --- | --- | --- | --- | --- | --- | --- | --- | --- | --- | --- | --- | --- | --- | --- | --- | --- | --- | --- | --- | --- | --- | --- | --- | --- | --- | --- | --- | --- | --- | --- | --- | --- | --- | --- | --- | --- | --- | --- | --- | --- | --- | --- | --- | --- | --- | --- | --- | --- | --- | --- | --- | --- | --- | --- | --- | --- | --- | --- | --- | --- | --- | --- | --- | --- | --- | --- | --- | --- | --- | --- | --- | --- | --- | --- | --- | --- | --- | --- | --- | --- | --- | --- | --- | --- | --- | --- | --- | --- | --- | --- | --- | --- | --- | --- | --- | --- | --- | --- | --- | --- | --- | --- | --- | --- | --- | --- | --- | --- | --- | --- | --- | --- | --- | --- | --- | --- | --- | --- | --- | --- | --- | --- | --- | --- | --- | --- | --- | --- | --- | --- | --- | --- | --- | --- | --- | --- | --- | --- | --- | --- | --- | --- | --- | --- | --- | --- | --- | --- | --- | --- | --- | --- | --- | --- | --- | --- | --- | --- | --- | --- | --- | --- | --- | --- | --- | --- | --- | --- | --- | --- | --- | --- | --- | --- | --- | --- | --- | --- | --- | --- | --- | --- | --- | --- | --- | --- | --- | --- | --- | --- | --- | --- | --- | --- | --- | --- | --- | --- | --- | --- | --- | --- | --- | --- | --- | --- | --- | --- | --- | --- | --- | --- | --- | --- | --- | --- | --- | --- | --- | --- | --- | --- | --- | --- | --- | --- | --- | --- | --- | --- | --- | --- | --- | --- | --- | --- | --- | --- | --- | --- | --- | --- | --- | --- | --- | --- | --- | --- | --- | --- | --- | --- | --- | --- | --- | --- | --- | --- | --- | --- | --- | --- | --- | --- | --- | --- | --- | --- | --- | --- | --- | --- | --- | --- | --- | --- | --- | --- | --- | --- | --- | --- | --- | --- | --- | --- | --- | --- | --- | --- | --- | --- | --- | --- | --- | --- | --- | --- | --- | --- | --- | --- | --- | --- | --- | --- | --- | --- | --- | --- | --- | --- | --- | --- | --- | --- | --- | --- | --- | --- | --- | --- | --- | --- | --- | --- | --- | --- | --- | --- | --- | --- | --- | --- | --- | --- | --- | --- | --- | --- | --- | --- | --- | --- | --- | --- | --- | --- | --- | --- | --- | --- | --- | --- | --- | --- | --- | --- | --- | --- | --- | --- | --- | --- | --- | --- | --- | --- | --- | --- | --- | --- | --- | --- | --- | --- | --- | --- | --- | --- | --- | --- | --- | --- | --- | --- | --- | --- | --- | --- | --- | --- | --- | --- | --- | --- | --- | --- | --- | --- | --- | --- | --- | --- | --- | --- | --- | --- | --- | --- | --- | --- | --- | --- | --- | --- | --- | --- | --- | --- | --- | --- | --- | --- | --- | --- | --- | --- | --- | --- | --- | --- | --- | --- | --- | --- | --- | --- | --- | --- | --- | --- | --- | --- | --- | --- | --- | --- | --- | --- | --- | --- | --- | --- | --- | --- | --- | --- | --- | --- | --- | --- | --- | --- | --- | --- | --- | --- | --- | --- | --- | --- | --- | --- | --- | --- | --- | --- | --- | --- | --- | --- | --- | --- | --- | --- | --- | --- | --- | --- | --- | --- | --- | --- | --- | --- | --- | --- | --- | --- | --- | --- | --- | --- | --- | --- | --- | --- | --- | --- | --- | --- | --- | --- | --- | --- | --- | --- | --- | --- | --- | --- | --- | --- | --- | --- | --- | --- | --- | --- | --- | --- | --- | --- | --- | --- | --- | --- | --- | --- | --- | --- | --- | --- | --- | --- | --- | --- | --- | --- | --- | --- | --- | --- | --- | --- | --- | --- | --- | --- | --- | --- | --- | --- | --- | --- | --- | --- | --- | --- | --- | --- | --- | --- | --- | --- | --- | --- | --- | --- | --- | --- | --- | --- | --- | --- | --- | --- | --- | --- | --- | --- | --- | --- | --- | --- | --- | --- | --- | --- | --- | --- | --- | --- | --- | --- | --- | --- | --- | --- | --- | --- | --- | --- | --- | --- | --- | --- | --- | --- | --- | --- | --- | --- | --- | --- | --- | --- | --- | --- | --- | --- | --- | --- | --- | --- | --- | --- | --- | --- | --- | --- | --- | --- | --- | --- | --- | --- | --- | --- | --- | --- | --- | --- | --- | --- | --- | --- | --- | --- | --- | --- | --- | --- | --- | --- | --- | --- | --- | --- | --- | --- | --- | --- | --- | --- | --- | --- | --- | --- | --- | --- | --- | --- | --- | --- | --- | --- | --- | --- | --- | --- | --- | --- | --- | --- | --- | --- | --- | --- | --- | --- | --- | --- | --- | --- | --- | --- | --- | --- | --- | --- | --- | --- | --- | --- | --- | --- | --- | --- | --- | --- | --- | --- | --- | --- | --- | --- | --- | --- | --- | --- | --- | --- | --- | --- | --- | --- | --- | --- | --- | --- | --- | --- | --- | --- | --- | --- | --- | --- | --- | --- | --- | --- | --- | --- | --- | --- | --- | --- | --- | --- | --- | --- | --- | --- | --- | --- | --- | --- | --- | --- | --- | --- | --- | --- | --- | --- | --- | --- | --- | --- | --- | --- | --- | --- | --- | --- | --- | --- | --- | --- | --- | --- | --- | --- | --- | --- | --- | --- | --- | --- | --- | --- | --- | --- | --- | --- | --- | --- | --- | --- | --- | --- | --- | --- | --- | --- | --- | --- | --- | --- | --- | --- | --- | --- | --- | --- | --- | --- | --- | --- | --- | --- | --- | --- | --- | --- | --- | --- | --- | --- | --- | --- | --- | --- | --- | --- | --- | --- | --- | --- | --- | --- | --- | --- | --- | --- | --- | --- | --- | --- | --- | --- | --- | --- | --- | --- | --- | --- | --- | --- | --- | --- | --- | --- | --- | --- | --- | --- | --- | --- | --- | --- | --- | --- | --- | --- | --- | --- | --- | --- | --- | --- | --- | --- | --- | --- | --- | --- | --- | --- | --- | --- | --- | --- | --- | --- | --- | --- | --- | --- | --- | --- | --- | --- | --- | --- | --- | --- | --- | --- | --- | --- | --- | --- | --- | --- | --- | --- | --- | --- | --- | --- | --- | --- | --- | --- | --- | --- | --- | --- | --- | --- | --- | --- | --- | --- | --- | --- | --- | --- | --- | --- | --- | --- | --- | --- | --- | --- | --- | --- | --- | --- | --- | --- | --- | --- | --- | --- | --- | --- | --- | --- | --- | --- | --- | --- | --- | --- | --- | --- | --- | --- | --- | --- | --- | --- | --- | --- | --- | --- | --- | --- | --- | --- | --- | --- | --- | --- | --- | --- | --- | --- | --- | --- | --- | --- | --- | --- | --- | --- | --- | --- | --- | --- | --- | --- | --- | --- | --- | --- | --- | --- | --- | --- | --- | --- | --- | --- | --- | --- | --- | --- | --- | --- | --- | --- | --- | --- | --- | --- | --- | --- | --- | --- | --- | --- | --- | --- | --- | --- | --- | --- | --- | --- | --- | --- | --- | --- | --- | --- | --- | --- | --- | --- | --- | --- | --- | --- | --- | --- | --- | --- | --- | --- | --- | --- | --- | --- | --- | --- | --- | --- | --- | --- | --- | --- | --- | --- | --- | --- | --- | --- | --- | --- | --- | --- | --- | --- | --- | --- | --- | --- | --- | --- | --- | --- | --- | --- | --- | --- | --- | --- | --- | --- | --- | --- | --- | --- | --- | --- | --- | --- | --- | --- | --- | --- | --- | --- | --- | --- | --- | --- | --- | --- | --- | --- | --- | --- | --- | --- | --- | --- | --- | --- | --- | --- | --- | --- | --- | --- | --- | --- | --- | --- | --- | --- | --- | --- | --- | --- | --- | --- | --- | --- | --- |

overall Production Stream	5.60E+06 gallon of methanol per year
Methanol Product Stream	0.9597 methanol mol fraction
Upstream Solar (1)	8 hours per day (365/year)
Downstream Solar (1)	24 hours per day (365/year)
Downstream Solar tot hrs	8000 per year

component	wt%
cellulose	68.25
Lignin	21.75
Ash	9.73
N/N2	0.61
S	1.22
O/O2	0.01
H2O	1.1

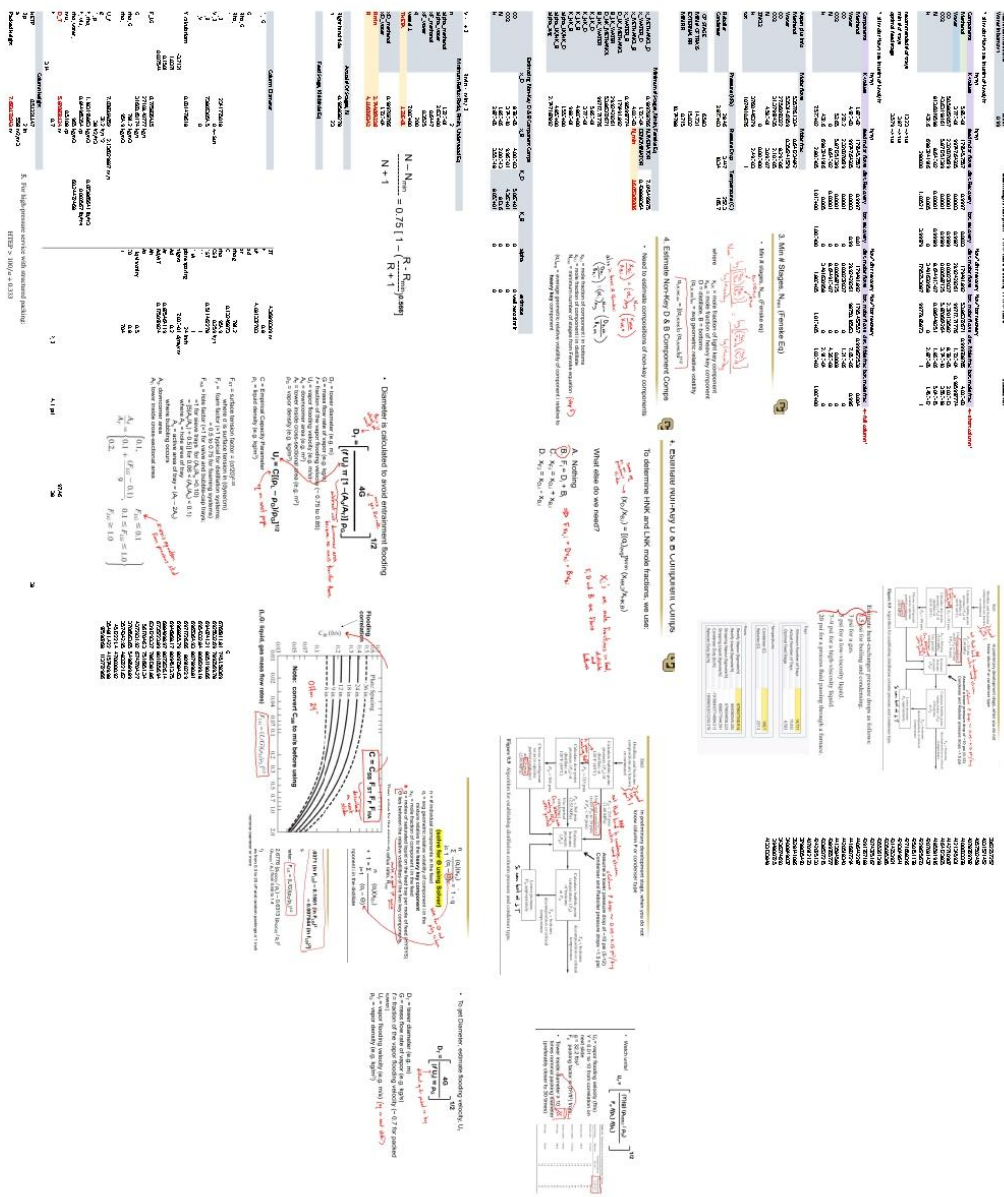
rxn #	Extent of rxn
1	0
2	0
3	0
4	0
5	0
6	1
7	10
8	10
9	10
10	10

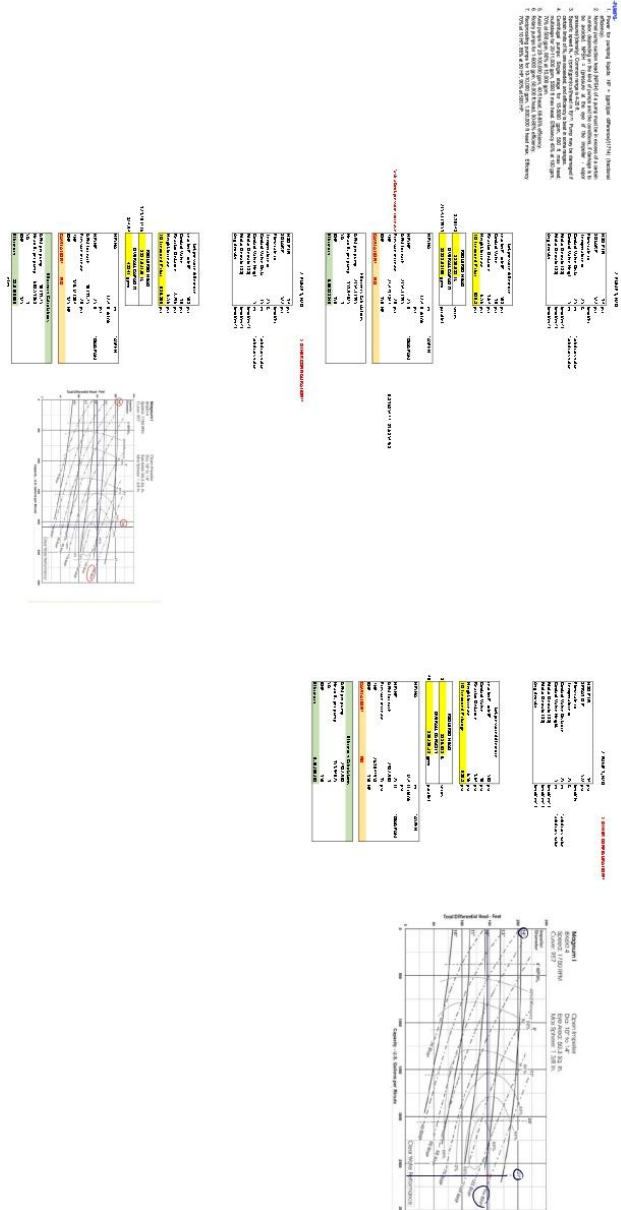
Rxn #	Conversion ZnO bed
6	1
7	1
8	0.45
9	0.45
10	0.45

Rxn #	Extent of rxn
1	0
2	0
3	0
4	0
5	0
6	1
7	1
8	1
9	1
10	1

Stoichiometry										
Component	Rxn # 1	Rxn # 2	Rxn # 3	Rxn # 4	Rxn # 5	Rxn # 6	Rxn # 7	Rxn # 8	Rxn # 9	Rxn # 10
GH1005 (cellulose)	1	N/A	-	-	1	1	1	1	1	-
H2O	6	7	-	-	1	1	1	1	1	1
CO	10	-	-	-	1	1	1	1	1	2
H2	13	1	1	1	3	-	-	-	-	3
CH10203 (lignin)	-	1	1	1	-	-	-	-	-	-
C2H2	-	-	1	1	-	-	-	-	-	-
Cl	-	-	-	1	-	-	-	-	-	-
HCl	-	-	-	-	2	-	2	-	-	-
CH4	-	-	-	-	1	-	-	-	-	-
ZnO	-	-	-	-	1	1	1	1	1	-
ZnS	-	-	-	-	1	1	1	1	1	-
ZnCl2	-	-	-	-	1	1	1	1	1	-
CO2	-	-	-	-	1	1	1	1	1	1
CO3H	-	-	-	-	1	1	1	1	1	1
CH3OH	-	-	-	-	1	1	1	1	1	1
CO2	44.01	-	-	-	-	-	-	-	-	-

Biomass	Avg MW





Compressor	1. Compressor	Mass Density	0.0830193 lb/gal
Compression of gas and recycle stream mix to 80 bars		Volumetric Flow	5441.95000 g/hr
Compressor Inlet Stream Pressure	35 psi	Mass Flow	1237.43363 lb/min
Compressor Output Stream Pressure	115 bar	Corrected Mass Flow	1237.43363 lb/min
Indicated Airflowpower	757.801.71 hp	1 Series	872.20721
Break Horsepower	757.801.71 hp	5 Parallel	
Net Work Required	757.801.37 %	Temperature Ratio	1.36704816
Efficiency	72 %	Gamma	1.370535
Outlet Temp	47.165 C		
Inlet Temp	891.57 F		
pressure Ratio	4.10 F		
	3.28571.4286		

Spray Quench Tank

Hot Stream Inlet [Stream 5] Temperature

Cold Stream Inlet [Stream 6] Temperature

Cold Stream Inlet [Stream 8] Temperature

Inlet flow rate

Hot Stream Inlet [Stream 5] Pressure

Hot Stream Outlet [Stream 6] Pressure

Cold Stream Outlet [Stream 8] Pressure

Inlet Temp

800 C

579.84 C

25.2041 C

309.84 C

4000.8000 l/min

rho [Density of H2O]

lambda [Heat of Evaporation of Water]

D0 [Drop Diameter]

k [Thermal conductivity]

T [Log mean temp difference between water and inlet]

Residence Time

Hot Stream Inlet [Stream 5] Temperature

Cold Stream Inlet [Stream 6] Temperature

Cold Stream Inlet [Stream 8] Temperature

Inlet flow rate

Hot Stream Inlet [Stream 5] Pressure

Hot Stream Outlet [Stream 6] Pressure

Cold Stream Outlet [Stream 8] Pressure

Inlet Temp

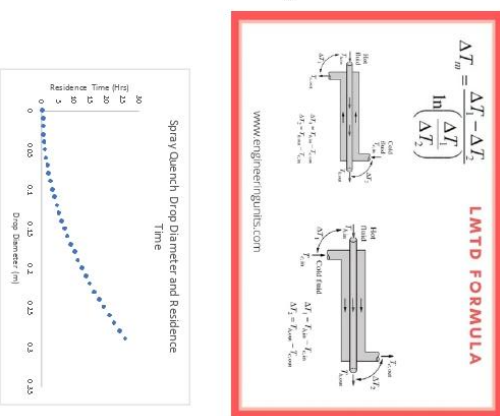
35 bar

35 bar

36 bar

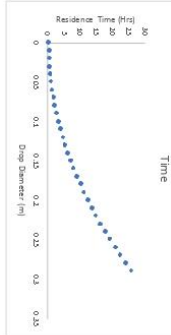
36 bar

H2O



Residence Time = volume of Reactor / Volumetric Flow rate

Volume of Reactor = Residence time * Volumetric Flow Rate



Symbol	Variable	Units
θ	Evaporation time	s
ρ	Density of drop (liquid)	kg/m ³
λ	Heat of vaporization of liquid	J/kg
D0	Drop diameter, initial, t = 0	m
M	Thermal conductivity	Jm/s/K
T	Log mean temperature difference between drop and gas	K

SCALING INPUTS FOR MID CONCENTRATION DESIGN (~4000X)

Assume:

Constant reactor temperature

Constant reactor heat duty

Steady state operation

Solar performance based on single-day, monthly averages

Hybrid operation for 24hr/day with fixed fraction for process down time

	Reactor Heat Duty Yearly Operation	217000 kWh/hour	Hours	Annual Solar Delivered Excess	Annual Solar GWh	Electrical for Hybrid (or Shortfall) Solar Hours Non-Solar Hours	Design Annual	Average (unweighted) Values η_s η_r $\eta_r - \eta_s$
Annual Net Energy Required to Process	633.6	GWhr		606.6	GWh	0.0	0.600	0.897
Annual Net Energy Required from Solar	1.00	GWhr		27.0	GWh	0.0	0.513	0.538
Daggett Yearly Hours of Direct Sunlight	633.6	GWhr					0.870	0.538
Reactor Temperature	1350	°C						0.446
Annual Weighted Efficiency	0.425							
Field Area Required	534950	m ²						
Heliostat Area/Tower	267459	m ²						
Tower Height	195.4	m						
# Towers Needed	2							
Total Heliostat Area	534918	m ²						
Annual Solar Energy to Process	633.6	GWhr						
	639.9764							
	633.6							
	627							
Within % of target Annual Energy from Solar								

SCALING INPUTS FOR HIGH CONCENTRATION DESIGN (~8000X)

Assume:

Constant reactor temperature

Constant reactor heat duty

Steady state operation

Solar performance based on single-day, monthly averages

Hybrid operation for 24hr/day with fixed fraction for process down time

	Reactor Heat Duty Yearly Operation	217000 2920	kWhr/hour Hours		Annual Solar Delivered Excess	Annual Solar GWhr GWh	Electrical! S Non-S
Annual Net Energy Required to Process	633.6	GWhr					
Nominal Fraction from Solar	1.00						
Annual Net Energy Required from Solar	633.6	GWhr					
Daggett Yearly Hours of Direct Sunlight	2787	kWhr/m ²					
Daggett Yearly Hours of Direct Sunlight	4870	Hours					
Reaction Temperature	1350	°C					
Annual Weighted Efficiency	0.496						
Field Area Required	458382	m ²	1375147 m ²				
Heliosat Area/Tower	91696	m ²	339.8055 acres				
Tower Height	184.8	m	338805.9 cost(\$)	< Design point tower height is 200m			
# Towers Needed	5						
Total Heliosat Area	458478	m ²					
Annual Solar Energy to Process	633.8	GWhr	Within 1% of target Annual Energy from Solar				

CAPITAL COST ESTIMATE					
User Input				Calc by Computer	
Name: Biomass Gasification Location: Month and				Date: 10/05/2022	
Type of Capital: Gmt					
Operating Hours per Year: 8,200					
Capacity: 66,000,000 Gt/hr				Life: 15 Years	
Lifetime: 15.75 Year per Month:				Cost: \$/hr	
Error cost of Land to install \$200/Cft. Cost: \$/hr				Item: \$/hr	Subtotal: \$/hr
Initial Infrastructure, Equipment, Methods					
Initial Equipment Purchased & Delivered					
Total Estimated Equipment Purchased & Delivered					
Mac. Equipment: Subtotal/Purchased Equipment Delivered					
Land Price Approach due to Peters, Zimmerman and West, 2003, from Table 22.17 in Slatler, et al., Processing Plant Type					
Overall Cost of Process: \$/hr Delivered					
Construction: 47					
Implementation and control: 36					
Equipment: 45					
Electrical: 11					
Buildings (Plant, Offices, Yard, Workshop): 15					
Service Factor: 70					
Total Direct and Indirect: 141					
Engineering and supervision: 33					
Total Direct and Indirect Plant Costs: 41					
Contractors, local and regional expenses: 26					
Permits: 44					
Pre of Capital Inv Invmt					
<hr/>					
Base Module Cost Method (FIM & FIM factors)					
Equipment at Mac. Module Level:					
FIM Cost: 650					
FIM Factor: 4.0					
Total: 2,600					
FIM Factor: 4.0					
Heat Exchanger 1: 142					
Heat Exchanger 2: 142					
Heat Exchanger 3: 142					
Heat Exchanger 4: 142					
FIM 1: 617					
FIM 2: 617					
Coke: 155					
Coke: 2,822 FIM					
Haul: Computer: 200					
Haul: Computer: 501					
Duration: 10475					
Duration: 4.16					
Duration: 15.86					
Conductor Minor: 32658					
Tower: 5908					
Total: 28,283					
<hr/>					
Subtotal (OC) from Total Base Module Cost w/ W. Factors					
Mac. Equipment: 10%					
Subtotal (OC) from Base Module Costs					
Subtotal (OC) Equipment Costs					
<hr/>					
Total: Base Module Costs for Fabricated Equipment					
Total: Base Module Costs for Process Machinery					
Total: Base Module Costs for Process Utilities					
Total: Costs for Initial Catalog - Ohmages					
Total: Base Module Costs for Computer & Instrumentation					
Total: Base Module Costs in (TBD) \$					
<hr/>					
Site Type: New Project					
Code of Site Preparation: 15%					
Code of Service Facilities: 25%					
Total: Overall Permanent Infrastructure (OPI):					
Cost of Contingencies and Contractors Fee: 20%					
Rate: Total Dependable Cost/1000					
Sum of Pd and TDC					
<hr/>					
Total: Current SS. (USOC)					
Site Factor: 100% of USOC Total					
Inflation: 4.0% for 27.0 yrs					
Local: 0.0%					
Total: Project Land/Cost: 0.0%					
TOTAL DEPENDABLE CAPITAL or FIXED CAPITAL INVESTMENT (TDC or FO)					
<hr/>					
WORKING CAPITAL					
Startup Raw Materials Inventory					
Quantity					
Units					
Price					
/					
/					
/					
/					
Total:					
Startup Spare Parts: 2.5% of live amount					
TOTAL: WORKING CAPITAL					
<hr/>					
Total: Net of L/L/G					
US Oil Coast: 1.00					
US South Coast: 1.05					
US Midwest: 1.10					
US West Coast: 1.25					
Mexico: 1.00					
Japan: 1.00					
Asia: 1.00					
India: 0.95					
<hr/>					
Project Type: Site Services					
New Project: 15%					
Project Addition: 5%					
<hr/>					
Processing Type: Column No.					
Gas: 2					
Solid/Fluids: 3					
Fluids: 4					
<hr/>					
Lang Factor Table: Bobds Bobds Fluids Fluids					
Overall Cost of Process: 1000					
Implementation and control: 200					
Implementation: 40					
Electrical: 100					
Buildings (of fixed vehicles): 25					
Yards: 25					
Service Factor: 400					
Total Direct Plant Cost: 2600					
Engineering: 250					
Construction: 300					
Contractors, local and regional: 211					
Contingency: 25					
Permits: 200					
<hr/>					

OPERATING COST ESTIMATE														
VARIABLE COST														
=USER INPUT			=CALC BY COMPUTER											
PRODUCT:	Methanol													
ANNUAL CAPACITY:	56,000,000 Gal per Year													
INGREDIENTS:	UNIT OF MEASURE	COST PER UNIT	UNITS OF INGRED/	COST PER Gal of PRODUCT (\$)										
	(kg)	(\$)	Gal/PRODUCT											
INGREDIENT NO. 1	kg	0.09	0.21358	biomass	0.019	4096.15	11960758	1054763.818						
INGREDIENT NO. 2	kg	0.00	216.86	methane	0.361	\$ 4,159,000.00	\$ 12,144,280,000.00	\$ 20,240,466.67						
INGREDIENT NO. 3	kg	0.0012	250.27	water	0.297	4799648.875	14014974715	\$ 16,640,471.30						
INGREDIENT NO. 4	kg	0.25	5.10	ZnO	1.274	97732.4	285378608	/1344652						
INGREDIENT NO. 5	kg	-3.5	0.038898571	carbon credit	-0.13615									
SUBTOTAL INGREDIENTS						1.951								
UTILITIES														
HP STEAM	kg	0.01729	8.4589E-13		0.000									
LP STEAM	kg	0.01257	6.14971E-13		0.000									
PROCESS WATER	gal													
COOLING WATER	m³	0.019	9.2955E-13		0.000									
INERT GAS	cf													
ELECTRICITY	kWh	0.06	0.0		0.000									
COMPRESSED AIR	cf													
LANDFILL	kg	554.8	9.90714E-06		0.005									
WASTE TREATMENT	kg	90.52	1.61643E-05		0.015									
SUBTOTAL UTILITIES						0.020								
CATALYSTS & CHEMICALS														
CATALYST														
CHEMICAL 1														
CHEMICAL 2														
CHEMICAL 3														
SUBTOTAL CATALYSTS & CHEMICALS														
PACKAGING MATERIALS														
PACKAGING LABOR														
BYPRODUCT CREDIT	MMBtu													
OTHER VARIABLE COSTS														
TOTAL VARIABLE COST					\$1.972 per Gal									
					\$110,408 k per Year									

OPERATING COST ESTIMATE			
FIXED COST			
	=USER INPUT		=CALC BY COMPUTER
PRODUCT:			
ANNUAL AnnCap:	56,000,000	Gal per Year	
TOTAL INVESTMENT (TPI):	\$19,800	k	
OPERATING LABOR & BENEFITS:			ANNUAL COST
NO. of OPERATORS:	48	calc in canvas	(\$k/yr)
ANNUAL WAGES	\$150	k PER OPERATOR	7,200
EMPL. BENEFITS @	40.0%	of WAGES	2,880
OPERATING SUPERVISION @		of WAGES	
SUBTOTAL OPERATING LABOR:			10,080
OPERATING SUPPLIES:		of WAGES	
MAINTENANCE:			
TOTAL MAINTENANCE @		OF INVESTMENT	
MAINTENANCE LABOR@		of TOTAL MAINT.	
MAINTENANCE MATERIAL @		of TOTAL MAINT.	
OVERHEAD:			
GEN. OH @	125.0%	of (OPR. WAGES + MAINT LABOR + OPR. SUPRV.)	9,000
LAB & TECHNICAL SUPPORT @		of INVESTMENT	
CORPORATE OVERHEAD:			
SALES & ADMINISTRATION		of INVESTMENT	
RESEARCH & DEVELOPMNT		of INVESTMENT	
SUBTOTAL CORPORATE OVERHEAD.....			
INSURANCE & LOCAL TAXES:			
	2.0%	of INVESTMENT	396
ROYALTIES:	\$ 0.0265	per annual Gal of Capacity	1,484
TOTAL FIXED COST (for cash flow calculations):		\$ 20,960	k per Year
		\$ 0.37	per Gal
DEPRECIATION:			
	of INVESTMENT		
Note: Do not include Depreciation if total Fixed Cost is to be used in Cash Flow Calc.			
TOTAL FIXED COST (for ROI calculations):		\$ 20,960	k per Year
		\$ 0.37	per Gal

CASH FLOW ANALYSIS

SELLER UNIT **SELLER UNIT** **SELLER UNIT**
SELLER UNIT **SELLER UNIT** **SELLER UNIT**
SELLER UNIT **SELLER UNIT** **SELLER UNIT**

TOTAL DIRECT COST OF CAMP = \$5,500.
SELLING PRICE = \$10,000 per unit
A. USE PERCENT = 50%
B. MARK UP VALUE = \$4,500
INCOME IS = EXPENSE ARE
INCOME = \$4,500
ANNUAL INCOME = \$45,000
ANNUAL EXPENSE = \$45,000

ROI CALCULATION
Total Ad Revenue - Total Ad Spend
Total Ad Spend * 100

PAI BACK PERIOD = **15.0%**
ROI = **4.6%**

Appendix C: Code

MATLAB and Python codes are present below.

Solar Reactor Code: Pages 133-137

Zinc Oxide Reactor Code: Pages 138-140

Methanol Reactor Code: Pages 141-144

Contents

- Appendix C: Solar Reactor Modeling
- Solar Reaction Kinetics
- Volume Domain
- Initial Conditions
- Solve ODE
- Data Handling
- Figure Plotting (Need To Change)

Appendix C: Solar Reactor Modeling

```
clear
clc
clear figure
```

Solar Reaction Kinetics

r1: C6H10O5+H2O=6CO+6H2 r2: C10H12O3+7H2O=10CO+13H2 r3: CO+H2O=CO2+H2 REVERSIBLE r4: CH4+H2O=CO+3H2

Volume Domain

```
volume_domain=linspace(0,50,300);
```

Initial Conditions

```
F_C6H10O5= 13.414*0.2778 %kmol/hr
F_C10H12O3= 37.7349*0.2778 %kmol/hr
F_H2O= 266380*0.2778 %mol/s
F_H2= 5.57321*10^6*0.2778 %kmol/hr
F_CO= 2.78661*10^6*0.2778 %kmol/hr
F_CO2= 0*0.2778 %kmol/hr
F_CH4= 259267*0.2778 %kmol/hr
T_0=298 %K

IC=[F_C6H10O5, F_C10H12O3, F_H2O, F_H2, F_CO, F_CO2, F_CH4, T_0];
```

Solve ODE

```
[Xsol, Ysol]=ode45('FinalDesignSolarReactorODE', volume_domain, IC)
```

Data Handling

```
F_C6H10O5=Ysol(:,1);
F_C10H12O3=Ysol(:,2);
F_H2O=Ysol(:,3);
F_H2=Ysol(:,4);
```

```
F_CO=Ysol(:,5);
F_CO2=Ysol(:,6);
F_CH4=Ysol(:,7);
T=Ysol(:,8);
```

Figure Plotting (Need To Change)

```
fig1=figure(1);
set(fig1, 'Name','Flow Rate');
plot(Xsol,F_C6H10O5)
hold on
plot(Xsol,F_C10H12O3)
hold on
plot(Xsol,F_H2O)
hold on
plot(Xsol,F_H2)
hold on
plot(Xsol,F_CO)
hold on
plot(Xsol, F_CO2)
hold on
plot(Xsol, F_CH4)
hold off
xlabel('Volume (L)');
ylabel('Flow Rate (mol/hr)');
legend("F_{C6H10O5}", "F_{C10H12O3}", "F_{H2O}", "F_{H2}", "F_{CO}", "F_{CO2}", "F_{CH4}")
title('Component Flow Rates')

fig2=figure(2);
set(fig2, 'Name','Temperature');
plot(Xsol,T)
xlabel('Volume (L)');
ylabel('Temperature(K)');
title('Temperature Energy Balance')
```

Published with MATLAB® R2022b

Contents

- [Output Variables](#)
- [Internal Variables](#)
- [ODE Definitions](#)

```
function [per_ode]=ode(X,Y)
```

Output Variables

```
F_C6H10O5=Y(1);
F_C10H12O3=Y(2);
F_H2O=Y(3);
F_H2=Y(4);
F_CO=Y(5);
F_CO2=Y(6);
F_CH4=Y(7);
T=Y(8);
```

Internal Variables

```
R=8.314*0.001    %kJ/(mol*K)
X=0.90 % conversion
phi = 4.7 %geometric factor

P=35

K1=(2.51*10^3)*exp(-112.6/(R*T))
K2=(6.74*10^-2)*exp(-37.3/(R*T))
K3=(3.04*10^-1)*exp(-36.6/(R*T))

H_rxn1 = 336.791;    %kJ/mol cellulose
H_rxn2 = 2459.472;   %kJ/mol lignin
H_rxn3 = 175.181 ;   %kJ/mol methane
H_rxn4 = -210.905;   %kJ/mol water-gas reaction

Cp1 =-0.011704*T+0.00067207*((T^2)/2) % Cellulose
Cp2 = 0.0314317*T+0.0003944*((T^2)/2) % Lignin
Cp3 = (0.033363)+0.02679*(0.00026105/T/sinh(0.00026105/T))^2+0.008896*(0.001169/T/cosh(0.001169/T))^2 % H2O
Cp4 = (0.027617)+0.00956*(0.002466/T/sinh(0.002466/T))^2+0.00376*(0.0005676/T/cosh(0.0005676/T))^2 % H2
Cp5 = (0.029108)+0.008773*(0.0030851/T/sinh(0.0030851/T))^2+0.008455*(0.0015382/T/cosh(0.0015382/T))^2 %CO
Cp6 = (0.02937)+0.03454*(0.001428/T/sinh(0.001428/T))^2+0.0264*(0.000588/T/cosh(0.000588/T))^2 % CO2
Cp7 = (0.033298)+0.079933*(0.0020869/T/sinh(0.0020869/T))^2+0.041602*(0.00099196/T/cosh(0.00099196/T))^2 % CH4

h_w = 0.0122 % W/m^2K
u_g = 3.2*10^-5 % Pa*s
A_i = 0.01824 % m^2
V_m = 0.365 % m^3
p_c = 15.2701 %kg/m^3
d_i = 0.1524 %m
h_m = 0.7189 %W/m^2K
T_m = 1723.15 %K
MW_c = 0.17117255 %kg/mol
T_w = 1723.15 %K
```

```

A_m = 109.5 %m^3
F_m = 51.1489*(1000/3600) %kmol/hr

F_T0 = (8.64498*10^6)*(1000/3600); % Sum of all entering flow rates

F_tot=F_C6H10O5+F_C10H12O3+F_H2O+F_H2+F_CO+F_CO2+F_CH4
P_C6H10O5 = F_C6H10O5/F_tot * P
P_C10H12O3 = F_C10H12O3/F_tot * P
P_H2O = F_H2O/F_tot * P
P_H2 = F_H2/F_tot * P
P_CO = F_CO/F_tot * P
P_CO2 = F_CO2/F_tot * P
P_CH4 = F_CH4/F_tot * P

k1=(K1*p_H2O)/(1+K2*p_H2O+K3*p_H2) %kJ/mol*bar*s
k2=(2.78*10^3)*exp((-1.26*10)/(R*T))
k3=(-9.59*10^4)*exp((-4.66*10)/(R*T))
k4=(3.0*10^8)*exp((-1.3*10^2)/(R*T))

```

ODE Definitions

```

r1=k1*(1-X)*sqrt(1-phi*log(1-X))
r2=k2*p_CO*p_H2O
r3=k3*p_CO2*p_H2
r4=k4*p_CH4*p_H2O

dF_C6H10O5=-r1
dF_C10H12O3=-r1
dF_H2O=-r1-r2+r3-r4
dF_CO=r1-r2+r3+r4
dF_H2=-r1+r2-r3+3*r4
dF_CO2=r2-r3
dF_CH4=-r4

Hpg=((h_m*A_m*f_m*MW_c)/(u_g*v_m*p_c))*(T-T_m)
Hwg=(h_w*pi*d_i)*(T-T_w)
SumFiCpi=(F_C6H10O5*Cp1)+(F_C10H12O3*Cp2)+(F_H2O*Cp3)+(F_H2*Cp4)+(F_CO*Cp5)+(F_CO2*Cp6)+(F_CH4*Cp7)

dT= (A_i*((H_rxn1*r1)+(H_rxn2*r1)+(H_rxn3*r4)+(H_rxn4*r2)+(H_rxn4*r3))-A_i*Hpg-A_i*Hwg)/SumFiCpi

per_ode=[dF_C6H10O5; dF_C10H12O3; dF_H2O; dF_H2; dF_CO; dF_CO2; dF_CH4; dT];

```

```
end
```

Published with MATLAB® R2022b

```
In [36]: import numpy as np
import math
import matplotlib.pyplot as plt
```

```
In [37]: def tp(T_m):
    e_m=1
    sigma=5.67*10**-8
    a=0.07297
    T_W=1723.15
    u_g=3.2*10**-5
    V_m=0.365
    p_m=32.10
    delth=7.7756*10**4
    MW_m=0.04011
    return (e_m*sigma*a*(T_W**4-T_m**4))/u_g+(V_m*p_m*(-delth))/MW_m
```

```
In [38]: def euler(func,y0,tf,delt):
    n = int(tf/delt)
    t = np.zeros(n+1)
    y = np.zeros(n+1)
    t[0] = 0
    y[0] = y0
    for i in range(0,n):
        t[i+1] = t[i] + delt
        y[i+1] = y[i] + delt*func(t[i])
    plt.plot(t,y)
    plt.xlabel("Volume (L)")
    plt.ylabel("Temperature of Particle (K)")
    plt.title("Volume and Temperature of Particle")
    return y[i+1]
```

```
In [39]: euler(tp,298,2,0.05)
```

```
Out[39]: 2234389616.508113
```

Contents

- [Appendix C: Zinc Oxide Reactor Modeling](#)
- [ZnO Reaction Kinetics](#)
- [Volume Domain](#)
- [Initial Conditions](#)
- [Solve ODE](#)
- [Data Handling](#)
- [Figure Plotting](#)

Appendix C: Zinc Oxide Reactor Modeling

```
clear
clc
clear figure
```

ZnO Reaction Kinetics

r1: $\text{ZnO} + \text{H}_2\text{S} = \text{ZnS} + \text{H}_2\text{O}$

Volume Domain

```
volume_domain=linspace(0,1,200);
```

Initial Conditions

```
F_H2S=0.311; %kmol/hr
F_ZnO=1200.8; %kmol/hr %we could assume PFR-like behavior
F_ZnS=0; %kmol/hr
F_H2O=0.69778e+06; %kmol/hr
T_0=298; %K
P_0=35; %Bar
%T_C0=600

IC=[F_H2S, F_ZnO, F_ZnS, F_H2O, T_0, P_0];
```

Solve ODE

```
[Xsol, Ysol]=ode45('FinalDesignZnOReactorODE', volume_domain, IC);
```

Data Handling

```
F_H2S=Ysol(:,1);
F_ZnO=Ysol(:,2);
F_ZnS=Ysol(:,3);
F_H2O=Ysol(:,4);
T=Ysol(:,5);
P=Ysol(:,6);
```

Figure Plotting

```
fig1=figure(1);
set(fig1, 'Name', "Concentration of H2S");
plot(Xsol,F_H2S)
hold on
plot(Xsol,F_ZnS)
hold on
xlabel('Volume (L)');
ylabel('Flow Rate (kmol/hr)');
legend("F_{H2S}", "F_{ZnS}")
title('Component Flow Rates')

fig2=figure(2);
set(fig2, 'Name', 'Temperature');
plot(Xsol,T)
xlabel('Volume (L)');
ylabel('Temperature(K)');
title('Temperature Energy Balance')

fig4=figure(4);
set(fig4, 'Name', 'Pressure')
plot(Xsol,P)
xlabel('Volume (L)');
ylabel('Pressure (bar)');
title('Pressure')
```

Contents

- Output Variables
- Internal Variables
- ODE Definitions

```
function [per_ode]=FinalDesignZnOReactorODE(X,Y)
```

Output Variables

```
F_H2S=Y(1);
F_ZnO=Y(2);
F_ZnS=Y(3);
F_H2O=Y(4);
T=Y(5);
P=Y(6);
```

Internal Variables

```
R_0=0.0765; %um
Z_v=0.6086; %unitless
x=0.90; %unitless
D_eff = 9.2*10^-14; %m^2/s
k_1 = 0; %unitless
C_pg = 5.97635*10^-8; %kJ/hr
m = 1.29*10^8; %kg/hr
h_g = 420.90 ; %W/m^2 K
a_v = 1; %m
T_s = 483; %K

%For Ergun Equation
G = 12.14*10^5 ; %mol/cm^2 s
rho = 0.02489377 ; %mol/L
D_p = 0.153 ; %um
phi = 0.15 ; %unitless
mu = 0.000143 ; %kg m/s

F_tot=F_H2S+F_ZnO+F_ZnS+F_H2O;
P_H2S = F_H2S/F_tot * P;
P_ZnO = F_ZnO/F_tot * P;
P_ZnS = F_ZnS/F_tot * P;
P_H2O = F_H2O/F_tot * P;
R = 0.08314; %L bar/mol K
C_H2S= P_H2S/R/T;
```

ODE Definitions

```
r1= 4*pi*R_0^2*C_H2S*(R_0*((Z_v+(1-Z_v)*(1-x))^(1/3)-(1-x)^(1/3))/((Z_v+(1-Z_v)*(1-x))^(1/3)*(1-x)^(1/3)*D_eff)+1/(1-x)^(2/3)*k_1)^(-1)*10^20;

dF_ZnO=-r1;
dF_H2S=-r1;
dF_ZnS=r1;
dF_H2O=r1;

dT=-h_g*a_v*(T-T_s)/(m*C_pg)*60^2*10^-3*34.1;

dP=(-G/(rho*D_p)*10^7)*((1-phi)/phi^3)*((150*(1-phi)*mu)/D_p*10^5/34.1+1.75*G)*10^-25; %some values are unit conversions

per_ode=[dF_ZnO; dF_H2S; dF_ZnS; dF_H2O; dT; dP] ;


```

```
end
```

.....

Published with MATLAB® R2022b

Contents

- [Appendix C: Methanol Reactor Modeling](#)
- [Methanol Reaction Kinetics](#)
- [Volume Domain](#)
- [Initial Conditions](#)
- [Solve ODE](#)
- [Data Handling](#)
- [Figure Plotting](#)

Appendix C: Methanol Reactor Modeling

```
clear
clc
clear figure
```

Methanol Reaction Kinetics

r1: CO+2H₂=CH₃OH r2: CO₂+H₂=CO+H₂O r3: CO₂+3H₂=CH₃OH+H₂O

Volume Domain

```
volume_domain=linspace(0,2000,2000);
```

Initial Conditions

```
F_CO= 537809.040 %kmol/hr
F_H2= 1363146.62 %kmol/hr
F_CH3OH= 241.87 %kmol/hr
F_CO2= 602.74 %kmol/hr
F_H2O= 535364.100 %kmol/hr
T_0=582.1500 %K
P_0=80 %Bar
T_C0=621.1500

IC=[ F_CO, F_H2, F_CH3OH, F_CO2, F_H2O, T_0, P_0, T_C0];
```

Solve ODE

```
[Xsol, Ysol]=ode45('FinalDesignMeOHReactorODE', volume_domain, IC)
```

Data Handling

```
F_CO=Ysol(:,1);
F_H2=Ysol(:,2);
F_CH3OH=Ysol(:,3);
F_CO2=Ysol(:,4);
F_H2O=Ysol(:,5);
```

```
T=Ysol(:,6);
P=Ysol(:,7);
T_C=Ysol(:,8);
```

Figure Plotting

```
fig1=figure(1);
set(fig1,'Name','Flow Rate');
plot(Xsol,F_CO)
hold on
plot(Xsol,F_H2)
hold on
plot(Xsol,F_CH3OH)
hold on
plot(Xsol,F_CO2)
hold on
plot(Xsol,F_H2O)
hold off
xlabel('Volume (L)');
ylabel('Flow Rate (mol/hr)');
legend("F_{CO}","F_{H2}","F_{CH3OH}","F_{CO2}","F_{H2O}")
title('Component Flow Rates')

fig2=figure(2);
set(fig2,'Name','Temperature');
plot(Xsol,T)
xlabel('Volume (L)');
ylabel('Temperature(K)');
title('Temperature Energy Balance')

fig3=figure(3);
set(fig3,'Name','Coolant Temperature');
plot(Xsol,T_C)
xlabel('Volume (L)');
ylabel('Temperature (K)');
title('Coolant Temperature')

fig4=figure(4)
set(fig4,'Name','Pressure')
plot(Xsol,P)
xlabel('Volume (L)');
ylabel('Pressure (bar)');
title('Pressure')
```

Published with MATLAB® R2022b

Contents

- Output Variables
- Internal Variables
- ODE Definitions

```
function [per_ode]=ode(X,Y)
```

Output Variables

```
F_CO=Y(1);
F_H2=Y(2);
F_CH3OH=Y(3);
F_CO2=Y(4);
F_H2O=Y(5);
T=Y(6);
P=Y(7);
T_C=Y(8)
```

Internal Variables

```
R=8.314
k1=(4.89*10^7)*exp(-113000/(R*T))
k2=(9.64*10^11)*exp(-152900/(R*T))
k3=(1.09*10^5)*exp(-87500/(R*T))

b_CO=(2.16*10^-5)*exp(46800/(R*T))
b_CO2=(7.05*10^-7)*exp(61700/(R*T))
b_H=(6.37*10^-9)*exp(84000/(R*T)) % Let b_H represent the ratio of b_H20/(b_h2)^0.5

K1=10^(5139/T-12.621)
K2=10^(-2073/T-2.029)
K3=10^(3066/T-10.592)

H_rxn1 = 162.3387404; %kJ/mol
H_rxn2 = -192.8416736; %kJ/mol
H_rxn3 = -206.7025002 ; %kJ/mol

Cp1 = (29108)+8773*(3085.1/T/sinh(3085.1/T))^2+8455*(1538.2/T/cosh(1538.2/T))^2;
Cp2 = (27617)+9560*(2466/T/sinh(2466/T))^2+3760*(576.6/T/cosh(576.6/T))^2;
Cp3 = (39252)+87900*(37.6/T/sinh(37.6/T))^2+53000*(896.7/T/cosh(896.7/T))^2;
Cp4 = (29370)+34540*(1428/T/sinh(1428/T))^2+26400*(588/T/cosh(588/T))^2;
Cp5 = (33363)+26790*(2610.5/T/sinh(2610.5/T))^2+8896*(1169/T/cosh(1169/T))^2;

Cp10 = 5.11 ; % Assuming that coolant specific heat is constant

U_catalyst = 368.3/273.15;

density=17.59
BP=0.41 % Bed Porosity
rho_bulk = density*(1-BP) ;
phi = 0.50; % Void Frac
rho_intrinsic = 440;

D_I=0.0254
tubes=16
L=0.48 % meters
a_s=D_I*L*tubes
a_c=pi*(D_I/2)^2*tubes
m_c = 10; % flowrate of coolant

G =(7.63648*10^6)/(a_s*1000)*density % Superficial mass velocity
```

```

g_c =1 ;  

D_p = 1/8*D_I; % Heuristic  

mu = 0.5;  

beta_0 =((G*(1-phi))/(rho_intrinsic*g_c*D_p*phi^3))*((150*(1-phi)*mu)/D_p+1.75*G)  

F_T0 = 2.437*10^6; % Sum of all entering flow rates  

F_tot=F_CO+F_CO2+F_H2+F_H2O+F_CH3OH;  

P_CO = (F_CO/F_tot * P);  

P_CO2 = F_CO2/F_tot * P;  

P_H2 = F_H2/F_tot * P;  

P_H2O = F_H2O/F_tot * P;  

P_CH3OH = F_CH3OH/F_tot * P;

```

ODE Definitions

```

r1=k1*b_CO*((P_CO*P_H2^(3/2)-P_CH3OH)/(P_H2^0.5*K1))/((1+b_CO*p_CO+b_CO2*p_CO2)*(P_H2^0.5+b_H*p_H2O))  

r2=k2*b_CO2*((P_CO*p_H2-p_CO*p_H20/K2)/((1+b_CO*p_CO+b_CO2*p_CO2)*(P_H2^(0.5)+b_H*p_H20)))  

r3=k3*b_CO2*((P_CO2*p_H2^(3/2)-(P_CH3OH*p_H20)/(P_H2^(3/2)*K3)))/((1+b_CO*p_CO+b_CO2*p_CO2)*(P_H2^0.5+(b_H*p_H20)))  

dF_CO=-r1+r2  

dF_H2=-2*r1-r2-3*r3  

dF_CH3OH=r1+r3  

dF_CO2=-r2-r3  

dF_H2O=r2+r3  

dT=(((U_catalyst/rho_bulk)*(T_C-T)+r1*H_rxn1+r2*H_rxn2+r3*H_rxn3)/(F_CO*Cp1+F_H2*Cp2+F_CH3OH*Cp3+F_CO2*Cp4+F_H2O*Cp5))  

dT_c=U_catalyst*a_s*(T-T_C)/(m_c*Cp10);  

dP=-(beta_0/(a_c*(1-phi)))*((80)/P)*(T/T_C)*(F_tot/F_T0))  

per_ode=[dF_CO; dF_H2; dF_CH3OH; dF_CO2; dF_H2O; dT; dP; dT_c] ;

```

```

end

```

Published with MATLAB® R2022b